BRIGARD& CASTRO
PROPIEDAD INTELECTUAL

Calle 70 A No. 4 – 41
BOGOTÁ – COLOMBIA
TEL: (571) 744 22 00
FAX: (571) 742 22 00
www.bc.com.co

As. 103303

Señor
DIRECTOR DIVISIÓN DE NUEVAS CREACIONES
SUPERINTENDENCIA DE INDUSTRIA Y COMERCIO
E. S. D.

REF: Expediente No. **07.021258**– solicitud de patente de invención a favor de **GENENTECH, INC** Título **ANTAGONISTAS ANTIBETA7 HUMANIZADOS Y USOS PARA ESTOS**

RESPUESTA A ARTICULO 46

JUAN PABLO CADENA SARMIENTO, portador de la tarjeta profesional No. 57.492 del C.S.J., obrando como apoderado de la sociedad solicitante me permito dar respuesta al oficio No. 05972 notificado el 18 de abril de 2012 presentando copia de los documentos solicitados en virtud del Artículo 46 de la Decisión 486.

PICARELLA D et. al.: "Monoclonal antibodies specific for beta 7 integrin and mucosal addressin cell adhesion molecule-1 (MADCAM-1) reduce inflammation in the colon of SCID mice reconstituted with CD45RBHIGH CD4+T cells". Journal of Immunology, The Williams and Wilkins Co. Caltimore, US, Vol. 158, pages 2099-2106.

SUN XUEYING et.al: "Beta 7 integrins contribute to skin graft rejection". Transplantation (Baltimore), vol. 74, no. 8, 27 October 2002 (2002-10-27), pages 1202-1203.

TIDSWELL M et. al.: "Structure-function analysis of the integrin beta subunit: Identification of domains involved in adhesion to MAdCAM-1". Journal of Immunology, Williams & Wilkins Co, US, vol.159, no. 3, 1 August 1997 (1997-08-01), pages 1497-1505.

LEE C V et. al.: "High-affinity human antibodies from Phage-displayed synthetic Fab Libraries with a single framework Scaffold". Journal of molecular biology, London, GB, vol. 30, no. 5, 23 July 2004 (2004-07-23), pages 1073-1093.

BRIGARD& CASTRO
PROPIEDAD INTELECTUAL

Calle 70 A No. 4 – 41
BOGOTÁ – COLOMBIA
TEL: (571) 744 22 00
FAX: (571) 742 22 00
www.bc.com.co

Anexos

- Artículos solicitados

Del Señor Director

JUAN PABLO CADENA SARMIENTO
T.P. No. 57.492 del C.SJ.
C.C. 80.410.337 de Usaquén
Calle 70 A No. 4 - 41

The Journal of Immunology

Monoclonal antibodies specific for beta 7 integrin and mucosal addressin cell adhesion molecule-1 (MAdCAM-1) reduce inflammation in the colon of scid mice reconstituted with CD45RBhigh CD4+ T cells

D Picarella, P Hurlbut, J Rottman, X Shi, E Butcher and DJ Ringler

J. Immunol. 1997;158;2099-2106

The Journal of Immunology is published twice each month by The American Association of Immunologists, Inc., 9650 Rockville Pike, Bethesda, MD 20814-3994.

Print ISSN: 0022-1767 Online ISSN: 1550-6606.

Monoclonal Antibodies Specific for β_7 Integrin and Mucosal Addressin Cell Adhesion Molecule-1 (MAdCAM-1) Reduce Inflammation in the Colon of *scid* Mice Reconstituted with CD45RB^{high} CD4$^+$ T Cells[1]

Dominic Picarella,[2]* Peter Hurlbut,* James Rottman,* Xiaojie Shi,* Eugene Butcher,† and Douglas J. Ringler*

Mucosal addressin cell adhesion molecule-1 (MAdCAM-1) is an adhesion protein expressed on endothelium in mucosal tissues that has been shown to play an important role in the selective homing of lymphocytes to intestinal mucosa and associated lymphoid tissue. To determine whether MAdCAM-1 or its ligand $\alpha_4\beta_7$ would be appropriate targets for therapeutic intervention in gut-associated inflammation, we tested the ability of rat mAbs specific for β_7 integrin and MAdCAM-1 to inhibit chronic colonic inflammation in *scid* mice reconstituted with CD4$^+$ T cells enriched for the CD45RB^{high} subpopulation. Abs specific for β_7 and MAdCAM-1 blocked recruitment of lymphocytes to the colitic colon, and more importantly, these Abs significantly reduced the severity of colonic inflammatory disease in this animal model. Therefore, the adhesive interactions mediated by $\alpha_4\beta_7$ and MAdCAM are intimately involved in leukocyte recruitment to gut in chronic inflammatory disease and may be relevant therapeutic targets for patients with inflammatory bowel disease. *The Journal of Immunology,* **1997, 158: 2099–2106.**

Mucosal addressin cell adhesion molecule-1 (MAdCAM-1)[3] is a member of the Ig supergene family that is expressed on mucosal endothelium and is involved in the selective homing of lymphocytes to normal mucosal tissues (1–3). The lymphocyte receptor for MAdCAM, $\alpha_4\beta_7$, defines a subpopulation of memory lymphocytes involved in mucosal immunity and mediates cell-cell and cell-matrix adhesion, signaling, trafficking, and regulation of immune responses in mucosal sites, particularly the gastrointestinal tract. Abs specific for MAdCAM-1 or for its lymphocyte receptor, $\alpha_4\beta_7$, inhibit normal homing of lymphocytes to the small intestine, Peyer's patch, or mesenteric lymph nodes (MLN) without inhibiting trafficking to nonmucosal tissues (3). As such, the adhesive interaction defined by $\alpha_4\beta_7$/MAdCAM-1 may represent a potent and organ-specific target for the therapeutic modulation of T cell-mediated inflammatory diseases of the gastrointestinal tract. However, the role of the $\alpha_4\beta_7$/MAdCAM-1 adhesion pathway in the recruitment of lymphocytes to the large intestine has not been examined, nor has its relevance been critically examined in inflammatory responses.

Previous studies in the cotton-top tamarin monkey (4, 5) have demonstrated that functional inhibition of $\alpha_4\beta_7$, using α_4- or β_7-specific mAbs, attenuates colonic inflammatory activity. However, because the α_4-specific Ab blocks both $\alpha_4\beta_1$ as well as $\alpha_4\beta_7$, and $\alpha_4\beta_7$ has ligands other than MAdCAM-1, it was not conclusively demonstrated that efficacy was the result of inhibition of $\alpha_4\beta_7$/MAdCAM-1 adhesive interactions. To examine this issue, T cell-mediated colitis was induced in *scid* mice by reconstitution with CD4$^+$ T cells enriched for the CD45RB^{high} subpopulation. Abs specific for β_7 and MAdCAM-1 together blocked recruitment of lymphocytes to the colitic colon in an organ-specific fashion and significantly reduced the severity of colonic inflammatory disease. The specificity of this treatment for gut-associated mucosal tissue was further supported by the observation that separate administration of MAdCAM-1-specific mAbs was sufficient to achieve similar anti-inflammatory effects. Therefore, the adhesive interactions mediated by $\alpha_4\beta_7$ and MAdCAM are intimately involved in leukocyte recruitment to gut in chronic inflammatory disease and may be relevant therapeutic targets for patients with inflammatory bowel disease.

Materials and Methods

Animals

BALB/cAnNTacfBR female mice (5–6 wk old) and *scid* female mice (C.B-17/IcrTac-*scid*fDF; 4 wk old) were purchased from Taconic Farms, Inc. (Germantown, NY), and housed under specific pathogen-free conditions in the LeukoSite animal facility.

Isolation of CD45RB^{high} T cells and reconstitution of scid *recipients*

BALB/c spleen cells were used as a source of CD4$^+$ T cells for reconstitution of *scid* recipient mice. Briefly, a single cell suspension was prepared in cold DMEM from several BALB/c spleens. Erythrocytes were lysed in a solution of 0.17 M ammonium chloride on ice for 10 min. After washing in DMEM, the cells were resuspended in warm (37°C) DMEM supplemented with 10% FCS and applied to a nylon wool column (pre-equilibrated at 37°C). After 1 h at 37°C, the nonadherent population, enriched for T cells, was eluted with warm DMEM/10% FCS. The cells were counted, washed, and resuspended to a density of 10×10^6 cells/ml in MACS buffer (PBS, 1% BSA, and 5 mM EDTA).

*LeukoSite, Inc., Cambridge, MA 02142; †Center for Molecular Biology in Medicine, Veterans Administration Medical Center, Palo Alto, CA 94304; and The Digestive Disease Center, Department of Medicine, Laboratory of Immunology and Vascular Biology, and Department of Pathology, Stanford University, Stanford, CA 94305

Received for publication August 30, 1996. Accepted for publication December 9, 1996.

The costs of publication of this article were defrayed in part by the payment of page charges. This article must therefore be hereby marked *advertisement* in accordance with 18 U.S.C. Section 1734 solely to indicate this fact.

[1] This work was supported by National Institutes of Health Small Business Innovation Research Grant R43 DK49883-01.

[2] Address correspondence and reprint requests to Dr. Dominic Picarella, LeukoSite, Inc., 215 First Street, Cambridge, MA 02142.

[3] Abbreviations used in this paper: MAdCAM-1, mucosal addressin cell adhesion molecule-1; MLN, mesenteric lymph node.

0022-1767/97/$02.00

The T cell-enriched population was further enriched for $CD4^+$ T cells using a MACS column (type RS 413-01, Miltenyi, Auburn, CA) prepared in accordance with the manufacturer's instructions. Briefly, cells were first reacted with a biotinylated rat mAb mixture consisting of anti-CD8a (1/1600–2000; clone 53-6.7, PharMingen, San Diego, CA), anti-B220 (1/1600–2000; clone RA3-682, PharMingen), anti-IA^d (1/100–200; clone 39-10-8, PharMingen), and anti-CD11b (1/100–200; clone M1/70, PharMingen) for 1 h on ice. The cells were washed, resuspended in 90 μl of buffer/10×10^6 cells, and mixed with 10 ml of streptavidin-conjugated Microbeads (481-01, Miltenyi)/10×10^6 cells. The reaction was performed for 20 min on ice, after which the mixture was applied to the MACS column. The flow-through population was highly enriched for $CD4^+$ T cells, as demonstrated by FACS analysis. After several washes, the cells were resuspended to a density of 10×10^6 cells/ml and reacted with FITC-conjugated anti-CD45RB (1/1000; clone 16A, PharMingen) and phycoerythrin-conjugated anti-CD4 (1/2000; clone RM4-5, PharMingen) for 1 h on ice.

As described in previous reports (6, 7), the $CD45RB^{high}$ population was sorted as the brightest 40 to 45% of the $CD4^+$ population, while the $CD45RB^{low}$ population was sorted as the dimmest 15 to 20% of the $CD4^+$ population. The sorted populations were subsequently washed with sterile saline and injected i.v. into recipient mice. The number of cells administered to each mouse varied from 5×10^4 to 1×10^6. The progression of disease was monitored as a function of loss of body weight.

Antibodies

YKIX 309.2 (rat IgG2a anti-canine CD4) (8, 9) and FIB 504 (rat IgG2a anti-murine β_7) (1) were produced by culture of the hybridoma cells in a hollow fiber cell bioreactor (Unisyn, San Diego, CA) and purified under endotoxin-free conditions by protein G affinity chromatography. MECA 367 (rat IgG2a anti-murine MAdCAM-1) (10) was purified from tissue culture supernatant under endotoxin-free conditions by protein G chromatography.

β_7/MAdCAM blockade in colitic scid *mice*

Colitic *scid* mice, reconstituted with $CD45RB^{high}$ T cells, were selected for blockade experiments on the basis of a statistically significant loss in body weight relative to control *scid* mice reconstituted with $CD45RB^{low}$ T cells. Typically, a statistically significant loss of body weight occurred within 6 to 8 wk of reconstitution, and by 2 to 3 mo, mean body weight had decreased by 15 to 25% of the initial or peak weight. Colitic mice (from 2–6 mo postreconstitution) were randomly distributed to different experimental groups. Analysis of variance was performed to confirm that there was no significant difference in body weight between experimental groups before the start of the experiment. Rat mAbs specific for β_7 integrin (FIB 504) and/or MAdCAM-1 (MECA 367) were administered either by daily i.p. injection of 100 μg each for a period of 14 days before adoptive transfer of ^{111}In-labeled MLN cells or by a single i.v. injection of a mixture of 250 μg of Ab with ^{111}In-labeled MLN cells. An equivalent amount of an isotype-matched rat mAb (YKIX 309.2) was administered under identical conditions and used as a control. Levels of rat IgG in plasma were determined at the conclusion of the blockade by ELISA and FACS analysis (see following sections) using TK1 cells and MAdCAM-transfected murine L1.2 cells.

^{111}In labeling and adoptive transfer

A single-cell suspension of MLN from BALB/c mice was prepared on ice in DMEM supplemented with 5% FCS. Erythrocytes were lysed as described previously, and the cells were resuspended to 100×10^6 cells/ml in DMEM plus 5% FCS. ^{111}In oxine (7.5 μCi; Amersham MediPhysics, Woburn, MA) was added for each 50×10^6 cells, and incubation proceeded for 20 min at room temperature with frequent agitation. The cells were washed and resuspended to 50×10^6 cells/ml, and 100 μl was injected i.v. into each recipient *scid* mouse. Tissues were harvested 24 h postinjection and counted for radioactivity in a Packard Cobra II gamma counter (Packard, Downers Grove, IL). Peyer's patches were not visible on a gross level in the small intestine of reconstituted *scid* mice and were not excised. Therefore, recruitment of labeled cells to the small intestine would also include trafficking to these sites. To assess nonspecific deposition of radiolabeled cells in tissues, some control mice received equal numbers of labeled cells fixed for 1 h on ice with 10% buffered formalin (Fisher Scientific Co., Fairlawn, NJ)

Histology, immunohistochemistry, and image analysis

For histologic analyses, tissue was fixed in 10% phosphate-buffered formalin (Fisher Scientific Co.), routinely processed (Hypercenter, Shandon Ltd., Pittsburgh, PA), and paraffin embedded. Sections were stained with hematoxylin and eosin.

Immunohistochemical staining was performed on 6-μm frozen sections. Briefly, tissue was snap-frozen in OCT medium (Miles, Inc., Elkhart, IN) in dry ice suspended in 2-methylbutane (EM Science, Gibbstown, NJ). Desiccated sections were fixed in ice-cold acetone (Fluka, Ronkonkoma, NY) for 10 min, washed with PBS, and blocked for 30 min at room temperature with PBS supplemented with 1% FCS, 10% normal rabbit serum, and 5% human AB serum. Sections were incubated overnight at 4°C with primary Ab and developed with Super Sensitive Detection Systems (AA000-5T; Biogenex, San Ramon, CA) using alkaline phosphatase-conjugated streptavidin and Fast Red as substrate, supplemented with levamisole to block endogenous alkaline phosphatase activity, in accordance with the manufacturer's instructions.

Quantitative, computer-assisted image analysis was performed on immunohistochemically stained, frozen sections using a Leica Quantimet 500 Image Analyzer (Leica, Deerfield, IL). Each section was surveyed in its entirety using a ×10 objective. The number of immunoreactive cells was enumerated on the basis of immunoreactive objects per area or the percentage of immunoreactive area in the section, as described previously (11).

Quantitation of plasma levels of Ab

Circulating levels of rat IgG2a mAb in plasma were determined by ELISA. Briefly, 96-well Nunc Maxi-Sorp plates (VWR Scientific Corp., Bridgeport, NJ) were coated overnight at 4°C with 10 μg/ml affinity-purified goat anti-rat IgG (Cappel, West Chester, PA). After blocking for 1 h at 37°C (PBS plus 1% BSA), plasma samples (appropriately diluted in PBS plus 1% BSA) were added to wells for 2 h at room temperature. After several washes, horseradish peroxidase-conjugated mouse anti-rat IgG (Jackson ImmunoResearch Laboratories, West Grove, PA) was added for 1 h at room temperature, followed by the addition of OPD substrate (Sigma Chemical Co., St. Louis, MO) for 10 to 15 min at room temperature. Purified rat IgG2a (ICN, Costa Mesa, CA) was used as a standard.

Bioactive Ab levels in plasma were determined by FACS analysis. Briefly, TK1 cells ($\alpha_4\beta_7^+$) or L1.2-MAd7 cells (MAdCAM-1^+) (12) were blocked with PBS and 2% normal mouse serum (Sigma Chemical Co., St. Louis, MO) for 30 min at 37°C, washed, and reacted with dilutions of plasma samples for 1 h on ice in 96-well V-bottom plates (Costar, Cambridge, MA). The cells were washed and then reacted with 5 μg/ml biotinylated rabbit anti-rat IgG (Vector, Burlingame, CA) on ice for 30 min, followed by reaction with streptavidin-PE (Southern Biotechnology Associates, Birmingham, AL) on ice for 30 min. Purified FIB 504 and MECA 367 were used as standards.

Results

The chronic colitis induced in scid mice reconstituted with $CD45RB^{high}$ T cells is associated with elevated levels of MAdCAM expression and infiltration of β_7^+ lymphocytes

Within 6 to 8 wk after reconstitution with $CD45RB^{high}$, but not $CD45RB^{low}$, T cells, *scid* recipient mice experienced a significant decrease in body weight. As previously described (6, 7, 13, 14), histologic features of the colon included infiltration of large numbers of mononuclear cells in the lamina propria and submucosa, epithelial immaturity with regions of ulceration, crypt dropout, loss of goblet cells, and crypt abscesses. MAdCAM-1 expression and the presence of β_7 integrin on infiltrating lymphocytes in the colon were analyzed by immunohistochemistry. The number of $\beta7^+$ cells (Fig. 1*A*) in the lamina propria and submucosa from colitic mice was similar to the number of $CD4^+$ T cells (Fig. 1*B*), suggesting that many or all of the infiltrating mononuclear cells expressed β_7 integrin. MAdCAM-1 expression in colon sections from *scid* mice reconstituted with $CD45RB^{low}$ T cells was limited to weakly immunoreactive venules in the lamina propria (Fig. 1*D*). This pattern and expression level was similar to those of normal C57Bl/6 mice (not shown). In contrast, in colon sections from *scid* mice reconstituted with $CD45RB^{high}$ T cells, MAdCAM-1^+ venules were more abundant, expressed higher levels of MAdCAM-1, and were present in submucosa, tunica muscularis, and lamina propria (Fig. 1*C*). Therefore, disease in colitic *scid* mice reconstituted with $CD4^+$ $CD45RB^{high}$ T cells was associated with

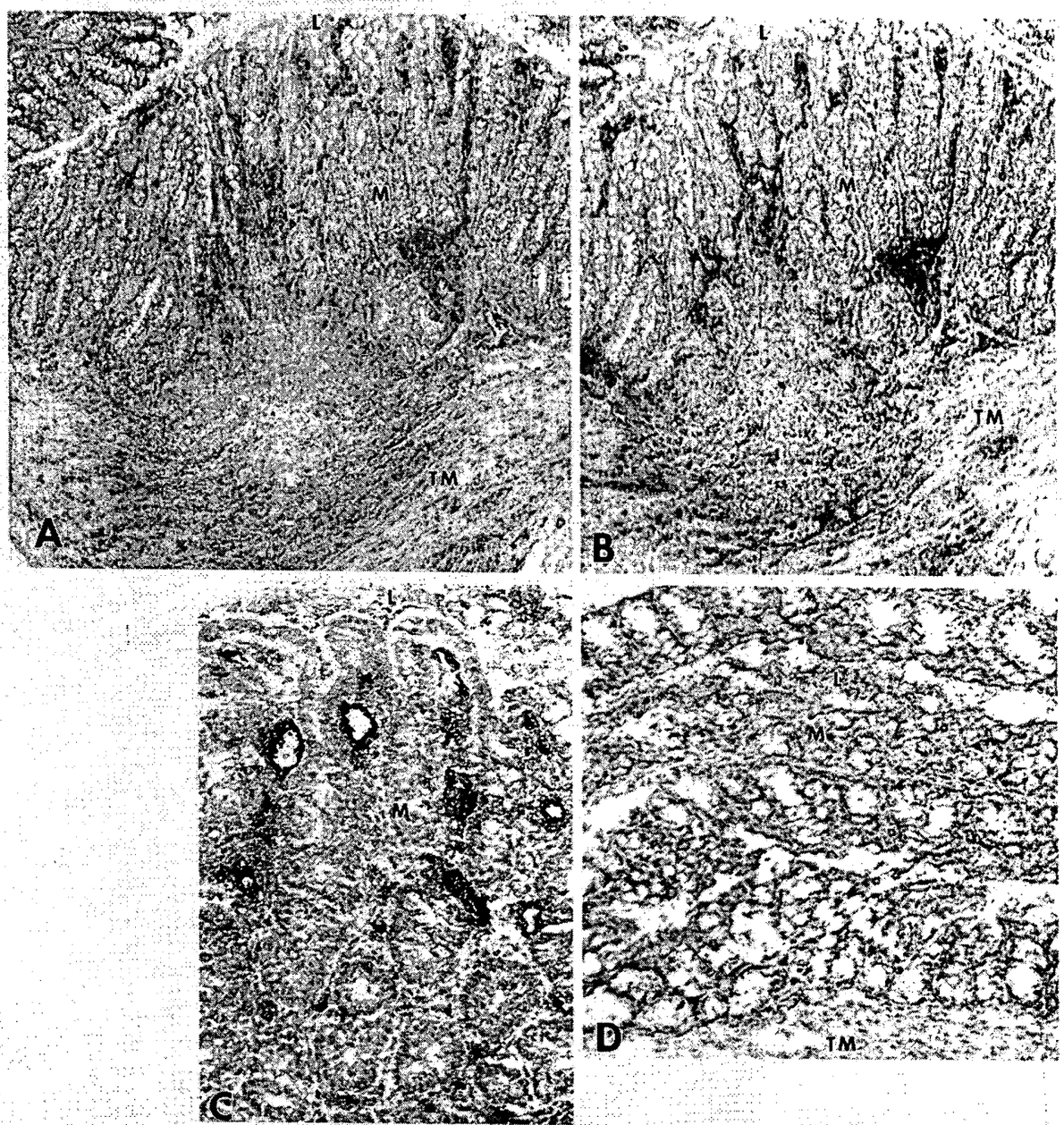

FIGURE 1. Colitis induced in *scid* mice is associated with enhanced MAdCAM-1 expression and infiltration of β_7^+ lymphocytes. Frozen sections were prepared from *scid* mice 6 mo postreconstitution with 1.1×10^5 $CD45RB^{high}$ or $CD45RB^{low}$ T cells. *A* and *B*, A severe transmural colitic lesion with lymphocytic infiltration in the mucosa (M) and tunica muscularis (TM) stained for β_7 integrin (*A*) or CD4 (*B*), demonstrating similar numbers of both cell types; magnification 300×. *C* and *D*, MAdCAM-1 expression in the mucosa of frozen colonic sections from colitic *scid* mice reconstituted with $CD45RB^{high}$ T cells (*C*) or age-matched control, noncolitic *scid* mice reconstituted with $CD45RB^{low}$ T cells (*D*); magnification 500×. MAdCAM-1 expression is greatly increased in inflamed colonic mucosa. L, lumen; M, mucosa; TM, tunica muscularis. Immunohistochemistry with Mayer's counterstain.

accentuated MAdCAM-1 expression and localization of lymphocytes bearing β_7.

β_7 and MAdCAM-1 are functionally involved in the recruitment of lymphocytes to sites of inflammation in the colon

To address the role of $\alpha_4\beta_7$ and MAdCAM-1 in the pathogenesis of colonic inflammation induced in *scid* mice, we conducted a series of experiments in which colitic *scid* mice (2–6 mo postreconstitution) were treated daily with rat mAbs specific for β_7 integrin, MAdCAM-1, both in combination, or an irrelevant isotype-matched control mAb in sufficient quantity to result in plasma concentrations of 100 to 400 μg/ml. These levels were well above the 50% inhibiting concentration (IC_{50}) of 50 to 100 ng/ml determined in an in vitro cell adhesion assay using murine TK1 cells and recombinant murine MAdCAM-C_k chimeric protein (not

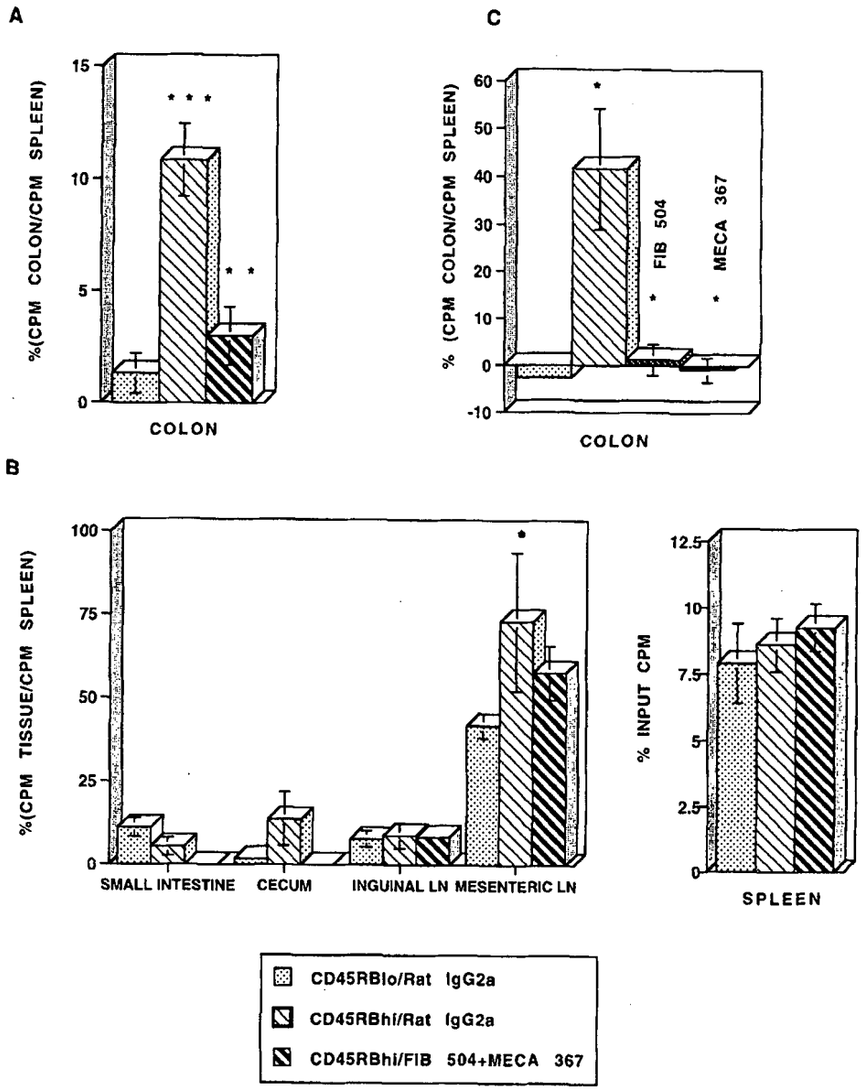

FIGURE 2. Assessment of β_7/MAdCAM-1 blockade *in scid mice by adoptive transfer of* ^{111}In-labeled MLN cells. Results for all tissues except spleen are expressed as a mean percentage (counts per minute for each tissue/counts per minute spleen) − background ± SEM. Results for the spleen are expressed as the percentage of input counts per minute − background ± SEM. Tissues were harvested and counted for radioactivity 24 h post-adoptive transfer. Statistical significance was determined using one-tailed Student's *t* test (*** indicates $p < 0.002$; **, $p < 0.005$; *, $p < 0.05$). *A* and *B*, mAb blockade in colitic *scid* mice (2–6 mo postreconstitution). One group ($n = 5$; mean loss of body weight (MLBW), 26.9% less than the control value) received a combination of FIB 504 (β_7-specific) and MECA 367 (MAdCAM-specific), while a colitic control group ($n = 5$; MLBW, 24.7% less than the control value) received an isotype-matched control Ab (YKIX 309.2) as described in *Materials and Methods*. Another control group consisted of mice reconstituted with CD45RB^{low} T cells ($n = 4$) that did not develop colitis. All mice were given daily i.p. injections of Abs for a period of 2 wk. ^{111}In-labeled MLN cells (5×10^6) were administered i.v. after treatment was completed. Recruitment of radiolabeled MLN cells to colon in colitic *scid* mice was increased 8.2-fold relative to recruitment in noncolitic control mice. *C*, Effect of a single dose of Ab administered with adoptive transfer of 5×10^6 ^{111}In-labeled cells. Colitic *scid* mice were injected i.v. with labeled cells combined with 250 μg of Rat IgG2a control Ab ($n = 4$; MLBW, 26.3% less than controls), FIB 504 ($n = 5$; MLBW 27.3% less than the control value), or MECA 367 ($n = 5$; MLBW, 29.1% less than the control value). Noncolitic *scid* mice were used as a control ($n = 5$). Recruitment of radiolabeled MLN cells to colon in colitic *scid* mice was increased >40-fold relative to recruitment in noncolitic control mice.

shown). Using quantitative adoptive transfer of ^{111}In-labeled MLN, recruitment of lymphocytes to the colon in colitic *scid* mice treated with an isotype-matched control Ab was significantly increased (typically 10- to 50-fold) relative to the basal level of recruitment to the colon in noncolitic *scid* mice reconstituted with CD45RB^{low} T cells ($p < 0.002$; Fig. 2*A*). Increased recruitment was only observed in the involved colon and the draining MLN ($p < 0.05$; Fig. 2*B*) and not in the small intestine or nonmucosal tissue, such as inguinal lymph node or spleen ($p > 0.1$; Fig. 2*B*). Treatment of colitic *scid* mice with a combination of β_7- and MAdCAM-specific rat mAbs inhibited recruitment to the colon by 72% ($p < 0.005$; Fig. 2*A*). When the efficacy of β_7- and MAdCAM-1-specific mAbs was evaluated independently following a single i.v. injection of labeled

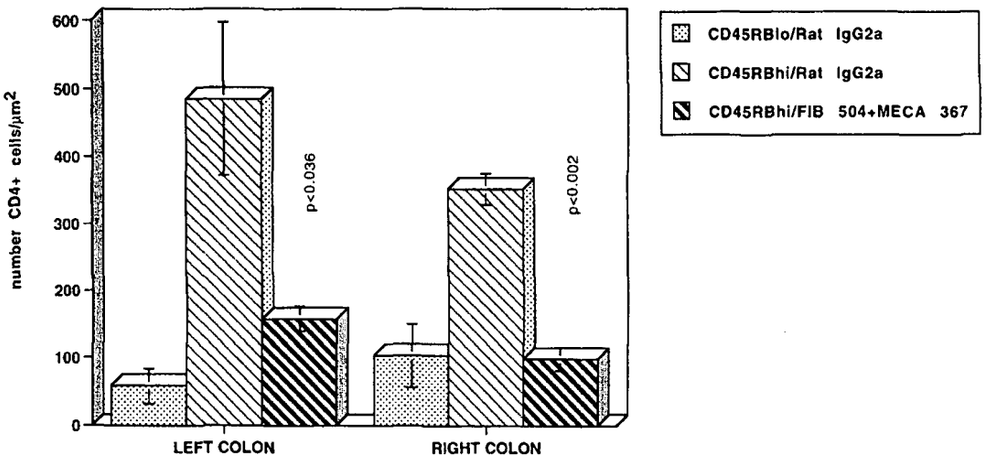

FIGURE 3. β_7/MAdCAM-1 blockade in colitic *scid* mice reduces the number of $CD4^+$ T cells in the lamina propria and submucosa. Computer-assisted image analysis was used to assess the relative numbers of $CD4^+$ cells in frozen sections of left and right colons of mice treated with a combination of FIB 504 (β_7-specific) and MECA 367 (MAdCAM-specific) or isotype-matched control Ab (YKIX 309.2). Sections were stained for CD4 using a biotinylated rat anti-mouse CD4 (clone AMS0409, Biosource, Camarillo, CA) and developed using a Fast Red detection system (BioGenex). Results are expressed as the mean number of $CD4^+$ cells per square micron of tissue area ± SEM ($n = 4$). Statistical significance was determined using one-tailed Student's *t* test.

cells and Ab, recruitment to the colon was inhibited by 97 and 98%, respectively ($p < 0.05$; Fig. 2*C*).

Blockade of β_7 integrin and MAdCAM reduces the severity of colitis in scid *mice*

Tissue sections from colitic animals given mAbs specific for β_7 and/or MAdCAM-1 were examined microscopically to assess whether inhibition of leukocyte recruitment was associated with histologic improvement of inflammatory activity. First, quantitative image analysis of frozen colonic sections was used to measure the number of infiltrating $CD4^+$ T cells in the mucosa and submucosa of animals in all experimental groups. In colitic *scid* mice given an irrelevant, isotype-matched mAb, the number of $CD4^+$ T cells was increased 8.5- and 3.5-fold in the left and right colons, respectively, compared with that in noncolitic *scid* mice reconstituted with $CD45RB^{low}$, $CD4^+$ T cells (Fig. 3). Treatment of colitic *scid* mice with a combination of β_7- and MAdCAM-specific Abs reduced the number of T cells in the left and right colons by 67% ($p < 0.036$) and 72% ($p < 0.002$), respectively (Fig. 3). Treatment with either Ab alone resulted in a similar reduction in the number of $CD4^+$ T cells in the colon, which achieved statistical significance with the MAdCAM-1-specific Ab, but not the β_7-specific Ab (not shown).

To determine whether a blockade of $CD4^+$ $\beta7^+$ lymphocyte recruitment with β_7- and/or MAdCAM-specific Abs was associated with improvement of colitis, a histologic scoring system was developed (Table I) and used to assess lesion severity in the epithelium, lamina propria/submucosa, and tunica muscularis of each section.

Mild lesions (score of 1) were characterized by focal to diffuse infiltration of the lamina propria/submucosa, with mononuclear cells consisting primarily of lymphocytes, occasional monocytes, macrophages, and rare multinucleate giant cells. The colonic epithelium overlying these areas was histologically normal, consisting primarily of goblet cells, enterocytes, and rare intraepithelial lymphocytes. In animals with moderate lesions (score of 2), the colonic mucosa was diffusely thickened. The mononuclear infiltrate caused focally extensive to diffuse expansion of the lamina propria and submucosa and compression of colonic crypts. The thickened mucosa was lined primarily by immature enterocytes characterized by cytoplasmic basophilia, numerous mitotic figures, and relatively few goblet cells. A greater number of intraepithelial lymphocytes was also present. With increasing lesion severity, the colonic mucosa was massively thickened, and the expanding mononuclear infiltrate bridged the epithelial basement membrane,

Table I. *Histologic scoring system*

Score	Severity	Criteria
Epithelium		
0	Normal	0–2 Leukocytes[a]/HPF[b]: normal mature goblet cells
1	Mild	3–10 Leukocytes/HPF; increased mitotic figures and immature crypt enterocytes
2	Moderate	10^+ Leukocytes/HPF; rare crypt abscesses
3	Severe	10^+ Leukocytes/HPF; fusion of crypts, multiple crypt abscesses and/or mucosal ulceration
Lamina propria/Submucosa		
0	Normal	Widely scattered leukocytes
1	Mild	Focal aggregates of leukocytes without expansion of lamina propria
2	Moderate	Diffuse leukocyte infiltration with expansion of the lamina propria, and/or focal bridging of the basement membrane
3	Severe	Diffuse leukocyte infiltration with extensive bridging of the basement membrane
Tunica muscularis		
0	Normal	Widely scattered leukocytes
1	Mild	Widely scattered leukocyte aggregates between muscle layers
2	Moderate	Leukocyte infiltration with focal effacement of the muscularis
3	Severe	Extensive leukocyte infiltration with transmural effacement of the muscularis

[a] The leukocytes observed were principally lymphocytes, with lesser numbers of macrophages, plasma cells, and rare multinucleate giant cells. However, within and adjacent to areas of mucosal ulceration and fistulas, neutrophils were commonly observed.
[b] HPF, high power (40×) field.

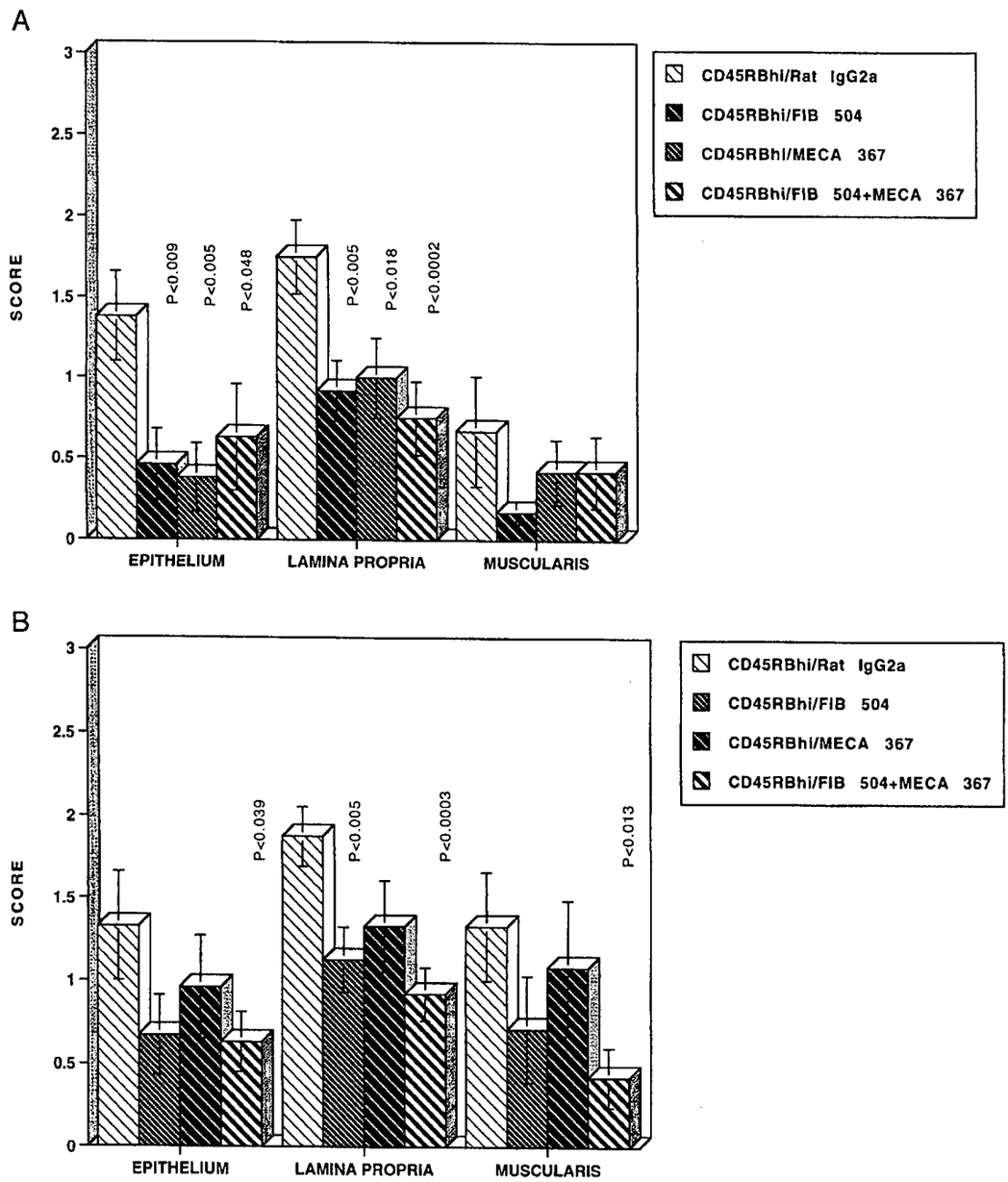

FIGURE 4. Histologic assessment of the severity of lesions from the left (*A*) and right (*B*) colons of *scid* mice reconstituted with CD45RB^{high} T cells and treated with FIB 504 (β_7-specific), MECA 367 (MAdCAM-1-specific), both in combination, or an irrelevant, isotype-matched control Ab (rat IgG2a). Results are expressed as the mean score of three sections per mouse, with four mice per treatment group, ± SEM (n = 4). Statistical significance was determined by one-tailed Student's t test.

causing effacement of colonic crypts, which resulted in crypt abscesses and crypt dropout. In more severe lesions, lymphocytes extended transmurally to the peritoneal surface, resulting in focally extensive effacement and necrosis of the tunica muscularis. The most severe lesions observed (score of 3) were fistulas characterized by colonic epithelial ulceration, transmural pyogranulomatous inflammation and necrosis, and localized peritonitis. While many of the colonic lesions were characteristic of ulcerative colitis, the presence of transmural fistulas and pyogranulomatous inflammation in some of the lesions was more characteristic of Crohn's disease.

The colonic epithelium of animals treated with Abs specific for β_7 and/or MAdCAM tended to be well differentiated and was characterized by fewer intraepithelial lymphocytes, crypt abscesses, and/or ulcers relative to epithelium from colitic control animals, resulting in statistically lower epithelial scores in all treatment groups in the left colon relative to epithelium from control colitic animals (Fig. 4*A*). In the right colon, a statistically significant effect of Ab treatment was achieved only for the combination of β_7- and MAdCAM-specific Abs ($p < 0.039$; Fig. 4*B*). In addition, mice treated with β_7 and/or MAdCAM-specific Abs had less mononuclear infiltration in the lamina propria and submucosa,

resulting in statistically lower histologic scores in the left (Fig. 4*A*; all treatment groups) and right colon (Fig. 4*B*; β_7-specific, $p < 0.005$; combination, $p < 0.003$) relative to those in colitic control mice (CD45RB^{high}/Rat IgG2a). Overall, treated animals had lower total scores than control animals, suggesting that treatment with β_7- or MAdCAM-specific Abs alone or in combination resulted in significant, albeit incomplete, reduction in colitic lesions.

Despite this improvement, no increase in body weight or resolution of rectal prolapse was observed in animals treated with mAbs specific for β_7 and/or MAdCAM (not shown). Treatment of colitic *scid* mice (2–6 mo postreconstitution) for 8 wk with sulfasalazine (100 mg/kg/day, orally) or with methylprednisolone acetate (Depo Medrol; 25 mg/kg/2 wk, s.c.) also failed to increase body weight (not shown). However, this treatment failed to result in significant histologic improvement in the severity of lesions in the colons of colitic *scid* mice (not shown). Collectively, these results suggest that treatment with β_7- or MAdCAM-specific Abs is effective at limiting colonic inflammation without inhibiting normal trafficking to nonmucosal tissues.

Discussion

Previous studies of lymphocyte trafficking to murine mucosal tissue demonstrated that Abs specific for MAdCAM-1 (3, 10) or for α_4 or β_7 integrins could block homing of lymphocytes to Peyer's patch and normal small intestinal lamina propria, but not peripheral lymph nodes (3, 15–17). In contrast, Abs specific for $\alpha_4\beta_1$ or its vascular ligand, vascular cell adhesion molecule-1, did not affect homing of lymphocytes to mucosal sites (3). The objective of this study was to examine the role of $\alpha_4\beta_7$ and, specifically, MAdCAM-1 in lymphocyte homing to inflamed colon and to determine whether blockade of $\alpha_4\beta_7$- and/or MAdCAM-1-mediated adhesion could influence the extent of chronic colonic inflammatory disease. The colitis induced in *scid* mice reconstituted with CD45RB^{high} CD4$^+$ T cells provided an excellent model to address these questions, as the colitic lesions are histologically similar to those observed in human inflammatory bowel disease, and unlike a number of other murine models of inflammatory bowel disease, the disease in the *scid* model is clearly T cell dependent and transferrable by T cells.

While β_7 is involved in many aspects of lymphocyte function among memory and effector lymphocytes, it is expressed preferentially by, and indeed may in part define by virtue of its role in mucosal homing, those lymphocytes involved in mucosal immune responses (18–21). In addition, the β_7 integrin chain associates with a second α-chain, αe, expressed at high levels by mucosal intraepithelial lymphocytes (22, 23). Thus, β_7-specific mAbs may have diverse effects on mucosal immune activities in addition to the effects on lymphocyte recruitment from the blood. On the other hand, MAdCAM-1 is, to date, thought to participate primarily, if not exclusively, at the level of lymphocyte extravasation. Collectively, therefore, the observed anti-inflammatory effects of β_7- or MAdCAM-1-specific mAbs suggest that inhibition of recruitment may be at least one critical element in the therapeutic effects observed in the present studies.

Based on quantitative inhibition of lymphocyte trafficking with β_7- or MAdCAM-1-specific mAbs, alone or in combination, our results suggest that MAdCAM-1 is an important ligand in directing the recruitment of lymphocytes bearing the $\alpha_4\beta_7$ integrin to the large intestine in mice with severe colitis. The effect of Ab treatment was specific for recruitment to mucosal tissue, since recruitment of ^{111}In-labeled lymphocytes to peripheral lymphoid tissue, such as inguinal lymph node and spleen, was not inhibited. In addition, treatment of severely colitic mice with Abs specific for either β_7 or MAdCAM-1 ameliorated histologic changes associated with colitis, based upon quantitative analysis of the number of CD4$^+$ T lymphocytes in the colonic mucosa and histologic assessment of mucosal inflammatory changes.

Although daily administration of Ab for 14 days was sufficient to maintain plasma concentrations of biologically active Ab well above the minimum amount necessary to inhibit static binding of a recombinant murine MAdCAM-C$_k$ chimeric protein to TK1 cells in vitro and inhibit recruitment of ^{111}In-labeled mononuclear cells from blood to colon, complete resolution of microscopic lesions in the colons of treated mice did not occur, nor did this treatment affect the loss of body weight associated with colitis in this model. Treatment of colitic *scid* mice with sulfasalazine or methylprednisolone acetate (Depo Medrol) also did not result in a significant increase in body weight. There are several possible explanations for these results. Although significant inhibition of recruitment of lymphocytes to colitic colon is observed following a 14-day Ab blockade, it is possible that a minor subpopulation of leukocytes, capable of sustaining ongoing inflammatory activity, requires higher concentrations of Ab to completely inhibit extravasation into colonic mucosa under shear conditions of blood flow in vivo. Alternatively, the efficacy of the Ab blockade may be limited to inhibition of extravasation of circulating leukocytes and may have only limited activity with regard to local proliferation of lymphocytes in the colonic mucosa and submucosa. As these lymphocytes may have a life span longer than the treatment course, a longer duration of Ab administration may be required for more complete resolution of colitic lesions. Finally, local production of cytokines by $\alpha_4\beta_7^-$ leukocytes in response to an environmental insult may play an important role in mediating tissue damage in this model.

While the failure of the Ab therapy to significantly affect the loss of body weight in this model is most likely due to incomplete resolution of the colitic lesions, the extent to which weight loss in this model is related to colitic activity is unclear. Previous studies with this model have demonstrated that Abs specific for TNF-α or IFN-γ, administered at the time of reconstitution, inhibit the severe loss of weight that accompanies the colitis, although such treatment does not preserve normal weight (14). While this result suggests that cytokines such as TNF-α or IFN-γ may play an important role in the development of cachexia in this model, the relative tissue distribution of cells actively producing these cytokines has not been described. Therefore, weight loss in this model may be related to systemic manifestations of lymphocyte reconstitution, only part of which involves inflammatory activity in the colon (6, 7, 13, 14, 24, 25).

This study represents the first demonstration that treatment with a MAdCAM-1-specific Ab is as effective as a β_7-specific Ab in blocking recruitment of lymphocytes to the colon in colitic animals. Collectively, the results of this study suggest that $\alpha_4\beta_7$ and MAdCAM-1 are intimately involved in the pathogenesis of colonic inflammation and, thereby, may represent potential therapeutic targets for novel approaches to the clinical management of patients with T cell-mediated inflammatory conditions of the gastrointestinal tract.

Acknowledgments

The authors gratefully acknowledge the assistance provided by Maris Handley with sorting the CD4 T cells and by Ken Ganley with maintaining the animals used in these studies. We thank Herman Waldmann for critically reviewing this manuscript.

References

1. Andrew, D. P., C. Berlin, S. Honda, T. Yoshimo, A. Hamann, B. Holzmann, P. J. Kilshaw, and E. C. Butcher. 1994. Distinct but overlapping epitopes are involved

in $\alpha_4\beta_7$-mediated adhesion to vascular cell adhesion molecule-1, mucosal addressin-1, fibronectin, and lymphocyte aggregation. *J. Immunol. 153:3847.*
2. Briskin, M. J., L. M. McEvoy, and E. C. Butcher. 1993. MAdCAM-1 has homology to immunoglobulin and mucin-like adhesion receptors and to IgA1. *Nature 363:461.*
3. Hamann, A., D. P. Andrew, D. Jablonski-Westrich, B. Holzmann, and E. C. Butcher. 1994. Role of α_4-integrins in lymphocyte homing to mucosal tissues in vivo. *J. Immunol. 152:3282.*
4. Podolsky, D. K., R. L. Lobb, N. King, C. D. Benjamin, B. Pepinsky, P. Sehgal, and M. deBeaumont. 1993. Attenuation of colitis in the cotton-top tamarin by anti-α_4 integrin monoclonal antibody. *J. Clin. Invest. 92:372.*
5. Hesterberg, P. E., D. Windsor-Hines, M. J. Briskin, D. Soler-Ferran, C. Merrill, C. R. Mackay, W. Newman, and D. J. Ringler. 1996. Rapid resolution of chronic colitis in the cotton top tamarin with an antibody to a gut homing integrin $\alpha_4\beta_7$. *Gastroenterology. 111:1373.*
6. Morrissey, P. J., K. Charrier, S. Braddy, D. Liggitt, and J. D. Watson. 1993. CD4$^+$ T cells that express high levels of CD45RB induce wasting disease when transferred into congenic severe combined immunodeficient mice: disease development is prevented by cotransfer of purified CD4$^+$ T cells. *J. Exp. Med. 178: 237.*
7. Powrie, F., M. W. Leach, S. Mauze, L. B. Caddle, and R. L. Coffman. 1993. Phenotypically distinct subsets of CD4$^+$ T cells induce or protect from chronic intestinal inflammation in C.B-17 *scid* mice. *Int. Immunol. 5:1461.*
8. Cobbold, S., and S. M. Metcalfe. 1994. Monoclonal antibodies that define canine homologues of human CD antigens. *Tissue Antigens 43:137.*
9. Watson, C. J. E., S. P. Cobbold, H. S. Davies, P. R. U. B. Rebello, H. Waldmann, R. Y. Calne, and S. M. Metcalfe. 1994. CD4 and CD8 monoclonal antibody therapy: strategies to prolong renal allograft survival in the dog. *Br. J. Surg. 80:1389.*
10. Streeter, P. R., E. Lakey-Berg, B. T. N. Rouse, R. F. Bargatze, and E. C. Butcher. 1988. A tissue-specific endothelial cell molecule involved in lymphocyte homing. *Nature 331:41.*
11. Rand, M. L., J. S. Warren, M. K. Mansour, W. Newman, and D. J. Ringler. 1996. Inhibition of T cell recruitment and cutaneous delayed-type hypersensitivty-induced inflammation with antibodies to monocyte chemoattractant protein-1. *Am. J. Pathol. 148:855.*
12. Berg, E. L., L. M. McEvoy, C. Berlin, R. F. Bargatze, and E. C. Butcher. 1993. L-selectin-mediated lymphocyte rolling on MAdCAM-1. *Nature 366:695.*
13. Powrie, F., M. W. Leach, S. Mauze, S. Menon, L. B. Caddle, and R. L. Coffman. 1994. Inhibition of Th1 responses prevents inflammatory bowel disease in *scid* mice reconstituted with CD45RB^{hi} CD4$^+$ T cells. *Immunity 1:553.*
14. Powrie, F., O. R. Correa, S. Mauze, and R. L. Coffman. 1994. Regulatory interactions between CD45RB^{high} and CD45RB^{low} CD4$^+$ T cells are important for the balance between protective and pathogenic cell-mediated immunity. *J. Exp. Med. 179:589.*
15. Issekutz, T. B. 1991. Inhibition of in vivo lymphocyte migration to inflammation and homing to lymphoid tissues by the TA-2 monoclonal antibody: a likely role for VLA-4 in vivo. *J. Immunol. 147:4178.*
16. Bargatze, R. F., M. A. Jutila, and E. C. Butcher. 1995. Distinct roles of L-selectin and integrins $\alpha_4\beta_7$ and LFA-1 in lymphocyte homing to Peyer's patch-HEV in situ: the multistep model confirmed and refined. *Immunity 3:99.*
17. Berlin, C., E. L. Berg, M. J. Briskin, D. P. Andrew, P. J. Kilshaw, B. Holzmann, I. L. Weissman, A. Hamann, and E. C. Butcher. 1993. $\alpha_4\beta_7$ integrin mediates lymphocyte binding to the mucosal vascular addressin MAdCAM-1. *Cell 74:185.*
18. Schweighoffer, T., Y. Tanaka, M. Tidswell, D. J. Erle, K. J. Horgan, G. E. G. Luce, A. I. Lazarovits, D. Buck, and S. Shaw. 1993. Selective expression of integrin $\alpha_4\beta_7$ on a subset of human CD4$^+$ memory T cells with hallmarks of gut-trophism. *J. Immunol. 151:717.*
19. Erle, D. J., M. J. Briskin, E. C. Butcher, A. Garcia-Pardo, A. I. Lazarovits, and M. Tidswell. 1994. Expression and function of the MAdCAM-1 receptor, integrin $\alpha_4\beta_7$, on human leukocytes. *J. Immunol. 153:517.*
20. Rott, L. S., M. J. Briskin, D. P. Andrew, E. L. Berg, and E. C. Butcher. 1996. A fundamental subdivision of circulating lymphocytes defined by adhesion to mucosal addressin cell adhesion molecule-1. *J. Immunol. 156:3727.*
21. Andrew, D. P., L. S. Rott, P. J. Kilshaw, and E. C. Butcher. 1996. Distribution of $\alpha_4\beta_7$ and $\alpha e\beta_7$ integrins on thymocytes, intestinal epithelial lymphocytes and peripheral lymphocytes. *Eur. J. Immunol. 26:897.*
22. Kilshaw, P. J., and S. J. Murant. 1991. Expression and regulation of β_7 (βp) integrins on mouse lymphocytes: relevance to the mucosal immune system. *Eur. J. Immunol. 21:2591.*
23. Cepek, K. L., C. M. Parker, J. L. Madara, and M. B. Brenner. 1993. Integrin $\alpha E\beta_7$ mediates adhesion of T lymphocytes to epithelial cells. *J. Immunol. 150:3459.*
24. Powrie, F. 1995. T cells in inflammatory bowel disease: protective and pathogenic roles. *Immunity 3:171.*
25. Leach, M. W., A. G. D. Bean, S. Mauze, R. L. Coffman, and F. Powrie. 1996. Inflammatory bowel disease in C.B-17 *scid* mice reconstituted with the CD45RB^{high} subset of CD4$^+$ T cells. *Am. J. Pathol. 148:1503.*

β7 INTEGRINS CONTRIBUTE TO SKIN GRAFT REJECTION

XUEYING SUN,[1,2] HAIQUAN QIAO,[1,3] JINYANG SHI,[1,4] JAGAT R. KANWAR,[1] WERNER MUELLER,[5] NORBERT WAGNER,[5] AND GEOFFREY W. KRISSANSEN[1,6]

Background. **Because integrins α4β7 and αEβ7 contribute to epidermotropism of T-cells during skin inflammation, we sought to study their role in skin allograft rejection.**

Methods. **Wild-type (WT) ($\beta7^{+/+}$) and β7 gene knockout ($\beta7^{-/-}$) C57BL/6 (H-2^b) mice and SJL/J (H-2^s) mice served as donors and recipients of allogeneic skin grafts. An anti-integrin β7 subunit mAb (FIB504.64) was used to treat WT $\beta7^{+/+}$ C57BL/6 recipients of skin grafts from SJL/J mice.**

Results. **WT C57BL/6 recipients acutely rejected skin from SJL/J mice in 13 days. In contrast, the survival of SJL/J skin on either $\beta7^{-/-}$ gene knockout or WT C57BL/6 recipients treated with anti-β7 subunit mAb, was prolonged by 6 to 7 additional days ($P<0.01$). The survival of skin allografts from either $\beta7^{-/-}$ or $\beta7^{+/+}$ C57BL/6 mice received by SJL/J recipients was not prolonged ($P>0.05$).**

Conclusions. **β7 integrins contribute to skin graft rejection, in accord with their role in mediating the epidermotropism of T-cells during skin inflammation.**

The β7 integrin α4β7 contributes to lymphocyte infiltration into chronically inflamed tissues by mediating lymphocyte adherence to high endothelial venules at chronically inflamed sites by means of its preferred ligand mucosal addressin cell adhesion molecule-1 (MAdCAM-1), whereas αEβ7 mediates the adhesion of intraepithelial lymphocytes to intestinal epithelia by an interaction with E-cadherin (*1*). The progression of type 1 diabetes and experimental autoimmune encephalomyelitis can be inhibited by antibody blockade of β7 integrins, or MAdCAM-1 (*2–4*), suggesting that β7 integrins play critical roles in mediating autoimmune inflammatory diseases.

Ultimately, allografts are rejected in β2 integrin-deficient cattle with leukocyte adhesion deficiency syndrome (*5*), suggesting that α4 and β7 integrins might be partly responsible for graft rejection. Blockade of α4 integrins with CS-1 peptides synergized with rapamycin to prevent the chronic rejection of cardiac allografts (*6*). Similarly, mAb blockade of vascular cell adhesion molecule-1 (VCAM-1), a vascular ligand for α4 integrins, promoted the long-term survival of cardiac allografts (*7*). αEβ7 is specifically upregulated by activated intratubular T-cells in acute renal allograft rejection, suggesting it might contribute to specific tissue damage (*8*). Given the latter findings, and the success of anti-β7 integrin blockade in attenuating inflammation in a number of autoimmune diseases, we sought to determine whether blockade of β7 integrins would inhibit the rejection of allogeneic skin grafts.

Eight- to ten-week-old mice of three different strains, namely integrin $\beta7^{+/+}$ wild-type (WT) C57BL/6 (H-2^b), $\beta7^{-/-}$ gene knock-out C57BL/6, and SJL/J (H-2^s), were used. Donors and recipients were always of the same sex, and each group had similar proportions of males and females. Full-thickness 1-cm^2 skin grafts that had been harvested from the tails of donors were implanted into graft beds on the thoracic wall of the recipients, in accordance with Animal Ethics Committee Approval (University of Auckland). The experimental endpoint was recorded when less than 25% of the graft remained. Results were either expressed as the median graft survival time (MST) or the percentage graft survival (percentage of mice having 25% or more donor tissue). Remaining graft tissue was serial sectioned (5 μm thick) and stained with hematoxylin-eosin. For antibody blockade, WT $\beta7^{+/+}$ C57BL/6 recipient mice were injected intraperitoneally with 200 μg of anti-β7 mAb FIB504.64 on days 0, 2, and 4. Results were statistically compared using a nonpaired Student *t* test and a log-rank test. A mixed lymphocyte reaction (MLR) was performed by the culturing of 5×10^5 responder splenocytes with an equal number of stimulator splenocytes previously treated with 50 μg/mL mitomycin C. Proliferation was assessed after 3 days by measuring incorporated (^{3}H) thymidine. The stimulation index equalled the counts per minute of MLR divided by the counts per minute of responder cells in the absence of stimulators.

Full major histocompatibility complex-mismatched heterotopic skin transplantation was performed using SJL/J (H-2^s) mice as skin donors and WT ($\beta7^{+/+}$) or $\beta7^{-/-}$ gene knockout C57BL/6 (H-2^b) mice as recipients. Table 1 shows that WT C57BL/6 recipients acutely rejected SJL/J donor skin grafts between 10 and 14 days posttransplantation. The grafts had an MST of 13 days (range 10–14) and were infiltrated with mononuclear cells (data not shown). In contrast, the $\beta7^{-/-}$ gene knockout recipients showed delayed rejection, such that SJL/J skin grafts were rejected within 16 to 23 days, with an MST of 20 days ($P<0.01$) (Table 1). To confirm these results, WT C57BL/6 recipients were injected thrice with the anti-integrin β7 subunit mAb FIB 504.64, on days 0, 2, and 4. MST was delayed to 19 days (range 16–20) ($P<0.01$), compared with 13 days (range 10–14) in control untreated mice. There was no significant difference ($P>0.05$) in the MSTs for the antibody-treated group versus the $\beta7^{-/-}$ gene knockout group. To investigate a potential graft versus host reaction, skin transplantation was performed using SJL/J mice as recipients and WT ($\beta7^{+/+}$) or $\beta7^{-/-}$ gene knockout C57BL/6 (H-2^b) mice as donors. SJL/J recipients similarly ($P>0.05$) rejected both WT and $\beta7^{-/-}$ gene knockout

This work was supported by the World Health Organization.

[1] Department of Molecular Medicine and Pathology, Faculty of Medicine and Health Science, University of Auckland, New Zealand.
[2] Department of Surgery, Qilu Hospital of Shandong University, Jinan, China.
[3] Department of Surgery, The First Clinical College of Harbin Medical University, Harbin, China.
[4] Virus Lab, The Second Affiliated Hospital of China Medical University, Shenyang, China.
[5] Institute for Genetics, University of Cologne, Cologne, Germany.
[6] Address correspondence to: Dr. Geoffrey Krissansen, Department of Molecular Medicine and Pathology, Faculty of Medicine and Health Science, University of Auckland, 85 Park Road, Grafton, Auckland, New Zealand. E-mail: gw.krissansen@auckland.ac.nz.

Received 25 February 2002. Accepted 4 June 2002.

DOI: 10.1097/01.TP.0000031946.28687.E1

TABLE 1. Survival of skin allografts

Group[a]	Donor	Recipient	Treatment	Graft survival (days)	Mean survival time (days ± SD)	P
1	SJL/J	WT C57BL/6	none	10,10,11,11,13,13,13,14,14,14	13 (±1.6)	
2	SJL/J	$\beta7^{-/-}$ C57BL/6	none	16,19,20,20,20,20,22,23,23,23	20 (±2.2)	<0.001[b]
3	SJL/J	WT C57BL/6	anti-β7 mAb	16,17,19,20,20	19 (±1.8)	<0.001[b]; 0.068[c]
4	WT C57BL/6	SJL/J	none	16,17,17,18,20	17 (±1.5)	
5	$\beta7^{-/-}$ C57BL/6	SJL/J	none	18,19,19,20,21	20 (±1.1)	0.069[d]

[a] The proportion of female mice in each group=group 1 (6/10), group 2 (5/10), group 3 (3/5), group 4 (3/5).
[b] Compared with group 1.
[c] Compared with group 2.
[d] Compared with group 4.
Abbreviation: WT, wild-type.

C57BL/6 skin grafts with MSTs of 17 and 20 days, respectively.

MLRs were performed using splenocytes from WT ($\beta7^{+/+}$) and $\beta7^{-/-}$ gene knockout C57BL/6 mice as both stimulators and responders, together with splenocytes from SJL/J mice. Splenocytes from $\beta7^{-/-}$ gene knockout mice generated slightly weaker responses than those of WT mice ($P<0.05$) (Fig. 1). Anti-β7 mAb blockade of responder WT splenocytes inhibited the MLR response to the level exhibited by responders from $\beta7^{-/-}$ gene knockout mice. Surprisingly, $\beta7^{-/-}$ stimulator splenocytes were slightly less efficient at inducing the proliferation of WT responders, suggesting that β7 integrins may be required for cell conjugate formation to enable T-cell costimulation.

This study shows that while β7 integrins are not essential for the rejection of skin allografts in mice, they nevertheless contribute to rejection. The β7 integrins appear to play only a minor role in activating antigraft T-cells and probably have a major role in vivo in mediating leukocyte infiltration into grafts. This is in accordance with previous studies, showing that $\beta7^{-/-}$ lymphocytes transmigrate poorly into gut-associated lymphoid tissue or the central nervous system in experimental autoimmune encephalomyelitis (*4*, *9*). Thus, although cutaneous lymphocyte antigen is important for T-cells to extravasate from blood into skin during normal immunosurveillance (*10*), β7 integrins appear to play key roles in the migration of lymphocytes to inflamed skin. In accord, α4β7 and αEβ7 integrins are expressed on epidermotropic T-cells in cutaneous T-cell lymphoma and spongiotic dermatitis, and the β7 integrin ligand VCAM-1 is up-regulated on microvascular endothelial cells in skin lesions (*11*). The expression of αEβ7 is markedly upregulated on skin T-cells in atopic dermatitis (*12*), and the αEβ7 ligand E-cadherin is found on epithelial cells in the skin (*13*).

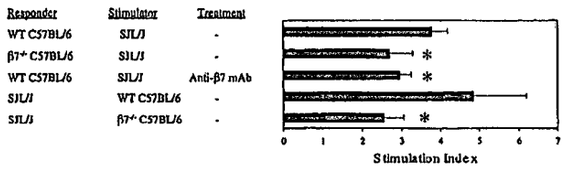

FIGURE 1. β7 integrins contribute weakly to mixed lymphocyte responses. Responder splenocytes (5 ×10⁵) were incubated for 3 days in the presence of 5 ×10⁵ mitomycin C-treated stimulator splenocytes. For antibody treatment, the anti-integrin β7 subunit mAb was added at 1 μg/well. Data are representative of four separate experiments. * $P<0.05$.

Acknowledgments. The authors thank Ms. Joanna Stewart of the Department of Community Health for help with statistics.

REFERENCES

1. Krissansen GW. Integrin superfamily. In: Robertson S, ed. The Encyclopedia of Life Sciences. Houndmills, Basingstoke, Hampshire: MacMillan Press, 2000.
2. Yang X, Sytwn H-K, McDevitt HO, et al. Involvement of β7 integrin and mucosal addressin cell adhesion molecule-1 (MAdCAM-1) in the development of diabetes in nonobese diabetic mice. Diabetes 1997; 46: 1542–1547.
3. Kanwar JR, Wang D, Krissansen GW. Prevention of a chronic progressive form of experimental autoimmune encephalomyelitis by an antibody against MAdCAM-1, given early in the course of disease progression. Immunol Cell Biol 2000; 78: 641–646.
4. Kanwar JR, Harrison JEB, Wang D, et al. Contributory role for β7 integrins in non-remitting experimental autoimmune encephalomyelitis. J Neuroimmunol 2000; 103: 146–152.
5. Muller KE, Rutten VP, Becker CK, et al. Allograft rejection in cattle with bovine leukocyte adhesion deficiency. Vet Immunol Immunopath 1995; 48: 55–63.
6. Coito AJ, Korom S, Hancock WW, et al. Blockade of α4β1-integrin-fibronectin adhesive interactions prevents chronic allograft rejection in sensitized recipients. Transplant Proc 1998; 30: 939–940.
7. Orosz CG, Ohyne RG, Pelletier RP, et al. Treatment with anti-vascular cell adhesion molecule antibody induces long-term murine cardiac allograft acceptance. Transplantation 1993; 56: 453–460.
8. Robertson H, Wong WK, Talbot D, et al. Tubulitis after renal transplantation: demonstration of an association between CD103⁺ T cells, transforming growth factor beta(1) expression and rejection grade. Transplant 2001; 71: 306–313.
9. Wagner N, Lohler J, Kunkel EJ, et al. Critical role for β7 integrins in formation of the gut-associated lymphoid tissue. Nature 1996; 382: 366–370.
10. Berg EL, Yoshino T, Rott LS, et al. The cutaneous lymphocyte antigen is a skin lymphocyte homing receptor for the vascular lectin endothelial cell-leukocyte adhesion molecule 1. J Exp Med 1991; 174: 1461–1466.
11. Schechner JS, Edelson RL, McNiff JM, et al. Integrins alpha(4)beta(7) and alpha(E)beta(7) are expressed on epidermotropic T cells in cutaneous T cell lymphoma and spongiotic dermatitis. Lab Invest 1999; 79: 601–607.
12. Devries IJM, Langeveldwildschut EG, Vanreijsen FC, et al. Nonspecific T-cell homing during inflammation in atopic dermatitis-expression of cutaneous lymphocyte-associated antigen and integrin alpha-E-beta-7 on skin-infiltrating T cells. J Allergy Clin Immunol 1997; 100: 694–701.
13. Brown DW, Furness J, Speight PM, et al. Mechanisms of binding of cutaneous lymphocyte-associated antigen-positive and alpha E beta 7-positive lymphocytes to oral and skin keratinocytes. Immunol 1999; 98: 9–15.

Structure-Function Analysis of the Integrin β_7 Subunit

Identification of Domains Involved in Adhesion to MAdCAM-1[1,2]

Mark Tidswell,[3]* Russell Pachynski,* Steve W. Wu,* Shi-Qiang Qiu,* Elizabeth Dunham,* Nancy Cochran,† Michael J. Briskin,† Peter J. Kilshaw,‡ Andrew I. Lazarovits,§ David P. Andrew,¶ Eugene C. Butcher,‖ Ted A. Yednock,# and David J. Erle*

β_7 integrins serve special roles in mucosal immunity. $\alpha_4\beta_7$-mediated adhesion to mucosal addressin cell adhesion molecule-1 (MAdCAM-1) directs lymphocyte homing to the gut, and $\alpha_E\beta_7$ mediates binding of lymphocytes to E-cadherin on epithelial cells. Since $\alpha_4\beta_7$ mediates adhesion to MAdCAM-1 but $\alpha_4\beta_1$ does not, we used β_7/β_1 chimeras to directly assess the importance of specific regions of β_7 in MAdCAM-1 binding. We found a region of β_7 (residues 46–386) that accounts for specificity of $\alpha_4\beta_7$ binding to MAdCAM-1. We also used human/mouse and human/rat chimeric β_7 subunits to map epitopes recognized by fifteen anti-β_7 mAbs. Six of seven Abs that block adhesion to MAdCAM-1 and E-cadherin (Fib 21, 22, 27, 30, 504; Act-1) mapped to amino acid residues 176–250. Residues 176–250 lie within the region of β_7 that specifies MAdCAM-1 binding and also within a region that has a predicted structure homologous to the metal ion-dependent adhesion site (MIDAS) domains of the integrin subunits α_L and α_M. Three new Abs that recognize β_7 in the presence of Mn^{2+}, but not Ca^{2+}, and promote adhesion to MAdCAM-1, mapped to amino acids 46–149. One blocking and five other Abs mapped to other regions (amino acids 387–725). We conclude that a MIDAS-like domain serves a critical role in β_7 integrin-mediated adhesion. *The Journal of Immunology,* 1997, 159: 1497–1505.

Integrins are heterodimeric adhesion receptors that mediate cell-cell and cell-extracellular matrix interactions. The β_7 integrin subfamily has two known members: $\alpha_4\beta_7$ and $\alpha_E\beta_7$. These β_7 integrins are expressed primarily by leukocytes and have helped define roles of specialized subsets of lymphocytes (see below). β_7 integrins are unique among known integrins in their ability to recognize certain ligands expressed on the surface of endothelial and epithelial cells in mucosal organs. Analyses of the β_1, β_2, and β_3 integrins have begun to provide some insights into the structural basis of integrin-ligand interactions. However, relatively little information about the structural basis of $\alpha_4\beta_7$- and $\alpha_E\beta_7$-mediated interactions with their unique ligands has been available.

$\alpha_4\beta_7$ is a lymphocyte homing receptor and plays a crucial role in the migration of these cells to the intestine and associated lymphoid tissue, such as Peyer's patches. $\alpha_4\beta_7$ mediates adhesion to a ligand on Peyer's patch high endothelial venules (HEV[4]) (1). The ligand on Peyer's patch HEV is MAdCAM-1, a glycoprotein in the Ig superfamily (2–4). MAdCAM-1 is expressed on Peyer's patch HEV, mesenteric lymph node HEV, and lamina propria venules within the gut (5, 6). Abs against α_4 or β_7 subunits inhibit attachment of circulating lymphocytes to Peyer's patch HEV in vivo (7, 8). Mice that are deficient in β_7 expression have a marked reduction in the number of lymphocytes in Peyer's patches and the intestine but normal numbers of lymphocytes in other organs (9). Memory T cells that recirculate preferentially to intestinal tissues express high levels of $\alpha_4\beta_7$, whereas those that recirculate to other organs are mostly $\alpha_4\beta_7^-$ (10). These $\alpha_4\beta_7^-$ memory T cells express a related integrin, $\alpha_4\beta_1$ (11–13). $\alpha_4\beta_1$ is not able to mediate cell adhesion to MAdCAM-1, although both $\alpha_4\beta_1$ and $\alpha_4\beta_7$ can mediate adhesion to VCAM-1 and fibronectin (4, 12, 14, 15).

Integrin $\alpha_E\beta_7$ mediates interaction of T cells with epithelial cells at mucosal surfaces. $\alpha_E\beta_7$ recognizes E-cadherin, an epithelial cell protein that has structural similarity to Ig superfamily adhesion molecules (16–19). Interaction of $\alpha_E\beta_7$ with E-cadherin is likely to be important in retention, migration, and proliferation of intraepithelial T cells.

Some information about the structural basis of β_7 integrin function has come from the analysis of anti-β_7 mAbs. Competitive Ab binding analysis indicates that Abs that block β_7-mediated adhesion can be assigned to at least five distinguishable (although not completely independent) epitopes (20). This finding is not surprising in light of studies of other integrin β subunits, which also reveal the involvement of multiple regions in ligand interactions (see *Discussion*). The locations of antigenically and functionally defined epitopes within the β_7 amino acid sequence have not been previously identified.

*The Lung Biology Center, Department of Medicine, University of California, San Francisco, CA 94143; †LeukoSite, Inc., Cambridge, MA 02142; ‡The Department of Immunology, the Babraham Institute, Babraham, Cambridge, United Kingdom; §Robarts Research Institute, London Health Sciences Centre, University of Western Ontario, London, Ontario, Canada; ¶Amgen, Inc., Boulder, CO 80301; ‖Laboratory of Immunology and Vascular Biology, Department of Pathology and the Digestive Disease Center, Stanford University, Stanford, CA 94305 and the Center for Molecular Biology and Medicine, Foothill Research Center, Veterans Affairs Medical Center, Palo Alto, CA 94304; and #Athena Neurosciences, South San Francisco, CA 94080

Received for publication March 3, 1997. Accepted for publication May 8, 1997.

The costs of publication of this article were defrayed in part by the payment of page charges. This article must therefore be hereby marked *advertisement* in accordance with 18 U.S.C. Section 1734 solely to indicate this fact.

[1] This work was supported in part by National Institutes of Health Grants K08HL03230 (to M.T.), R01HL52004 (to D.J.E.), and AI37832 (to E.C.B.), and an American Lung Association of California Young Investigator Award (to M.T.).

[2] The rat β_7 partial cDNA sequence has been submitted to GenBank (accession number AF003598).

[3] Address correspondence and reprint requests to Dr. Mark Tidswell, Lung Biology Center, Box 0854, University of California at San Francisco, San Francisco, CA 94143. E-mail address: easd@itsa.ucsf.edu

[4] Abbreviations used in this paper: HEV, high endothelial venule; MAdCAM-1, mucosal addressin cell adhesion molecule-1; MIDAS, metal ion-dependent adhesion site; CLIBS, cation- and ligand-influenced binding sites.

0022-1767/97/$02.00

We performed a structure-function analysis of the β_7 subunit by constructing, expressing, and characterizing β_7 chimeras. We constructed β_7/β_1 chimeric subunits by replacing regions of the β_1 subunit with homologous regions of β_7. This resulted in the identification of regions of the β_7 subunit that account for the MAdCAM-1 binding specificity of the $\alpha_4\beta_7$ integrin. We subsequently used human/mouse and human/rat chimeric β_7 subunits to localize the epitopes recognized by adhesion blocking and nonblocking Abs. We also produced and mapped three new anti-β_7 Abs that promote adhesion and recognize epitopes of β_7 that are influenced by cation. Results from these analyses point to the importance of a putative metal ion-dependent adhesion site (MIDAS)-like region of the β_7 subunit in $\alpha_4\beta_7$ interaction with MAdCAM-1.

Materials and Methods

Cells

K562 human erythroleukemia cells (α_4^-, β_7^-, β_1^+; American Type Culture Collection, Rockville, MD; CCL 243) and RPMI 8866 B lymphoma cells ($\alpha_4\beta_7^+$, β_1^-; (12, 21)) were maintained in RPMI 1640 supplemented with 10% FCS, penicillin, streptomycin, and glutamine. 293 human kidney cells (ATCC CRL-1573) and TK-1 mouse lymphoma cells (1) were maintained in DMEM supplemented with 10% FCS, penicillin, streptomycin, and glutamine.

Antibodies to human and mouse β_7

The mouse anti-human β_7 integrin subunit Abs 2G3, 2B8, and 10F8 were raised against $\alpha_4\beta_7$ integrin immunopurified from lysates of RPMI 8866 cells using the anti-α_4 integrin Ab GG5/3. Mice were immunized as previously described (22). Hybridoma supernatants were screened for differential reactivity with RPMI 8866 cells in the presence and absence of Mn^{2+}. The rat monoclonal anti-β_7 Abs Fib 21, Fib 22, Fib 27, Fib 30, Fib 504, and LS722 (15, 20) have been previously described. The rat anti-β_7 Abs M293, M298, M300, and M301 have been described elsewhere (23). Production of the mouse mAb Act-1, which recognizes human $\alpha_4\beta_7$ (11), has been described (24). Hybridoma supernatants or purified IgG preparations were used for flow cytometry and adhesion assays.

Integrin cDNAs

Human cDNAs encoding the β_7, β_1, and α_4 integrin subunits have been previously described (25–27). Three nonoverlapping cDNA fragments spanning the entire mouse β_7 open-reading frame were produced by RT-PCR from TK-1 cell RNA using oligonucleotide primers modeled after the previously reported mouse β_7 sequence (28). A silent mutation that produced an *MluI* site at nucleotide 532 was incorporated into the primers to facilitate chimera production. A fragment of rat β_7 cDNA homologous to nucleotides 585–1265 of human β_7 cDNA was produced by homology PCR. Mixtures of oligonucleotide primers were designed based on conserved portions of the human and mouse β_7 sequences. The forward primer mixture was 5′ AATTAATCTAGATGGAYCTNAGNTAYTCNATGAARG AYGA 3′, and the reverse primer mixture was 5′ AATTAAGAATTCRTCC ATDATNAGYTGNACNACRTT 3′, where D indicates A, G, or T; N indicates A, C, G, or T; R indicates A or G; Y indicates C or T; and underlining indicates *XbaI* and *EcoRI* sites introduced to facilitate cloning of PCR products. These primers were used to amplify cDNA prepared using RNA purified from Sprague Dawley rat splenocytes. The sequences of the cloned mouse and rat cDNA fragments were determined after subcloning into pBluescript. The mouse fragment sequences agreed exactly with the previously reported mouse β_7 cDNA sequence (28). The rat β_7 partial cDNA sequence has been submitted to GenBank (accession number AF003598).

Construction of chimeric and mutant cDNAs

Construction of chimeric cDNAs involved the use of naturally occurring restriction sites and additional restriction sites introduced by incorporation of silent mutations into PCR primers and the use of splice overlap extension PCR. Restriction sites allowed for joining of portions of β_7 cDNAs at three sites (site numbers specify the amino acid residue corresponding to the restriction site): residue 170 (*MluI*), residue 381 (*BclI*), and residue 554 (*SacI*). To join β_7 cDNAs at other sites, and to construct β_7/β_1 chimeras, splice overlap extension PCR was used (29). This technique was also used to generate point mutations at residue 250 of the human and mouse β_7 subunits (see *Results*). PCR was performed using *Taq* polymerase (Promega, Madison, WI), *Pfu* polymerase (Stratagene, La Jolla, CA), or a mixture of *Pfu* and KlenTaq (Ab Peptides, St. Louis, MO) according to the manufacturers' instructions.

Expression of integrin cDNAs in K562 cells

Eight million K562 cells in log growth phase were cotransfected with 25 μg of pCDM8-α_4 and 5 μg of pBK-neo (Stratagene, La Jolla, CA) by electroporation (950 μF, 200 V, 13 Ω; Electro Cell Manipulator 600, BTX, San Diego, CA). Stable clones of K562-α_4 transfectants were produced by limiting dilution cloning following selection in medium containing G418 (Life Technologies, Grand Island, NY) at 500 μg/ml. K562-α_4 cells were then retransfected with human β_7, mouse β_7, or β_7 subunit chimeric cDNA subcloned into the pCEP4 expression vector (Invitrogen, San Diego, CA) using the same electroporation protocol (25 μg plasmid per transfection). Stable transfectants were selected in medium containing hygromycin (Calbiochem, La Jolla, CA) at 500 μg/ml. K562-α_4hβ_7 and K562-α_4mβ_7 cells were cloned by limiting dilution. Where necessary, other transfected cells were enriched for chimeric β_7 expression by positive selection of Fib 504-labeled cells using magnetic beads coupled to sheep anti-rat IgG (Dynal Inc., Lake Success, NY).

Transient expression of chimeric β_7 subunits in 293 cells

For two chimeric β_7 subunit cDNAs, hβ_7(170–231Δm) and hβ_7(231–554Δm), transient expression was used to analyze Ab recognition. 293 cells were cotransfected with 1 μg each of pCEP4-α_4 and pCEP-chimeric β_7 using Lipofectamine (Life Technologies) according to the instructions of the manufacturer. Surface expression was analyzed after 24 to 48 h using flow cytometry.

Construction and purification of human MAdCAM-1 IgG fusion protein

Human MAdCAM-1 cDNA (6) was used as a template for PCR amplification of the entire extracellular region of human MAdCAM-1 using the forward primer 5′ GGAAGCTTCCACCATGGATTTCGGACTGGCCC 3′ and the reverse primer 5′ GGACTAGTGGTTTGGACGAGCCTGTTG 3′, where underlining indicates *HindIII* and *SpeI* sites introduced to facilitate cloning. A 1-kb fragment encompassing the CH1, H, CH2, and CH3 regions of human IgG1 was isolated from a humanized CD18 heavy chain clone (30) by excision with *SpeI* and *EcoRI*. This constant region fragment and the MAdCAM-1 extracellular domain fragment were ligated in a three way ligation to the vector pEE12 (31, 32). The resulting construct was sequenced across the entire MAdCAM-1 portion to confirm proper sequence and fusion of segments. Permanent NSO cell lines (Celltech, Ltd., Berkshire, U.K.) secreting human MAdCAM-1 Ig chimera were selected after transfection by electroporation and growth in a glutamine free media as previously described (33). Cloned lines were adapted to growth in spinner culture, and the MAdCAM-1 Ig chimera was purified by protein A chromatography. Media for maintenance of NSO-secreting lines was DMEM high glucose with Glutamine Systems supplements (JRH Biosciences, Lenexa, KS) and 10% dialyzed FBS (Life Technologies).

MAdCAM-1 adhesion assay

For adhesion assays, 4-mm wells on 21-well glass slides (Structure Probe, West Chester, PA) were coated overnight at 4°C with 10 μl of MAdCAM-IgG (0.025–5 μg/ml in 20 mM HEPES, 150 mM NaCl), and then blocked with 5% BSA for 2 h at 37°C. Transfected K562 cells (40,000 cells in 15 μl of adhesion assay buffer: 150 mM NaCl, 10 mM HEPES, pH 7.4, 1 mM $CaCl_2$, 1 mM $MgCl_2$, with or without $MnCl_2$) were added to each well and allowed to adhere for 90 min at room temperature. Unless otherwise specified, adhesion assays were performed using wells coated with 4 ng of MAdCAM-1 IgG (10 μl of a 0.4 μg/ml solution) and in the presence of 1 mM $MnCl_2$. Nonadherent cells were removed by briefly dipping the slides 2 to 3 times in a chamber containing adhesion assay buffer. Adherent cells were fixed and stained by immersing slides in a solution containing 0.5% crystal violet, 20% methanol, and 1% formaldehyde in water for 1 h at room temperature and counted using a video microscope. For Ab blocking experiments, cells were preincubated for 15 min at 4°C. Purified mAbs were used at a concentration of 10 μg/ml. Ab-containing supernatants were used in saturating amounts as determined by flow cytometry. All assays were performed at least in duplicate.

Flow cytometric analysis

K562 transfectants were incubated with saturating amounts of unconjugated anti-β_7 or control Ab at 4°C in buffer that contained 10 mM HEPES, pH 7.4, and 150 mM NaCl. Buffer also contained 1 mM $CaCl_2$ and 1 mM $MgCl_2$ unless otherwise specified. Phycoerythrin-conjugated mouse anti-rat Ig (Chromaprobe Inc., Mountain View, CA), phycoerythrin-conjugated

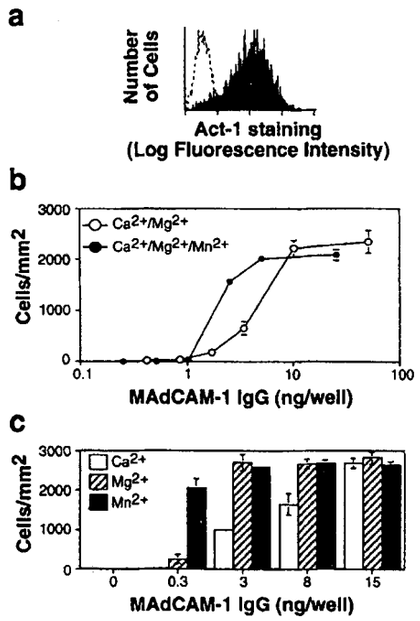

FIGURE 1. Heterologous expression of functional $\alpha_4\beta_7$ on K562 cells. *a*, Detection of human and mouse β_7 on the surface of transfected cells. K562 cells were transfected with human α_4 cDNA alone (K562-α_4) or with human α_4 plus human β_7 cDNA (K562-α_4hβ_7). Stable transfectants were analyzed by flow cytometry using the anti-$\alpha_4\beta_7$ Ab Act-1 (K562-α_4, open histogram; K562-α_4hβ_7, filled histogram). *b*, K562-α_4hβ_7 cell adhesion to MAdCAM-1 is increased by Mn^{2+}. Adhesion to MAdCAM-1-IgG fusion protein was determined in the presence of 1 mM Ca^{2+} plus 1 mM Mg^{2+} or 1 mM Ca^{2+} plus 1 mM Mg^{2+} plus 1 mM Mn^{2+}. *c*, Effects of various divalent cations on K562-α_4hβ_7-mediated cell adhesion to MAdCAM-1. Adhesion assay was performed in HEPES-buffered saline with the addition of 1 mM Ca^{2+}, 1 mM Mg^{2+}, or 1 mM Mn^{2+}.

goat anti-mouse (γ-specific) Ig (Boehringer Mannheim, Indianapolis, IN), or FITC-conjugated rat anti-mouse Ig (Chromaprobe Inc.) was used to detect anti-β_7 Ab-labeled cells. Fib 22 is a rat IgM Ab and was detected using FITC-conjugated goat anti-rat IgM (Boehringer Mannheim). To determine the effects of cation on Ab binding, cells were incubated with Ab at room temperature in the same buffer with the addition of varying amounts of $CaCl_2$, $MnCl_2$, and/or $MgCl_2$ as specified.

Results

Heterologous expression of functional $\alpha_4\beta_7$ on K562 cells

We developed a heterologous expression system to allow us to characterize Abs against β_7 and to produce and characterize chimeric β_7 subunits. K562 ($\alpha_5\beta_1^+$ α_4^- β_7^-) cells were transfected with human α_4 cDNA to obtain $\alpha_4\beta_1^+$ cells (K562-α_4; data not shown). The K562-α_4 cells were then retransfected with human (hβ_7) β-$_7$ subunit cDNA, and $\alpha_4\beta_7$ expression was detected with the complex-specific mAb Act-1 (Fig. 1*a*). Cells transfected with both α_4 and β_7 (K562-α_4hβ_7) adhered to MAdCAM-1 in the presence of Ca^{2+} and Mg^{2+} (1 mM each), and adhesion was increased by addition of Mn^{2+} (also at 1 mM) (Fig. 1*b*). Cells transfected with α_4 alone (K562-α_4) did not adhere to MAdCAM-1 (see below). To further characterize the effects of cations on $\alpha_4\beta_7$-mediated adhesion, we examined the adhesion of K562-α_4hβ_7 cells to MAdCAM-1 when only Ca^{2+}, Mg^{2+}, or Mn^{2+} was present (Fig. 1*c*). Mn^{2+} promoted adhesion even at low MAdCAM-1 concentrations, Mg^{2+} was effective at moderate MAdCAM-1 concentrations, and Ca^{2+} promoted adhesion only at relatively high

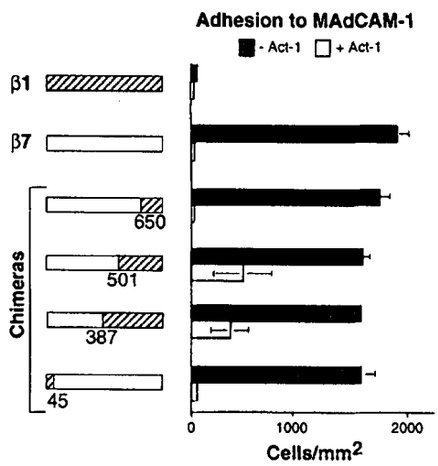

FIGURE 2. Chimeric β_7/β_1 subunits mediate adhesion to MAdCAM-1. K562-α_4 cells, which express α_4 associated with endogenous full-length β_1 (hatched bar), failed to adhere to MAdCAM-1-IgG. K562-α_4 cells transfected with either full-length human β_7 (open bar) or the four β_7/β_1 chimeras did adhere to MAdCAM-1-IgG. Wells were coated with 4 ng MAdCAM-1-IgG, and 1 mM Mn^{2+} was added during all steps of the assay. Representative data from one of three experiments is shown. Adhesion to MAdCAM-1-IgG was determined in the absence or presence of anti-$\alpha_4\beta_7$-blocking Ab, Act-1. The incomplete blocking of adhesion of two of the β_7/β_1 chimeras to MAdCAM-1 by Act-1 was a reproducible, and unexplained, finding. SE is shown by error bars. When not visible, error was <5%.

MAdCAM-1 concentrations. No adhesion was seen when assays were conducted using cation-free medium with or without EDTA or EGTA (data not shown). Similar effects of divalent cations have been reported for β_2 and β_3 integrin-mediated adhesion (34, 35).

Use of chimeric β_7/β_1 subunits to identify a β_7 subunit domain that specifies MAdCAM-1 binding

Previous reports indicate that $\alpha_4\beta_7$ can mediate MAdCAM-1 adhesion but $\alpha_4\beta_1$ cannot (4, 12). Others have reported Mn^{2+} can induce cell lines to weakly adhere to MAdCAM-1 via $\alpha_4\beta_1$ (36). In our adhesion assays using K562-α_4 transfectants, $\alpha_4\beta_1$ was unable to mediate adhesion to MAdCAM-1 even in the presence of Mn^{2+} (Fig. 2). K562-α_4 cells (which did not adhere to MAdCAM-1) and K562-α_4hβ_7 cells (which did adhere to MAdCAM-1) had equivalent surface expression of α_4 subunit, and K562-α_4 cells adhered to VCAM-1 and fibronectin via $\alpha_4\beta_1$ (data not shown). These data indicate that α_4-transfected K562 cells expressed functional $\alpha_4\beta_1$ but were unable to utilize this receptor to adhere to MAdCAM-1.

We produced human β_7/β_1 chimeric subunits by replacing portions of the β_1 subunit cDNA with homologous portions of the β_7 subunit cDNA to analyze the ability of various regions of the β_7 subunit to specify binding to MAdCAM-1. Four β_7/β_1 chimeric subunits were produced and expressed on the cell surface (Fig. 2). Three of these chimeric subunits were designed so that the change from β_1 to β_7 encoding sequence occurred at intron-exon boundaries (37). These three subunits contained the amino acid residues encoded by exons 2 to 13 of β_7 (residues 1–650), exons 2 to 11 of β_7 (1–501), or exons 2 to 9 of β_7 (1–387). (Exon 1 of the β_7 genomic DNA encodes 5'-untranslated sequences.) A fourth chimera was also expressed. It was designed so that the the first 45 amino acid residues of β_7 (including the signal peptide and a unique amino-terminal 20-amino acid extension not present in

other β subunits) were replaced by the corresponding shorter amino-terminal region of β_1. Each of these four β_7/β_1 chimeras was expressed at levels comparable to that seen with full-length β_7 transfectants as determined by staining with Act-1, and Fib Abs that recognize hβ_7 (not shown). Transfectants expressing these four β_7/β_1 chimeras adhered to MAdCAM-1 as efficiently as did transfectants expressing full-length β_7 (Fig. 2). Since replacement of β_1 amino acid residues 46–798 and 1–386 by the homologous portions of β_7 produced MAdCAM-1 binding equivalent to full-length β_7, these results demonstrate that the region of β_7 containing amino acid residues 46–386 plays a critical role in adhesion to MAdCAM-1. Attempts to use additional chimeras to further pinpoint the region of β_7 required for MAdCAM-1 specificity were unsuccessful: substitution of β_1 regions 1–327, 1–171 plus 190–798, or 150–798 with homologous regions of β_7 resulted in chimeras that could not be detected at the cell surface (data not shown).

Characterization of Anti-β_7 Ab function using transfected K562 cells

We used Abs against mouse β_7 to block Mn^{2+}-dependent adhesion of K562-α_4 mβ_7 to MAdCAM-1. In agreement with a previous report (20), we found that the Fib Abs (Fib 21, 22, 27, 30, 504) blocked adhesion, and M298 and LS722 Abs did not block adhesion. In previous studies, M301 blocked adhesion to MAdCAM-1 partially, and only in the absence of activation (20). We saw minimal inhibitory effect of M301 in our system. The adhesion of K562-α_4hβ_7 to MAdCAM-1 was also inhibited by the Fib Abs, which cross-react with human β_7, and by the anti-human $\alpha_4\beta_7$ Ab Act-1.

The ability of the anti-mouse β_7 Abs M293 and M300 (23) to block adhesion of $\alpha_4\beta_7$ to MAdCAM-1 has not been previously studied. We used K562-α_4 mβ_7 in assays of adhesion to MAdCAM-1. M300 inhibited adhesion, but M293 did not.

Characterization of Abs that recognize cation and ligand-influenced domains of β_7

Since Mn^{2+} promotes β_7 integrin-mediated adhesion, we attempted to produce Abs that preferentially bound to β_7 in the presence of Mn^{2+}. The novel Abs 2G3, 10F8, and 2B8 were raised against purified human $\alpha_4\beta_7$ integrin and stained RPMI 8866 cells in the presence of Mn^{2+}, but not in the presence of Ca^{2+} (see below). Two lines of evidence indicated that these Abs specifically recognize human β_7: 1) 2G3, 10F8, and 2B8 stain cells expressing human $\alpha_4\beta_7$ (K562-α_4hβ_7), but not cells expressing human α_4 with mouse β_7 (K562-α_4 mβ_7) (Fig. 3*a*); and 2) these Abs detect a protein with the appropriate mobility for β_7 (~107 kDa) by immunoblotting lysates from K562-α_4hβ_7 transfectants (only when samples were electrophoresed under nonreducing conditions, data not shown).

We further characterized the effect of ligand and cations on 2G3 staining of β_7. The 2G3 epitope was induced by MAdCAM-1 in solution. Addition of soluble MAdCAM-1 increased 2G3 staining of K562-α_4hβ_7 cells in the absence of Mn^{2+} (Fig. 3*b*). To determine the effect of different divalent cations individually on the ability of 2G3 to recognize the β_7 subunit, we stained K562-α_4hβ_7 cells with 2G3 in the presence of varying concentrations of Ca^{2+}, Mg^{2+}, or Mn^{2+} (Fig. 3*c*). When Ca^{2+} (0.1–1 mM) was added to the incubation and wash buffers, 2G3 staining was decreased. Mn^{2+} and Mg^{2+} (0.1–1 mM) increased 2G3 staining. To further test whether Ca^{2+} inhibited 2G3 staining of hβ_7 we added either EGTA or EDTA to the buffered solution used for staining, without addition of cation. Addition of either chelating agent produced high intensity staining of β_7 by 2G3 confirming that Ca^{2+} has an inhibitory effect on 2G3 staining (Fig. 3*d*).

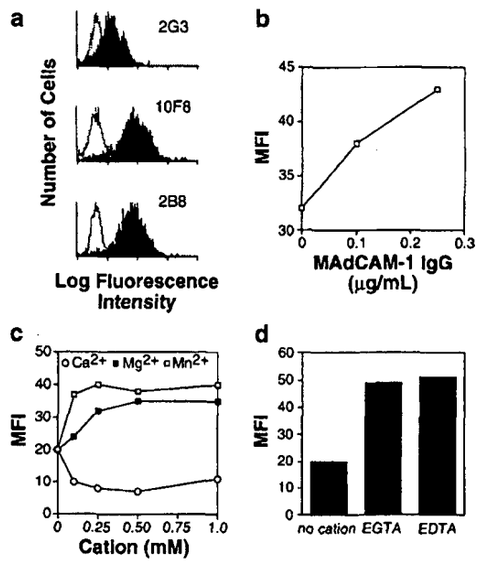

FIGURE 3. Ligand and cation influence 2G3, 10F8, and 2B8 staining of β_7. *a*, 2G3, 10F8, and 2B8 recognize human β_7 in the presence of Mn^{2+} cation. Flow cytometry analyses of K562-α_4mβ_7 (open histogram) and K562α_4hβ_7 (solid histogram) stained with 2G3, 10F8, or 2B8. 1 mM Mn^{2+} was present throughout. *b*, Soluble MAdCAM-1-IgG fusion protein increases 2G3 staining. MAdCAM-1 at a concentration of either 0.1 μg/ml or 0.25 μg/ml was added to K562-α_4hβ_7 cells during staining with 2G3, in a HEPES-buffered saline containing 1 mM Mg^{2+} and 1 mM Ca^{2+}, but no Mn^{2+}. Mean fluorescent intensity (MFI) is shown. *c*, 2G3 recognition of β_7 is inhibited by Ca^{2+}, and increased by Mn^{2+} or Mg^{2+}. K562-α_4hβ_7 cells were stained by 2G3 in buffer containing no added cation, or 0.1 to 1 mM Mn^{2+}, Mg^{2+}, or Ca^{2+}. *d*, Divalent cation-chelating agents increase the staining of β_7 by 2G3. EGTA (1 mM) or EDTA (1 mM) were added to all solutions during staining of K562-α_4hβ_7 cells.

We also examined the effect of 2G3, 10F8, and 2B8 Abs on adhesion of cells to MAdCAM-1. These Abs had no effect on adhesion of K562-α_4hβ_7 cells to MAdCAM-1 under conditions of near-maximal adhesion (1 mM Mn^{2+} included in assay buffer, Fig. 4*a*). However, the Abs markedly increased adhesion of K562-α_4hβ_7 cells to MAdCAM-1 under conditions of submaximal adhesion (1 mM Ca^{2+} and Mg^{2+} only; Fig. 4*b*). The increase in cell adhesion achieved using these Abs was similar to that produced by the addition of Mn^{2+}.

Mapping epitopes of anti-β_7 Abs on human/mouse chimeric β_7 subunits

The epitopes recognized by species-specific anti-human β_7 and anti-mouse β_7 Abs were mapped using chimeric human/mouse β_7 subunits. Initially, we expressed human β_7, mouse β_7, and six chimeric β_7 subunits designed so that the entire β_7 sequence of both species could be surveyed for epitopes. Expression of the chimeric subunit was detected by the Fib series of Abs (Fib 21, 22, 27, 30, 504) and by M301, all of which are known to recognize both mouse and human β_7 (Fig. 5, and data not shown). Chimeric β_7 constructs were expressed on the cell surface at levels comparable to hβ_7 and mβ_7 as demonstrated by Fib 504 staining (Fig. 5). The chimeric subunits mediated cell adhesion at levels equivalent to hβ_7 and mβ_7 (data not shown). Together with the staining by cross-species-reactive anti-β_7 Abs, this is evidence that the chimeric subunits fold, and pair with α_4, normally.

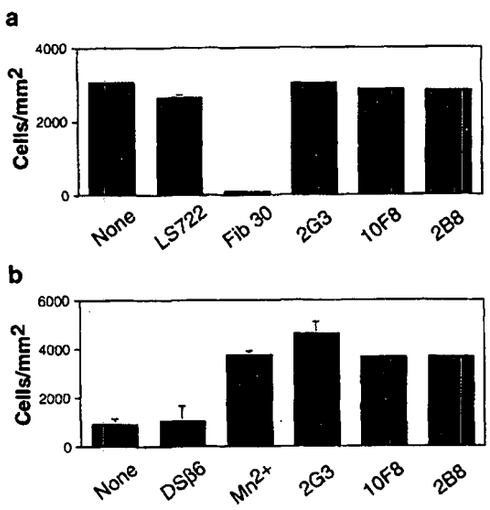

FIGURE 4. Effect of 2G3, 10F8, and 2B8 Abs on $\alpha_4\beta_7$-mediated adhesion to MAdCAM-1. *a*, 2G3, 10F8, and 2B8 do not block $\alpha_4\beta_7$-mediated adhesion to MAdCAM-1. Adhesion of K562 transfectants to MAdCAM-1-IgG was measured in the presence of 1 mM Ca^{2+}, 1 mM Mg^{2+}, and 1 mM Mn^{2+}. Controls included no added Ab, nonblocking anti-β_7 Ab LS722, and blocking anti-β_7 Ab Fib 30. *b*, 2G3, 10F8, and 2B8 increase $\alpha_4\beta_7$-mediated adhesion to MAdCAM-1 in the absence of Mn^{2+}. K562 transfectants were allowed to adhere to MAdCAM-1 IgG in the presence of 1 mM Ca^{2+} plus 1 mM Mg^{2+}. The adhesion assay was performed without Ab (None), with an irrelevant control Ab (DSβ_6), with the addition of Mn^{2+}, and with each of the three novel Abs (2G3, 10F8, and 2B8).

We were able to map each of the human- or mouse-specific Abs unambiguously using the human/mouse chimeric constructs (Table I). The anti-mouse β_7 Ab M291 recognized all constructs containing the mouse β_7 residues 554–802 and did not recognize any constructs containing the homologous human sequence. We assigned the epitope 558–726 to M291 since there are no differences between the mouse and human sequence in the region 554–557 and the β_7 extracellular domain is predicted to end at residue 726. All of the other Abs that we mapped on human/mouse chimeric β_7 subunits recognized amino acids in the region 170–554 of hβ_7 or mβ_7. We next constructed additional chimeric subunits that subdivided this large middle portion of the β_7 subunit (Table I). Act-1 recognized amino acids in the region 231–281 of human β_7 (see below). M293, M298, M300, and LS722 mapped to residues 387–542 of the mouse β_7 subunit. We assigned these Abs to the epitope 387–542 since there are no differences between human and mouse β_7 sequences in the regions 381–387 and 542–554.

Antibody epitope mapping data was also obtained using the β_7/β_1 chimeras (not shown). M301 recognized the β_7/β_1 chimera containing β_7 residues 1–650 but not the chimera containing β_7 residues 1–501. The M301 epitope was therefore assigned to residues 501–650 of β_7. Consistent with the results obtained using human/mouse and human/rat β_7 chimeras, Act-1 and all of the Fib Abs tested recognized each of the β_7/β_1 chimeras.

The new calcium-inhibited, adhesion-promoting anti-β_7 Abs 2G3, 10F8, and 2B8 recognized constructs that contained the N-terminal sequence of human β_7 (amino acids 1–170). These Abs also recognized the β_7/β_1 chimeric subunit in which the first 45 amino acids up to the first conserved cysteine residue of β_7 were replaced by the homologous sequence of the β_1 subunit. We assigned the epitopes of 2G3, 10F8, and 2B8 to amino acids 46–149 since there are no differences between the human and mouse β_7 sequences in the region 150–170.

Act-1 requires serine 250 for specific recognition of the human β_7 subunit

Comparison of the human and mouse β_7 sequences between residues 231–281, required for Act-1 binding, revealed only one amino acid difference. A serine residue is present at position 250 in hβ_7, and an asparagine residue at the same position in mβ_7. We constructed two point mutations: N250S (mouse β_7 with asparagine 250 mutated to serine) and S250N (serine 250 to asparagine; for convenience this mutation was inserted into the mβ_7 (170–554Δh), which had previously been shown to bind Act-1 in the same way as human β_7). N250S and S250N were transfected into K562-α_4 cells, resulting in expression of functional $\alpha_4\beta_7$ heterodimers (Fig. 6). Act-1 bound to and inhibited the function of N250S but not S250N, demonstrating that a single amino acid difference at residue 250 completely accounts for the difference in Act-1 recognition of human and mouse β_7.

Mapping epitopes of anti-β_7 Abs on human/rat chimeric β_7 subunits

The Act-1 epitope is within a region of the β_7 subunit predicted to have structural similarity to the metal ion-dependent adhesion site (MIDAS) of the integrin α_M and α_L subunits (see *Discussion*). To determine whether epitopes recognized by rat Abs (Fib 21, 22, 27, 30, 504) that recognize both human and mouse β_7 map within the MIDAS-like domain, we constructed a human/rat chimeric β_7 subunit. We cloned a fragment of rat β_7 cDNA that encodes a sequence homologous to human β_7 amino acid residues 170–381, which roughly corresponds to the MIDAS-like domain (residues 150–332). We then generated a chimeric subunit, hβ_7(170–381 Δrat) that contained the homologous rat β_7 sequence in place of residues 170–381 of the human β_7 sequence. This construct was transfected into K562-α_4 cells. The rat Ab M301, which minimally reduces adhesion to MAdCAM-1, did stain hβ_7(170–381 Δrat) transfectants. This indicates that the chimera was expressed on the surface and that the M301 epitope lies outside the 170–381 region (Table I). The rat β_7 sequence has an asparagine residue at residue 250, and, as expected, hβ_7(170–381 Δrat) was not recognized by Act-1 (Table I). hβ_7(170–381 Δrat) transfectants adhered to MAdCAM-1, demonstrating that the chimera was functional (data not shown).

The five Fib Abs, which are all rat Abs that recognize both mouse and human β_7 and block adhesion to MAdCAM-1, did not recognize hβ_7(170–381 Δrat) (Table I). This finding indicates that these Abs depend upon a structure within the 170–381 region of both human and mouse β_7, but absent from the homologous region of rat β_7. Comparison of the sequences of human, mouse, and rat β_7 in the region 170–381 reveals six amino acid residues that are identical in human and mouse but differ in the rat sequence. We have assigned the Fib Ab epitopes to the region 176–237, since all six of these residues are within this region. Epitope assignments, and functions, of all Abs described in this study are shown in Table II.

Discussion

The purpose of this study was to identify regions of the β_7 subunit that have special importance for ligand binding. To directly analyze the functional importance of specific regions of β_7 in MAdCAM-1 binding, we constructed and expressed human β_7/human β_1 chimeric subunits (Fig. 2). Since $\alpha_4\beta_7$ mediates adhesion to MAdCAM-1 but $\alpha_4\beta_1$ does not, this method allowed us to identify a region of β_7 that has unique properties required for

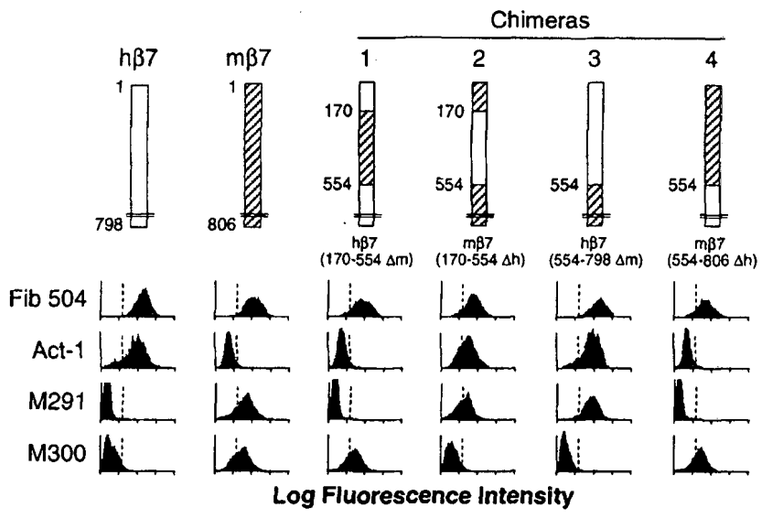

FIGURE 5. Expression of human/mouse chimeric β_7 subunits and Ab epitope mapping. Recognition of chimeric subunits by anti-β_7 Abs. Full-length human and mouse β_7 subunits and human/mouse chimeric β_7 subunits are illustrated at the top. K562-α_4 cells were retransfected with cDNAs encoding these subunits to obtain stable $\alpha_4\beta_7$ expressing cells. These cells were stained using the Abs Fib 504 (rat anti-human or mouse β_7), Act-1 (mouse anti-human $\alpha_4\beta_7$), M291 and M300 (both rat anti-mouse β_7). In each histogram, vertical dashed lines indicate the boundary between unstained and stained cells. Approximately 99% of cells incubated with an irrelevant negative control Ab were classified as unstained using this threshold.

Table I. *Recognition of human /mouse β_7 chimeras by anti-β_7 antibodies*[a]

β7 Construct	Antibody Recognition								
	M301	Fib	Act-1	M291	M293	M298	M300	LS722	2G3[†]
Human wt β7	+	+	+	–	–	–	–	–	+
Mouse wt β7	+	+	–	+	+	+	+	+	–
hβ7 (1-170 Δ m)	+	+	+	–	–	–	–	–	–
mβ7 (1-170 Δ h)	+	+	–	+	+	+	+	+	+
hβ7 (170-554 Δ m)	+	+	–	–	+	+	+	+	+
mβ7 (170-554 Δ h)	+	+	+	+	–	–	–	–	–
hβ7 (554-802 Δ m)	+	+	+	+	–	–	–	–	+
mβ7 (554-798 Δ h)	+	+	–	–	+	+	+	+	–
hβ7 (170-231 Δ m)	+	+	+	nd	nd	nd	nd	–	nd
hβ7 (231-554 Δ m)	+	+	–	nd	nd	nd	nd	+	nd
hβ7 (170-381 Δ m)	+	+	–	–	–	–	–	–	nd
mβ7 (281-554 Δ h)	+	+	–	+	–	–	–	–	nd
mβ7 (170-281 Δ h)	+	+	+	+	+	+	+	+	nd
mβ7 (170-354 Δ h)	+	+	+	+	+	+	+	+	nd
hβ7 (170-381Δrat)	+	–	–	nd	nd	nd	nd	nd	nd

[a] Human, mouse, and human/mouse chimeric β_7 cDNAs were expressed by retransfecting K562-α4 cells. A minus sign (–) indicates that Ab staining was similar to that seen with a negative control Ab; a plus sign (+) indicates that Ab staining was substantially greater than that seen with the negative control. All chimeric subunits were expressed on the cell surface as indicatred in the M301 and Fib columns (all of the Fib Ab, Fib 21, 22, 27, 30, and 504 were tested). *None of the five Fib Ab recognized the human/rat chimeric subunit (bottom row).*

[†] The Abs 2G3, 10F8, and 288 shared the same pattern of reactivity with chimeric human/mouse subunits.

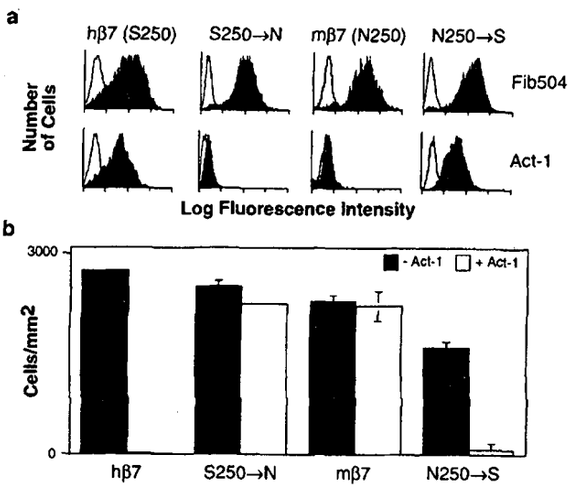

FIGURE 6. Act-1 recognition of human β_7 is dependent upon serine 250. *a*, Act-1 binding depends upon serine 250. Act-1-stained K562-α_4 cells transfected with cDNAs encoding authentic human β_7 (which has a serine residue at position 250, "hβ_7 (S250)") but failed to stain cells transfected with mouse β_7 cDNA (which has an asparagine residue at position 250). A human/mouse β_7 chimera containing residues 170–554 of the human sequence (mβ_7 (170–554Δh)) was stained by Act-1 (not shown), but the mutation of serine 250 to asparagine ("S250→N," mβ_7 (170–554Δh, S250N)) led to loss of staining. Conversely, expression of a mouse β_7 cDNA altered only by mutation of asparagine 250 to serine ("N250→S") led to appearance of the Act-1 epitope. *b*, *Substitutions at residue 250 do not affect* MAdCAM-1 binding but do affect the ability of Act-1 to inhibit binding. MAdCAM-1 adhesion of K562 cells transfected with the cDNAs hβ_7, S250→N, mβ_7, and mβ_7 (N250→S) was determined in the absence or presence of Act-1 Ab.

MAdCAM-1 adhesion. We found that this unique functional activity lies within a portion of the β_7 subunit (residues 46–386) that contains the epitopes recognized by six blocking Abs and three Abs that recognize epitopes influenced by cation and ligand. We mapped the epitopes of function-blocking, nonblocking, and cation- and ligand-influenced Abs using interspecies human/mouse or human/rat β_7 chimeric subunits (Figs. 5 and 6, and Table I). The assignment of epitopes is summarized in Table II and Figure 7. The most remarkable finding from these studies is that six of seven Abs that block $\alpha_4\beta_7$-mediated adhesion to MAdCAM-1 can be mapped to epitopes within a single short region of the β_7 subunit (amino acid residues 176–250). Five of these Abs (Fib 21, 22, 27, 30, 504) were previously shown to block $\alpha_E\beta_7$-mediated interaction with epithelial cells (20). In the light of previous data pertaining to the structure and function of integrin subunits, our results strongly suggest that a metal ion-dependent adhesion site-like (MIDAS-like) domain of the β_7 subunit (residues 150–332) plays a critical role in ligand binding and in determining ligand specificity.

Table II summarizes epitope-mapping data and functional data obtained in this study and previous studies. A comparison of mapping data from this study and from a previous study that defined

Table II. *Physical mapping and functional properties of anti-β_7 Ab*[a]

mAb	Amino Acid Epitope	Functional Epitope	MAdCAM-1 Blocking (% Inhibition)	VCAM-1 Blocking	Fibronectin Blocking	Species Specificity
2G3	46–149		↑ adhesion[b]	ND	ND	h β_7
10F8	46–149		↑ adhesion	ND	ND	h β_7
2B8	46–149		↑ adhesion	ND	ND	h β_7
Fib 21	176–237	C	95 ± 5	+	+	m or h β_7
Fib 22	176–237	C	97 ± 1	+	+	m or h β_7
Fib 27	176–237	D1	49 ± 8	+	+	m or h β_7
Fib 30	176–237	D1	86 ± 1	+	+	m or h β_7
Fib 504	176–237	D2	91 ± 3	+	+	m or h β_7
Act-1	250		99 ± 2	−	+	α_4 + h β_7
M293	387–542		17 ± 2	ND	ND	m β_7
M298	387–542	B1	8 ± 6	−	−	m β_7
M300	387–542		81 ± 8	ND	ND	m β_7
LS722	387–542	B2	6 ± 5	−	−	m β_7
M301	501–650	A	27 ± 7	−	−	m or h β_7
M291	558–726		ND	ND	ND	m β_7

[a] Amino acid epitopes were mapped using the human/mouse β_7, human/rat β_7, and β_7/β_1 chimeric subunits. Epitope assignments were further narrowed by comparing the human and mouse (or rat) sequences and eliminating identical residues as possible recognition sites. The ability to block adhesion to MAdCAM-1 was determined as described in *Materials and Methods* and is expressed here as % of inhibition of cell adhesion relative to a no Ab control (± SE). Functional epitope designations (A–D) were assigned by Andrew et al. (20), based on groups of Ab that cross-inhibited recognition of β_7, and these functional classes were subdivided (D1 and D2, e.g.) by ligand-blocking properties of Ab. The abilities of Ab to block binding to VCAM-1 and fibronectin were previously described (20). Fib 22, previously reported to recognize only mouse β_7, was shown in this study to recognize both mouse and human β_7.

[b] 2G3, 10F8, and 2B8 increase $\alpha_4\beta_7$-mediated cell adhesion to MAdCAM-1.

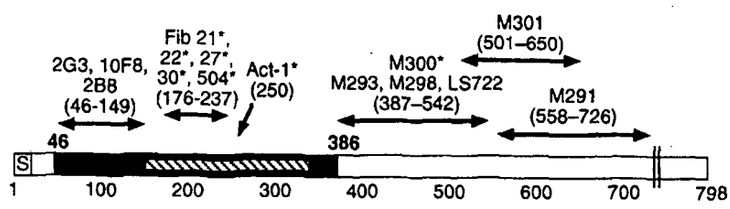

FIGURE 7. Summary of the β_7 subunit structure/function analysis. The β_7 subunit, including the signal peptide ("S"), the extracellular domain (residues 25–726), the transmembrane domain (double vertical lines), and the cytoplasmic domain is depicted at the bottom. Physical mapping data for anti-β_7 Abs are summarized at the top. Abs that block adhesion to MAdCAM-1 are indicated by asterisks. The β_7/β_1 chimera results indicate that β_7 residues 46–386 (solid bar) provide MAdCAM-1 binding specificity. Residues 150–332 (cross-hatched bar) comprise the putative MIDAS-like domain of β_7.

"functional epitopes" recognized by groups of cross-inhibitory Abs (20) reveals a close correlation. Functional epitope A corresponds to the M301 epitope (residues 501–650). Functional epitope B is recognized by M298 (nonblocking, B1) and LS722 (aggregating, B2), and corresponds to the structural domain recognized by these two Abs (residues 387–542) in our study. Functional epitopes C, D1, and D2, defined by the Fib series of Abs, correspond to residues 176–237. Six of seven Abs that inhibited the adhesion of $\alpha_4\beta_7$-transfected K562 cells to MAdCAM-1 could be mapped to residues 176–250. M300, another Ab with blocking activity in our assay, mapped to a distinct region (residues 387–542). Since our results with β_7/β_1 chimeric subunits demonstrate that amino acids 46–386 specify MAdCAM-1 binding, it is likely that M300 Ab acts from a distance to alter ligand binding (see below). While M301 (residues 501–650) had minimal effect on adhesion in our assay, it has previously been shown to block the adhesion of unstimulated (but not PMA-stimulated) mouse lymphocytes to MAdCAM-1, indicating that M301 can have some inhibitory activity (20). It is not surprising that adhesion-blocking Abs map to more than one region of β_7 since blocking Abs against other integrins also map to multiple regions of these molecules (38). This may indicate that more than one domain of the β subunit is directly involved in ligand binding, that two or more regions that are separated in the primary sequence are nearby in the tertiary structure, or that certain Abs perturb ligand binding without directly blocking access to the binding site (for example, by inducing a distant conformational change that interferes with ligand binding). Nonetheless, the mapping of six function-blocking Abs to a single small region (residues 176–250) of β_7 indicates that this region has a special role in adhesion.

We produced, characterized, and mapped the epitopes of three new anti-β_7 Abs, 2G3, 10F8, and 2B8. These Abs were identified by screening hybridoma supernatants for the ability to stain β_7 in the presence, but not in the absence, of Mn^{2+} (Fig. 3). Since all three Abs had similar properties, one (2G3) was selected for more detailed study. In addition to Mn^{2+}, 2G3 staining could also be induced by Mg^{2+}. In contrast, Ca^{2+} inhibited Ab binding. There was a general correlation between expression of the 2G3 epitope and the level of β_7-mediated adhesion produced in the presence of different cations: Mn^{2+} was the most potent inducer of the epitope and of adhesion, Mg^{2+} was intermediate, and Ca^{2+} inhibited the epitope and was the weakest at promoting adhesion (Figs. 1*c* and 3*c*). However, this correlation no longer held in the presence of chelating agents. As expected, no adhesion to MAdCAM-1 was seen when chelating agents were added to the medium. However, both EDTA and EGTA stimulated 2G3 binding (Fig. 3*d*), presumably by preventing Ca^{2+} from binding to $\alpha_4\beta_7$. Two previously described anti-integrin β_1 Abs, 9EG7 and 15/7, also recognize epitopes that are induced by either Mn^{2+} or EDTA/EGTA and inhibited by Ca^{2+} (22, 39, and our unpublished observations).

There were also interactions between 2G3 binding and ligand binding. Soluble MAdCAM-1 induced the 2G3 epitope (Fig. 3*b*). 2G3 (and the other two novel Abs, 10F8 and 2B8) strongly promoted cell adhesion to MAdCAM-1 in the absence of Mn^{2+} (Fig. 4*b*). In this

regard, 2G3 is similar to the anti-β_1 Ab 15/7, which recognizes a ligand-occupied/active conformation of the receptor. When occupied by ligand, 15/7 binds to β_1 integrin to stabilize the adhesive interaction.

Additional Abs with the ability to recognize other integrin β subunits in the presence of Mn^{2+} or ligand, and to increase adhesion to ligand, have been previously described. Such anti-β integrin Abs map to cation- and ligand-influenced binding sites (CLIBS) (39). The new Abs we produced behaved as CLIBS Abs. However, 2G3, 10F8, and 2B8 staining of β_7 was induced by Mg^{2+}, whereas the staining by some CLIBS Abs, AP-5 (anti-β_3) (40) and 9EG7 (anti-β_1) (39), is not induced (or inhibited) by Mg^{2+}. 2G3, 10F8, and 2B8 differed from previously reported CLIBS Abs in important respects. First, they were specific for β_7 and provided insight into the interaction of $\alpha_4\beta_7$ with MAdCAM-1. Second, the epitopes of 2G3, 10F8, and 2B8 were mapped to a region of the β_7 subunit not previously known to be a region for CLIBS Ab recognition.

2G3, 10F8, and 2B8 Abs map to the amino terminus of β_7 (amino acids residues 46–149; Table I, Table II, and Fig. 7). This region of the β_7 subunit is separate from the MIDAS-like domain (residues 150–332), and the putative cation binding region (β_7 residues 150–172; homologous to the cation binding domain in the β_3 subunit (41)). Cation- and/or ligand-induced Abs against other integrins have been mapped to different regions of the β subunit. The ligand-induced Ab AP-5 recognizes the extreme amino terminus of β_3 (residues 1–6) (40); the 15/7 Ab maps to the central domain of the β_1 subunit, homologous to β_7 residues 385–457 (42); other CLIBS Abs map to MIDAS-like domains of the β subunits (22, 38), or to cysteine-rich regions of the β_1, β_2, or β_3 integrin subunits (homologous to β_7 subunit residues 467–798) (39, 40, 43). The new Abs 2G3, 10F8, and 2B8 map to a region of the β_7 subunit that has not previously been implicated in the interaction with cation or ligand. Our results suggest that the conformation of β_7 amino acids 46–149 is strongly influenced by ligand and cation.

The β_7/β_1 chimera and epitope mapping results both indicate that a MIDAS-like domain of β_7 plays an important role in ligand binding (Fig. 7). MIDAS is a feature of the integrin α_L and α_M subunits identified in the crystal structure of the I domains of these subunits (44, 45). I domains (also known as A domains) are found in the extracellular portion of some integrin α subunits, and isolated I domains are able to bind some integrin ligands (46). Five oxygenated residues within the I domain coordinate binding of metal ions. It has been proposed that an additional coordinating residue may be supplied by the ligand, accounting for the metal ion dependence of ligand binding. Integrin β subunits share homology with I domain sequences (44). The putative MIDAS-like domains of integrin β subunits have a predicted arrangement of metal ion coordinating residues, α helices, and β sheets that is similar to the α_L and α_M MIDAS domain structures. Epitopes of six of the ligand binding-blocking Abs that we mapped fall within the MIDAS-like domain, and the MIDAS-like domain is contained within the region of β_7 that conferred MAdCAM-1 adhesion in the β_7/β_1 chimera experiments (Fig. 7). Studies involving integrin cross-linking to ligand, Ab epitope mapping, and analysis of mutant integrins indicate that the MIDAS-like domains of other integrin β subunits, including β_1, β_2, β_3, and β_6, are also crucial for ligand binding (38, 47–51). The Act-1 epitope lies in a region of the MIDAS-like domain of β_7 (residues 230–267) that is highly conserved among integrin β subunits and is implicated in ligand binding and as well as subunit association in β_1, β_2, and β_3. (52, 53).

The MIDAS-like domain of integrin β subunits may also play a direct role in association with the α subunit. In support of this possibility, a short peptide from the β_3 MIDAS-like domain has been shown to associate with α_{IIb} in vitro, and mutations in the same region of the β_2 and β_3 subunit MIDAS-like domains (54, 55) interfere with subunit association. The Act-1 Ab maps to the homologous region of the β_7 subunit. Act-1 recognizes $\alpha_4\beta_7$ but not $\alpha_E\beta_7$ (11, and data not shown). This may indicate that the Act-1 epitope includes residues from both α_4 and β_7, or that the region of the β_7 subunit recognized by Act-1 can be conformationally altered or masked by the associated α subunit. The location of the Act-1 epitope therefore suggests that the MIDAS-like domain of β_7 may be involved in association with the α subunit.

The MIDAS-like domain of β_7 is likely to be important for the interaction of lymphocytes with endothelial cells and epithelial cells in vivo. Since five Abs (Fib 21, 22, 27, 30, and 504) that block $\alpha_E\beta_7$-mediated binding to epithelial cells (20) map to the MIDAS-like domain, this domain is likely to play a key role in lymphocyte-epithelial cell interactions, as well as $\alpha_4\beta_7$-MAdCAM-1-mediated lymphocyte-endothelial cell interactions. The anti-$\alpha_4\beta_7$ Ab Act-1 that maps to the MIDAS-like domain of β_7 (residue 250) has therapeutic effects in cotton top tamarins with colitis (56). Although Act-1 efficiently inhibits $\alpha_4\beta_7$-mediated adhesion of lymphocytes to MAdCAM-1, the therapeutic effect of this Ab in colitis is not associated with a substantial decrease in intestinal lymphocytes. Act-1 binding to $\alpha_4\beta_7$ can directly influence lymphocyte proliferation (57) and protein tyrosine phosphorylation (A.I.L. and M.T., unpublished results), suggesting that recruitment-independent effects of Ab may be important in vivo. Agents such as Act-1 that are directed at the β_7 MIDAS-like domain can have diverse effects in vitro and in vivo, and may be of therapeutic value in colitis or other diseases involving mucosal immune responses.

Acknowledgments

The authors thank Drs. Y. Takada for providing human α_4 integrin cDNA, D. Sheppard for providing cell lines and Abs, and I. Weissman for providing TK-1 cells.

References

1. Holzmann, B., B. McIntyre, and I. L. Weissman. 1989. Identification of a murine Peyer's patch-specific lymphocyte homing receptor as an integrin molecule with an alpha chain homologous to human VLA-4. *Cell 56:37.*
2. Streeter, P. R., E. L. Berg, B. T. N. Rouse, R. F. Bargatze, and E. C. Butcher. 1988. A tissue-specific endothelial cell molecule involved in lymphocyte homing. *Nature 331:41.*
3. Nakache, M., E. Berg, P. Streeter, and E. C. Butcher. 1989. The mucosal vascular cell addressin is a tissue specific endothelial cell adhesion molecule for circulating lymphocytes. *Nature 337:179.*
4. Berlin, C., E. L. Berg, M. J. Briskin, D. P. Andrew, P. J. Kilshaw, B. Holzmann, I. L. Weissman, A. Hamann, and E. C. Butcher. 1993. $\alpha_4\beta_7$ integrin mediates lymphocyte binding to the mucosal vascular addressin MAdCAM-1. *Cell 74:185.*
5. Briskin, M. J., L. M. McEvoy, and E. C. Butcher. 1993. MAdCAM-1 has homology to immunoglobulin and mucin-like adhesion receptors and to IgA1. *Nature 363:461.*
6. Shyjan, A. M., M. Bertagnolli, C. J. Kenney, and M. J. Briskin. 1996. Human mucosal addressin cell adhesion molecule-1 (MAdCAM-1) demonstrates structural and functional similarities to the $\alpha_4\beta_7$-integrin binding domains of murine MAdCAM-1, but extreme divergence of mucin-like sequences. *J. Immunol. 156: 2851.*
7. Bargatze, R. F., M. A. Jutila, and E. C. Butcher. 1995. Distinct roles of L-selectin and integrins $\alpha_4\beta_7$ and LFA-1 in lymphocyte homing to Peyer's patch-HEV in situ: the multistep model confirmed and refined. *Immunity 3:99.*
8. Hamann, A., D. P. Andrew, D. Jablonski-Westrich, B. Holzmann, and E. C. Butcher. 1994. Role of α_4-integrins in lymphocyte homing to mucosal tissues in vivo. *J. Immunol. 152:3282.*
9. Wagner, N., J. Löhler, E. J. Kunkel, K. Ley, E. Leung, G. Krissansen, K. Rajewsky, and W. Müller. 1996. Critical role for β_7 integrins in formation of the gut-associated lymphoid tissue. *Nature 382:366.*
10. Abitorabi, M. A., C. R. Mackay, E. H. Jerome, O. Osorio, E. C. Butcher, and D. J. Erle. 1996. Differential expression of homing molecules on recirculating lymphocytes from sheep gut, peripheral, and lung lymph. *J. Immunol. 156:3111.*
11. Schweighoffer, T., Y. Tanaka, M. Tidswell, D. J. Erle, K. J. Horgan, G. E. Ginther Luce, A. I. Lazarovits, D. Buck, and S. Shaw. 1993. Selective expression

of integrin $\alpha_4\beta_7$ on a subset of human CD4$^+$ memory T cells with hallmarks of gut tropism. *J. Immunol. 151:717.*

12. Erle, D. J., M. J. Briskin, E. C. Butcher, A. Garcia-Pardos, A. Lazarovits, and M. Tidswell. 1994. Expression and function of the MAdCAM-1 receptor integrin $\alpha_4\beta_7$ on human leukocytes. *J. Immunol. 153:517.*
13. Rott, L. S., M. J. Briskin, D. P. Andrew, E. L. Berg, and E. C. Butcher. 1996. A fundamental subdivision of circulating lymphocytes defined by adhesion to mucosal addressin cell adhesion molecule-1: comparison with vascular cell adhesion molecule-1 and correlation with β_7 integrins and memory differentiation. *J. Immunol. 156:3727.*
14. Chan, B. M. C., M. J. Elices, E. Murphy, and M. E. Hemler. 1992. Adhesion to vascular cell adhesion molecule 1 and fibronectin: comparison of $\alpha_4\beta_1$ (VLA-4) and $\alpha_4\beta_7$ on the human B cell line JY. *J. Biol. Chem. 267:8366.*
15. Ruegg, C., A. A. Postigo, E. E. Sikorski, E. C. Butcher, R. Pytela, and D. J. Erle. 1992. Role of integrin $\alpha_4\beta_7/\alpha_4\beta_P$ in lymphocyte adherence to fibronectin and VCAM-1 and in homotypic cell clustering. *J. Cell Biol. 117:179.*
16. Cepek, K. L., S. K. Shaw, C. M. Parker, G. J. Russell, J. S. Morrow, D. L. Rimm, and M. B. Brenner. 1994. Adhesion between epithelial cells and T lymphocytes mediated by E-cadherin and the $\alpha_E\beta_7$ integrin. *Nature 372:190.*
17. Karecla, P. I., S. J. Bowden, S. J. Green, and P. J. Kilshaw. 1995. Recognition of E-cadherin on epithelial cells by the mucosal T cell integrin α_{M290} β_7 ($\alpha_E\beta_7$). *Eur. J. Immunol. 25:852.*
18. Overduin, M., T. S. Harvey, S. Bagby, K. I. Tong, P. Yau, M. Takeichi, and M. Ikura. 1995. Solution structure of the epithelial cadherin domain responsible for selective cell adhesion. *Science 267:386.*
19. Karecla, P. I., S. J. Green, S. J. Bowden, J. Coadwell, and P. J. Kilshaw. 1996. Identification of a binding site for integrin $\alpha_E\beta_7$ in the N-terminal domain of E-cadherin. *J. Biol. Chem. 271:30909.*
20. Andrew, D. P., C. Berlin, S. Honda, T. Yoshino, A. Hamann, B. Holzmann, P. J. Kilshaw, and E. C. Butcher. 1994. Distinct but overlapping epitopes are involved in $\alpha_4\beta_7$-mediated adhesion to vascular cell adhesion molecule-1, mucosal addressin-1, fibronectin, and lymphocyte aggregation. *J. Immunol. 153:3847.*
21. Stupack, D. G., S. Stewart, W. G. Carter, E. A. Wayner, and J. A. Wilkins. 1991. B lymphocyte fibronectin receptors: expression and utilization. *Scand. J. Immunol. 34:761.*
22. Yednock, T. A., C. Cannon, C. Vandevert, E. G. Goldbach, G. Shaw, D. K. Ellis, C. Liaw, L. C. Fritz, and L. I. Tanner. 1995. $\alpha_4\beta_1$ integrin-dependent cell adhesion is regulated by a low affinity receptor pool that is conformationally responsive to ligand. *J. Biol. Chem. 270:28740.*
23. Kilshaw, P. J., and S. J. Murant. 1991. Expression and regulation of β_7 (β_P) integrins on mouse lymphocytes: relevance to the mucosal immune system. *Eur. J. Immunol. 21:2591.*
24. Lazarovits, A. I., R. A. Moscicki, J. T. Kurnick, D. Camerini, A. K. Bhan, L. G. Baird, M. Erikson, and R. B. Colvin. 1984. Lymphocyte activation antigens. I. A monoclonal antibody, anti-Act I, defines a new late lymphocyte activation antigen. *J. Immunol. 133:1857.*
25. Erle, D. J., C. Ruegg, D. Sheppard, and R. Pytela. 1991. Complete amino acid sequence of an integrin β subunit (β_7) identified in leukocytes. *J. Biol. Chem. 266:11009.*
26. Giancotti, F. G., and E. Ruoslahti. 1990. Elevated levels of the $\alpha_5\beta_1$ fibronectin receptor suppress the transformed phenotype of Chinese hamster ovary cells. *Cell 60:849.*
27. Kamata, T., W. Puzon, and Y. Takada. 1995. Identification of putative ligand-binding sites of the integrin $\alpha_4\beta_1$ (VLA-4, cd49d/CD29). *Biochem. J. 305:945.*
28. Hu, M. C.-T., D. T. Crowe, I. L. Weissman, and B. Holzmann. 1992. Cloning and expression of mouse integrin β_P(β_7): a functional role in Peyer's patch-specific lymphocyte homing. *Proc. Natl. Acad. Sci. USA 89:8254.*
29. Horton, R. M., Z. Cai, S. N. Ho, and L. R. Pease. 1990. Gene splicing by overlap extension: tailor-made genes using the polymerase chain reaction. *Biotechniques 8:528.*
30. Sims, M. J., D. G. Hussal, S. Brett, W. Rowan, M. J. Lockyer, A. Angel, A. P. Lewis, G. Hale, H. Waldman, and J. S. Crowe. 1993. A humanized CD18 antibody can block function without cell destruction. *J. Immunol. 151:2296.*
31. Stephens, P. E., and M. L. Cockett. 1989. The construction of a highly efficient and versatile set of mammalian expression vectors. *Nucleic Acids Res. 17:7110.*
32. Bebbington, C. R., and C. C. G. Hentschel. 1987. *The Use of Vectors Based on Gene Amplification for the Expression of Cloned Genes in Mammalian Cells.* Academic Press, New York.
33. Cockett, M. L., C. R. Bebbington, and G. T. Yarranton. 1990. High level expression of tissue inhibitor of metalloproteinases in Chinese hamster ovary cells using glutamine synthetase gene amplification. *Biotechnology 8:662.*
34. Staatz, W. D., S. M. Rajpara, E. A. Wayner, W. G. Carter, and S. A. Santoro. 1989. The membrane glycoprotein Ia-IIa (VLA-2) complex mediates the Mg^{++}-dependent adhesion of platelets to collagen. *J. Cell Biol. 108:1917.*
35. Elices, M. J., L. A. Urry, and M. E. Hemler. 1991. Receptor functions for the integrin VLA-3: fibronectin, collagen, and laminin binding are differentially influenced by Arg-Gly-Asp peptide and by divalent cations. *J. Cell Biol. 112:169.*
36. Strauch, U. G., A. Lifka, U. Gosslar, P. J. Kilshaw, J. Clements, and B. Holzmann. 1994. Distinct binding specificities of integrins $\alpha_4\beta_7$ (LPAM-1), $\alpha_4\beta_1$ (VLA-4), and $\alpha_{IEL}\beta_7$. *Int. Immunol. 6:263.*
37. Jiang, W. M., D. Jenkins, Q. Yuan, E. Leung, K. H. Choo, J. D. Watson, and G. W. Krissansen. 1992. The gene organization of the human β_7 subunit, the common beta subunit of the leukocyte integrins HML-1 and LPAM-1. *Int. Immunol. 4:1031.*
38. Takada, Y., and W. Puzon. 1993. Identification of a regulatory region of integrin β_1 subunit using activating and inhibiting antibodies. *J. Biol. Chem. 268:17597.*
39. Bazzoni, G., D. T. Shih, C. A. Buck, and M. E. Hemler. 1995. Monoclonal antibody 9EG7 defines a novel β_1 integrin epitope induced by soluble ligand and manganese, but inhibited by calcium. *J. Biol. Chem. 270:25570.*
40. Honda, S., Y. Tomiyama, A. J. Pelletier, D. Annis, Y. Honda, R. Orchekowski, Z. Ruggeri, and T. J. Kunicki. 1995. Topography of ligand-induced binding sites, including a novel cation-sensitive epitope (AP5) at the amino terminus, of the human integrin β_3 subunit. *J. Biol. Chem. 270:11947.*
41. D'Souza, S. E., T. A. Haas, R. S. Piotrowicz, V. Byers-Ward, D. E. McGrath, H. R. Soule, C. Cierniewski, E. F. Plow, and J. W. Smith. 1994. Ligand and cation binding are dual functions of a discrete segment of the integrin β_3 subunit: cation displacement is involved in ligand binding. *Cell 79:659.*
42. Puzon-McLaughlin, W., T. A. Yednock, and Y. Takada. 1996. Regulation of conformation and ligand binding function of integrin $\alpha_5\beta_1$ by the β_1 cytoplasmic domain. *J. Biol. Chem. 271:16580.*
43. Du, X., M. Gu, J. W. Weisel, C. Nagaswami, J. S. Bennett, R. Bowditch, and M. H. Ginsberg. 1993. Long range propagation of conformational changes in integrin $\alpha_{IIb}\beta_3$. *J. Biol. Chem. 268:23087.*
44. Lee, J. O., P. Rieu, M. A. Arnaout, and R. Liddington. 1995. Crystal structure of the A domain from the alpha subunit of integrin CR3 (CD11b/CD18). *Cell 80: 631–8.*
45. Qu, A., and D. J. Leahy. 1995. Crystal structure of the I-domain from the CD11a/CD18 (LFA-1, $\alpha_L\beta_2$) integrin. *Proc. Natl. Acad. Sci. USA 92:10277.*
46. Ueda, T., P. Rieu, J. Brayer, and M. A. Arnaout. 1994. Identification of the complement iC3b binding site in the β_2 integrin CR3 (CD11b/CD18). *Proc. Natl. Acad. Sci. USA 91:10680.*
47. Puzon-McLaughlin, W., and Y. Takada. 1996. Critical residues for ligand binding in an I domain-like structure of the integrin β_1 subunit. *J. Biol. Chem. 271:20438.*
48. Goodman, T. G., and M. L. Bajt. 1996. Identifying the putative metal ion dependent adhesion site in the β_2 (CD18) subunit required for $\alpha_L\beta_2$ and $\alpha_M\beta_2$ ligand interactions. *J. Biol. Chem. 271:23729.*
49. Tozer, E. C., R. C. Liddington, M. J. Sutcliffe, A. H. Smeeton, and J. C. Loftus. 1996. Ligand binding to integrin $\alpha_{IIb}\beta_3$ is dependent on a MIDAS-like domain in the β_3 subunit. *J. Biol. Chem. 271:21978.*
50. Huang, X. Z., A. Chen, M. Agrez, and D. Sheppard. 1995. A point mutation in the integrin β_6 subunit abolishes both $\alpha_v\beta_6$ binding to fibronectin and receptor localization to focal contacts. *Am. J. Respir. Cell Mol. Biol. 13:245.*
51. Bergelson, J. M., and M. E. Hemler. 1995. Integrin-ligand binding: do integrins use a "MIDAS touch" to grasp an Asp? *Curr. Biol. 5:615.*
52. Wardlaw, A. J., M. L. Hibbs, S. A. Stacker, and T. A. Springer. 1990. Distinct mutations in two patients with leukocyte adhesion deficiency and their functional correlates. *J. Exp. Med. 172:335.*
53. Bajt, M. L., M. H. Ginsberg, A. L. Frelinger, M. C. Berndt, and J. C. Loftus. 1992. A spontaneous mutation of integrin $\alpha_{IIb}\beta_3$ (platelet glycoprotein IIb-IIIa) helps define a ligand binding site. *J. Biol. Chem. 267:3789.*
54. Steiner, B., A. Trzeciak, G. Pfenninger, and W. Kouns. 1993. Peptides derived from a sequence within β_3 integrin bind to platelet $\alpha_{IIb}\beta_3$ (GPIIb-IIIa) and inhibit ligand binding. *J. Biol. Chem. 268:6870.*
55. Djaffar, I., and J. P. Rosa. 1993. A second case of variant of Glanzmann's thrombasthenia due to substitution of platelet GPIIIa (integrin β_3) Arg214 by Trp. *Hum. Mol. Genet. 2:2179.*
56. Hesterberg, P., D. Winsor-Hines, M. J. Briskin, D. Soler-Ferran, C. Merrill, C. R. MacKay, W. Newman, and D. J. Ringler. 1996. Rapid resolution of chronic colitis in the cotton-top tamarin with an antibody to a gut homing integrin $\alpha_4\beta_7$. *Gastroenterology 111:1373.*
57. Woodside, D. G., T. K. Teague, and B. W. McIntyre. 1996. Specific inhibition of T lymphocyte coactivation by triggering integrin β_1 reveals convergence of β_1, β_2, and β_7 signaling pathways. *J. Immunol. 157:700.*

doi:10.1016/j.jmb.2004.05.051 J. Mol. Biol. (2004) 340, 1073–1093

JMB

Available online at www.sciencedirect.com

SCIENCE DIRECT®

ELSEVIER

High-affinity Human Antibodies from Phage-displayed Synthetic Fab Libraries with a Single Framework Scaffold

Chingwei V. Lee, Wei-Ching Liang, Mark S. Dennis, Charles Eigenbrot Sachdev S. Sidhu and Germaine Fuh*

Department of Protein Engineering, Genentech Inc. 1 DNA Way, South San Francisco, CA 94080, USA

**Corresponding author*

Phage-displayed synthetic antibody libraries were built on a single human framework by introducing synthetic diversity at solvent-exposed positions within the heavy chain complementarity-determining regions (CDRs). The design strategy of mimicking natural diversity using tailored codons had been validated previously with scFv libraries, which produced antibodies that bound to antigen, murine vascular endothelial growth factor (mVEGF), with affinities in the 100 nM range. To improve library performance, we constructed monovalent and bivalent antigen-binding fragment (Fab) libraries, and explored different CDR-H3 diversities by varying the amino acid composition and CDR length. A Fab with sub-nanomolar affinity for mVEGF was obtained from a library with CDR-H3 diversity designed to contain all 20 naturally occurring amino acids. We then expanded the library by increasing the variability of CDR-H3 length and using tailored codons that mimicked the amino acid composition of natural CDR-H3 sequences. The library was tested against a panel of 13 protein antigens and high-affinity Fabs were obtained for most antigens. Furthermore, the heavy chain of an anti-mVEGF clone was recombined with a library of light chain CDRs, and the affinity was improved from low nanomolar to low picomolar. The results demonstrated that high-affinity human antibodies can be generated from libraries with completely synthetic CDRs displayed on a single scaffold.

Keywords: phage display; affinity improvements; antibody engineering; designed CDR

Introduction

In vitro combinatorial libraries have been used to produce antibodies with high affinity and specificity, and to improve our understanding of antibody structure and function using technologies such as phage display,[1–3] ribosomal display,[4] bacterial display[5] and yeast display.[6] In the last decade, phage display has been the most widely applied technology capable of either improving the properties of monoclonal antibodies (mAbs) from diverse natural sources, or generating mAbs from naïve repertoires.[7]

The two types of *in vitro* antibody libraries, natural and synthetic, are distinguished by the source of their repertoires. Most antibody libraries to date have been derived, totally or in part,[8–11] from the natural repertoires by cloning the antibody variable domain genes from naïve[12–14] or immunized[15,16] individuals. The diversity of natural antibody libraries is contributed by the hypervariable complementarity-determining region (CDR) sequences presented on multiple

Abbreviations used: CDR, complementarity-determining region; CDR-H*n*, (where $n = 1, 2,$ or 3), heavy chain CDR 1, 2, or 3; CDR-L*n*, (where $n = 1, 2$ or 3), light chain CDR 1, 2 or 3; cP3, C-terminal domain of the M13 bacteriophage gene-3 minor coat protein; Fab, antigen binding fragment; Ig, immunoglobulin; mAb, monoclonal antibody; VH domain, heavy chain variable domain; VL domain, light chain variable domain; mVEGF, murine vascular endothelial growth factor; scFv, single-chain variable fragment; PBS, phosphate buffered saline; BSA, bovine serum albumin; ELISA, enzyme-linked immunosorbant assay; TMB, tetramethylbenzidine.

E-mail address of the corresponding author: gml@gene.com

frameworks, and the recombination of light and heavy chains.[17] The performance of such libraries, measured by the affinities of derived antibodies, is determined predominantly by their library sizes,[14] which is often limited by the efficiencies of transformation of the library DNA into *Escherichia coli*. Synthetic libraries, on the other hand, have designed diversities introduced with synthetic DNA. Synthetic antibody libraries that have been reported employ either single[18–21] or multiple frameworks.[22–24] Synthetic libraries built on multiple frameworks, such as the HUCAL libraries,[22–24] have been used to obtain antibodies with affinities in the low nanomolar range against some antigens. For single-framework libraries, diversity depends solely on the degeneracy of synthetic DNA used to vary the CDR loop sequences. Both the diversity design and the library size are crucial for the performance of a synthetic library. Synthetic antibody libraries built on a single framework offer many advantages (e.g. ease of library construction and analysis of the derived antibodies), especially when using a framework derived from humanized 4D5 that has been optimized for protein expression and has been used successfully in therapeutics.[21,25] However, the question remains whether a single framework can present CDR binding loops with sufficient diversity to produce a library that is capable of generating high-affinity antibodies against diverse antigens. Frameworks serve as a source of diversity for natural antibodies, since they provide the structural scaffolding for CDR loops.[26–28] Many framework residues can influence the binding affinities of antibodies.[29]

We previously developed a synthetic antibody phage library using the template of a single framework with diversification restricted to the heavy chain.[30] A subset of CDR positions was chosen for diversification using criteria of high solvent exposure and/or especially high variability among natural antibody sequences. These positions were randomized using tailored codons designed for a bias toward amino acids found in natural antibodies. The concept was validated with libraries built on the humanized 4D5 framework in the single-chain variable fragment (scFv) format, and libraries of this type generated antibody fragments with affinities in the 100 nM range.[30]

In this study, we further explored the concept of restricting synthetic diversity to mimic natural diversity in order to generate highly functional antibody libraries. To improve upon the previous libraries, we first chose to convert to a Fab format. However, our first attempt with a Fab library using the same diversity design as our first scFv library resulted in >5 μM binding clones (G.F., unpublished results). This may have resulted from the lower display of Fab on phage relative to the display of scFv. To improve the display of functional Fab, the diversities allowed in CDR-H1 and CDR-H2 was limited to closely mimic the natural diversity, and different designs for CDR-H3 were explored. A reduction in the diversity of the CDR-H1 and H2 degeneracy by 10^4-fold from the design for scFv library could be accomplished without sacrificing the coverage of natural diversities, and the performance of the Fab library was improved to a level similar to that of our initial scFv library. Various CDR-H3 designs were then explored to enhance significantly the ability to generate high-affinity binding clones. The affinities of these selected heavy chain fragments were further improved to the low picomolar range by introducing additional diversity into the light chain CDRs. To expand the library so that it could generate antibodies to any antigen, we further increased the length of CDR-H3, since length is a key component of the diversities of CDR-H3 in natural antibodies.[31–33] This library was screened against a panel of 13 protein antigens and, in most cases, produced Fabs with affinities of under ten nanomolar or low nano-molar without the need for further affinity maturation.

Results

Diversity design for CDR-H1 and CDR-H2

For the generation of heavy chain libraries in the Fab format, a set of positions within CDR-H1 and CDR-H2 was chosen for randomization in a manner similar to that previously described for libraries constructed in an scFv format, which we refer to as Lib-v1 in what follows.[30] For the new Fab libraries, positions 30–33 in CDR-H1, and 50, 52, 53, 54, 56 and 58 in CDR-H2 were randomized (Figure 1). In addition, framework position 49 was allowed a limited diversity to reflect the variations in natural antibody sequences. We modified the previous diversity design used in Lib-v1 by fine-tuning the diversity to more closely mimic the natural repertoire (Table 1). The first step in the fine-tuning was the determination of the "target diversity" based on the natural diversity observed at each position. The CDR sequences of approximately 3600 human antibodies in the Kabat database†[34] were aligned and at each position the amino acids were ranked by the frequency of occurrence. For example, Ser is the commonest amino acid residue at position 30, as it appeared in 68% of natural antibodies, followed by Thr (18%), Asn (4%), Arg (2.5%), Asp (1.9%) and Gly (1.8%). These six amino acids together account for over 90% of the natural antibody sequences, and were therefore designated as the "target diversity" for this position (Table 1). The same operation was performed for each of the other positions, and the target diversity was chosen for each position.

Next, tailored degenerate codons were designed to encode for the target diversity at each position.

† www.kabatdatabase.com

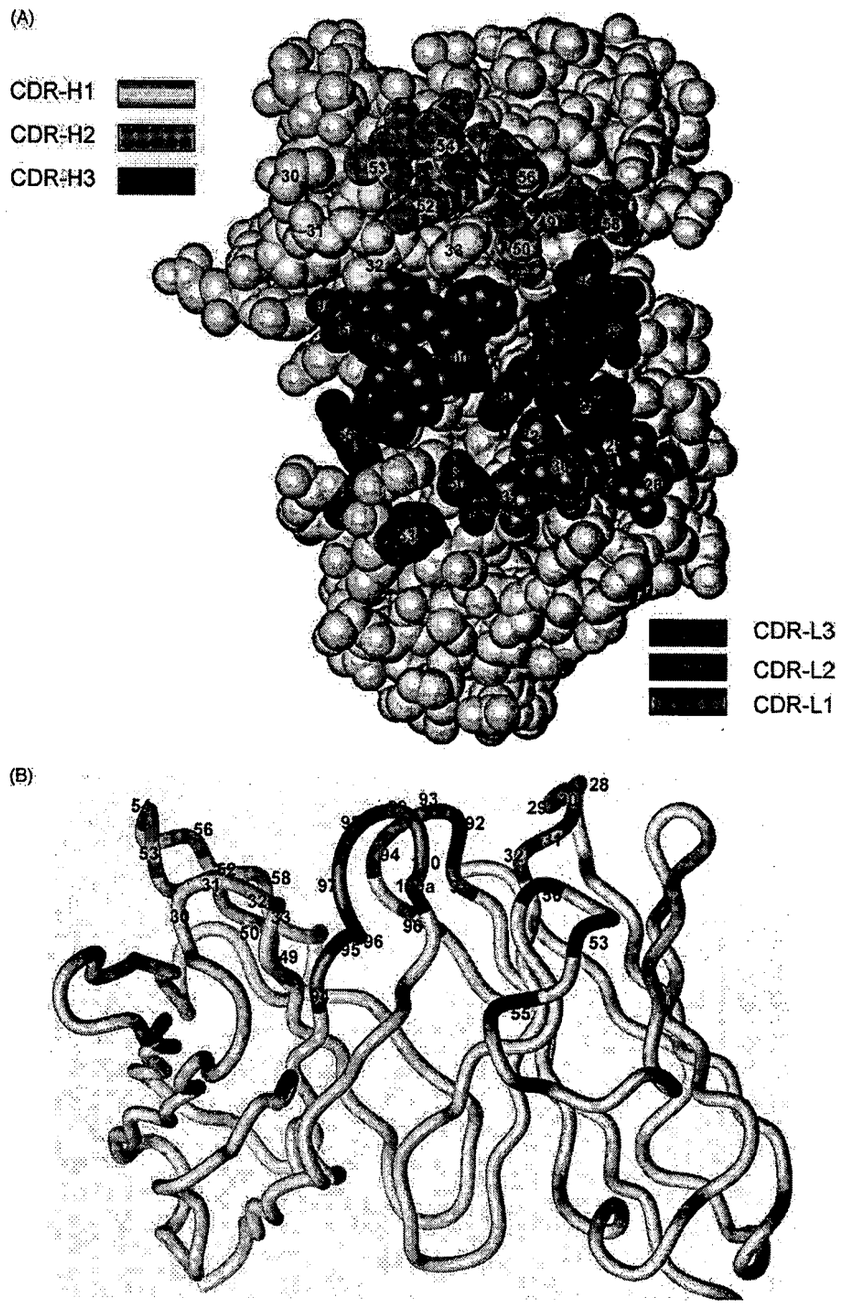

Figure 1. The CDR residues chosen for randomization in the Fab phage libraries. The top–down view of the CDR binding loops of h4D5 as a space-filling model (A) and the side view of the variable domain as a worm (B) are shown, highlighting the residues chosen for randomization in heavy chain CDR-H1 (yellow), CDR-H2 (green) and CDR-H3 (blue), and light chain CDR-L1 (pink), CDR-L2 (magenta) and CDR-L3 (red). The Kabat numbering is used in this and subsequent Figures.[34]

The tailored codons were evaluated by two criteria (Table 1). First, the best codon should encode the minimum number of amino acid residues not found in the target diversity and should also exclude cysteine and stop codons. Second, coverage of the target diversity by the degenerate codon should be as high as possible, with coverage of the highest-ranking amino acids a priority. More emphasis was placed on the first criterion than the second, since we believe removing unwanted

Table 1. Target diversity and design diversity of CDR-H1 and CDR-H2 for the heavy chain library

Positions	Target diversity: Prevalence in natural antibodies (%)											Design diversity			
												Codon	Residues encoded	Coverage (%)	Oligonucleotide
H1-K30	S	T	N	R	D	G						*AVT*	STN	90	H1 a-d
	68	18	4	3	2	2									
H1-D31	S	N	G	T	D	R	A					*RRT*	SNGD	82	H1 a,b
	50	13	10	10	9	2	1					*RVM*	SNGTDRA **E**	95	H1 c,d
H1-T32	Y	S	N	G	F	A						*WMY*	YSN **T**	80	H1 a-d
	64	9	7	4	3	3									
H1-Y33	A	Y	W	G	S	D	T	N	V			*KMT*	AYSD	57	H1 a,c
	22	20	17	14	12	3	3	2	2			*KGG*	WG	31	H1 b,d
H2-A49	G	S	A									*GST*	GA	77	H2 a-c
	58	22	19												
H2-R50	R	Y	W	V	G	I	E	A	S	N	L	*DGG*	RWG	35	H2 a
	17	10	9	9	9	8	8	6	6	6	4	*DHT*	YVIASN **DFT**	45	H2 b
												GAA	E	8	H2 c
H2-Y52	S	Y	N	K	I	R	D	T				*DMT*	SYNDT **A**	74	H2 a-c
	26	25	17	8	5	3	3	3							
H2-T53	S	D	Y	G	H	N	I	T	W			*DMT*	SDYNT **A**	66	H2 a-c
	24	20	11	10	9	8	5	3	2						
H2-N54	G	S	D	N	K	F	T					*RRC*	GSDN	81	H2 a-c
	37	26	11	7	6	5	4								
H2-Y56	S	T	N	D	Y	E	G	A				*DMT*	STNDYA	81	H2 a-c
	28	16	15	10	10	5	5	2							
H2-R58	Y	N	D	R	S	I	T	H				*DAC*	YND	69	H2 a-c
	32	25	12	7	4	4	3	2							

CDR positions selected for randomization in CDR-H1 and H2 are listed with the template h4D5 residues. Target diversity is a group of residues that were selected because they cover over 90% of the approximately 3500 human antibody sequences in the Kabat database.[34] The prevalence (%) of each residue in natural sequences is listed under each residue. Design diversity is a group of residues encoded by a tailored degenerate codon (in italics) so that the coverage (%) of natural target diversity by one codon or a combination of codons (as for position 50) was close to 70% or higher. Diversity was designed to minimize the residues not included in the target diversity (bold text). Several H1 or H2 oligonucleotides were mixed for the mutagenesis reaction for library construction (see Materials and Methods).

degeneracy to limit the library diversity is more important than attempting to cover all amino acids in the target diversity for CDR-H1 and CDR-H2. At most positions, the highest-ranking three to six amino acid residues were easily encoded by tailored degenerate codons. However, at some positions it was not straightforward to encode a significant proportion of the target diversity without including unwanted diversity. For example, positions 33 and 50 were the most variable positions in CDR-H1 and CDR-H2, respectively; several different degenerate codons were employed to cover them. The coverage of the target diversity by the degenerate codons was in the range of 66–95%, which is at least as good if not better than the design for Lib-v1. All together, the degenerate codons for CDR-H1 and H2 encoded $\sim 10^6$ unique DNA sequences; this was $\sim 10^4$-fold lower than the DNA degeneracy encoded previously in Lib-v1. The encoded diversity of amino acid sequences was ~500 for CDR-H1 and $\sim 10^4$ for CDR-H2. These synthetic diversity designs for CDR-H1 and CDR-H2 were employed to construct phage-displayed Fab libraries with several different CDR-H3 diversity designs.

Construction of the first generation CDR-H3 library

CDR-H3 is located at the center of the antigen-binding site (Figure 1), and it is the most variable amongst the six CDRs in natural antibodies, both in terms of amino acid composition, length, and conformation.[26,27,35,36] As a result, CDR-H3 is often the most important determinant for the specificity of antibodies,[37] and we explored different strategies to introduce the diversity within this loop.

In the Kabat numbering scheme, CDR-H3 is defined as the sequence from positions 95–102. However, we noted that the C-terminal boundaries of natural CDR-H3 sequences are not highly variable, but rather, usually contain either Phe-Asp-Tyr or Ala-Met-Asp-Tyr immediately preceding position 103. As the h4D5 CDR-H3 contains an Ala-Met-Asp-Tyr motif at its C-terminal boundary, we decided to leave this region constant in our design. At the N-terminal boundary of CDR-H3, we changed the framework slightly from that of the h4D5 sequence (Ser93-Arg94) to the sequence found most commonly amongst human antibodies in the Kabat database (Ala93-Arg/Lys94). For our first-generation library (Lib-1), we designed two mutagenic oligonucleotides that inserted mainly DVK codons between these boundaries and varied the N or C termini of the loop (Table 2); a similar design strategy was used previously in scFv Lib-v1. The CDR-H3 length was fixed at 11 residues, which is the length found in h4D5 (Table 2). The DVK codon encodes for 12

Table 2. CDR-H3 diversity designs for generating heavy chain libraries, Lib-1 and Lib-2

Library	Oligonucleotide	S93	R94	CDR-H3 positions 95–102 (h4D5 residue)												Length	Degeneracy
				W95	G96	G97	D98	G99	F100	·	·	Y100a	A100b	M100c	D101	Y102	
Lib-1	DVK 1	A	R/K	*DVK*	*DVK*	*DVK*	*DVK*	*DVK*	*NNK*	·	·	Y	A	M	D	Y	11	1×10^8
	DVK 2	A	R/K	W	*NVT*	*DVK*	*DVK*	*DVK*	*DVK*	·	·	W/S/A/G/T/R	A	M	D	Y	11	8×10^6
Lib-2-DVK	DVK 1	A	R/K	*DVK*	*DVK*	*DVK*	*DVK*	*DVK*	*DVK*	·	·	Y	A	M	D	Y	11	3×10^8
	DVK 2	A	R/K	W	*NVT*	*DVK*	*DVK*	*DVK*	*NNK*	·	·	W/S/A/G/T/R	A	M	D	Y	11	8×10^6
	DVK 3	A	R/K	*DVK*	*DVK*	*DVK*	*DVK*	*DVK*	*DVK*	·	·	W/S/A/G	A	M	D	Y	11	1×10^8
	DVK 4	A	R	*DVK*	*DVK*	*DVK*	*DVK*	*DVK*	*DVK*	*DVK*	·	Y	A	M	D	Y	12	6×10^8
	DVK 5	A	R	*DVK*	*DVK*	*DVK*	*DVK*	*DVK*	*DVK*	*DVK*	·	W/S/A/G/T/R	A	M	D	Y	12	4×10^9
	DVK 6	A	R	*DVK*	*DVK*	*DVK*	*DVK*	*DVK*	*DVK*	*DVK*	*DVK*	Y	A	M	D	Y	13	1×10^8
	DVK 7	A	R	*DVK*	*DVK*	*DVK*	*DVK*	*DVK*	*DVK*	*DVK*	*DVK*	W/S/A/G/T/R	A	M	D	Y	13	7×10^8
Lib-2-NVT	NVT 1	A	R/K/T	*NVT*	*NVT*	*NVT*	*NVT*	*NVT*	*NVT*	·	·	Y	A	M	D	Y	11	3×10^6
	NVT 2	A	R/K/T	W	*NVT*	*NVT*	*NVT*	*NVT*	*NVT*	·	·	*NVT*	A	M	D	Y	11	3×10^6
	NVT 3	A	R/K	W	*NVT*	*NVT*	*NVT*	*NVT*	*NVT*	*NVT*	·	W/S/A/G	A	M	D	Y	12	2×10^7
	NVT 4	A	R/K	*NVT*	W	*NVT*	*NVT*	*NVT*	*NVT*	*NVT*	·	W/S/A/G	A	M	D	Y	12	2×10^7
	NVT 5	A	R/K	*NVT*	*NVT*	W	*NVT*	*NVT*	*NVT*	*NVT*	·	W/S/A/G	A	M	D	Y	12	2×10^7
	NVT 6	A	R/K	*NVT*	*NVT*	*NVT*	*NVT*	*NVT*	W	*NVT*	·	W/S/A/G	A	M	D	Y	12	2×10^7
	NVT 7	A	R/K	*NVT*	*NVT*	*NVT*	*NVT*	*NVT*	*NVT*	W	·	W/S/A/G	A	M	D	Y	12	2×10^7
	NVT 8	A	R/K	W	*NVT*	*NVT*	*NVT*	*NVT*	*NVT*	·	·	W/S/A/G/T/R	A	M	D	Y	11	2×10^6
	NVT 9	S	R	*NVT*	*NVT*	*NVT*	*NVT*	*NVT*	*NVT*	*NVT*	*NVT*	Y	A	M	D	Y	13	4×10^8
Lib-2-NNS	NNS 1	A	R	*NNS*	*NNS*	*NNS*	*NNS*	*NNS*	*NNS*	·	·	Y	A	M	D	Y	11	1×10^9
	NNS 2	A	R	*NNS*	*NNS*	*NNS*	*NNS*	*NNS*	*NNS*	·	·	W/S/A/G/T/R	A	M	D	Y	11	6×10^9

Different designs in oligonucleotides for CDR-H3 for Lib-1 and Lib-2 are listed with their lengths and calculated DNA degeneracies (Degeneracy). The randomized positions are shown with either the degenerate codon (italics) or the amino acids (plain text) allowed by genetic codons.

amino acids (Tyr, Ala, Arg, His, Asp, Ser, Thr, Asn, Pro, Gly, Trp and Cys) with at least one amino acid from each category of amino acids: aromatic (Phe, Trp, Tyr), aliphatic (Ile, Leu, Val, Ala, Met), basic (Lys, Arg, His), acidic (Asp, Glu), polar (Ser, Thr, Asn, Gln), and conformational (Pro, Gly, Cys). We constructed two libraries that displayed either monovalent (Lib-1-Fab containing 2.1×10^9 unique members) or bivalent (Lib-1-Fab.zip containing 1.8×10^9 unique members) Fabs with CDR-H1, CDR-H2, and CDR-H3 diversified as described above. Previous studies have shown that bivalent display resulted in an avidity effect that increased the efficiency of capture of antigen-specific Fabs with immobilized antigens.[38]

The libraries were cycled separately through rounds of binding selections with immobilized mVEGF antigen. After three rounds of selection, individual clones were analyzed by phage enzyme-linked immunosorbant assay (ELISA) to identify specific anti-mVEGF binding clones that were defined as clones exhibiting ELISA signals at least tenfold greater on mVEGF coated plates in comparison with signals on plates coated with an irrelevant protein, for example, bovine serum albumin (BSA). The monovalent and bivalent library pools after three rounds of sorting contained 21% and 70% positive clones, respectively. DNA sequencing of 67 positive clones from the monovalent library revealed four unique sequences, while 47 bivalent positive clones were represented by nine unique sequences (Table 3). For a different antigen, the bivalent library (Lib-1) yielded binding clones but the monovalent library did not (data not shown). Thus, it appears that the bivalent display resulted in a greater number of positive clones representing a more diverse population of unique sequences, consistent with previous reports that efficiency of antibody selection improved as valency of display on phage increased.[38,39]

We next looked for a correlation between the affinity of a positive clone and its prevalence within the selected population to see if affinity was the driving force in selection (Table 4). In the monovalent pool, the highest-affinity clone (mV-202) was also the most prevalent clone (42% of sequenced binders). However, this correlation between affinity and prevalence was absent among the remaining clones. The two low-affinity clones (mV-201 and mV-204) were more prevalent than the clone with the second highest affinity (mV-203). This may be accounted for by the significant variations we observed in the level of display among different clones. In the bivalent pool, one high-affinity clone (mV-304) accounted for 57% of sequenced clones, but the other high-affinity clone (mV-307) represented only 4% of the sequenced clones. Thus, while there appears to be some correlation between affinity and prevalence among selected binders, there are considerable discrepancies that suggest other factors in addition to affinity (e.g. levels of protein expression) influenced the selection process. Our previous scFv library (Lib-v1), which used a similar design for CDR-H3 diversity, yielded a greater number of unique anti-mVEGF binders but the highest affinities were comparable to those obtained with the current Fab libraries.[30] These results are consistent with the fact that scFvs are displayed more efficiently than Fabs on phage particles and, thus, the scFv format allows for the selection of a larger population of binding clones representing a greater range of affinities.

Construction of the second-generation CDR-H3 library

We next constructed a second-generation library (Lib-2) with the aim of comparing the performance of different CDR-H3 designs in generating high-affinity Fabs, with the hopes of improving on the results obtained with the first-generation library design. Three sub-libraries were constructed to test three different degenerate codons for generating CDR-H3 diversity. Lib-2-DVK (4.1×10^9 unique members) using the degenerate DVK codon was constructed with a pool of seven mutagenic oligonucleotides to allow for a diversity of loop lengths from 11 to 13 (Table 2). The other two sub-libraries used either an NVT degenerate codon (Lib-2-NVT, 5.0×10^8 unique members) or an NNS degenerate codon (Lib-2-NNS, 8.0×10^8 unique members). The NVT codon encodes 11 amino acids with 12

Table 3. Effect of CDR-H3 designs on the best affinities from the libraries, Lib-1 and Lib-2

Library	H3 codon	Library size ($\times 10^9$)	Positive (%)	Unique/sequenced	Best affinity (nM)	H3 oligo
Lib-1-Fab	DVK	2.1	21	4/67	200	DVK1
Lib-1-Fab.zip	DVK	1.8	70	9/47	41	DVK1
Lib-2-Fab	DVK	4.1	80	4/50	0.6	NNS1
	NVT	0.5				
	NNS	0.8				

The results from selections for binding to mVEGF are shown for Lib-1 in the Fab or Fab.zip format and Lib-2 in Fab format with three different CDR-H3 designs. Lib-2-DVK, -NVT or -NNS were generated separately and pooled together for selection experiments. The percentage specific binding clones after three rounds of selection are shown as positive (%). The number of clones with unique DNA sequences out of the total number of clones sequenced are shown as unique/sequenced. Best affinity shows the lowest IC_{50} values measured among the unique clones using a competition ELISA. The H3 oligonucleotides from which the CDR-H3 sequences of the best clones were derived are indicated as H3 oligo (see Table 2 for description of the oligonucleotides).

Table 4. The deduced amino acid sequences and binding affinities of mVEGF binding clones from Lib-1 and Lib-2

Library	Clone	CDR-H1				CDR-H2							CDR-H3										H3 oligo	IC_{50}	Frequency (%)
		30	31	32	33	49	50	52	53	54	56	58	93	94	95	96	97	98	99	100	·	100a			
Lib-1-Fab	mV-201	T	S	N	G	A	Y	S	S	N	Y	Y	A	R	W	S	R	A	S	F	·	Y	DVK1	>5 μM	22
	mV-202	T	G	T	D	A	I	T	Y	D	S	Y	A	K	A	G	D	R	E	G	·	Y	DVK1	200 nM	42
	mV-203	T	D	S	G	G	R	S	Y	S	S	N	A	K	W	P	W	Y	N	A	·	W	DVK2	700 nM	9
	mV-204	S	N	T	A	G	I	N	Y	G	T	T	A	R	E	S	G	R	G	G	·	Y	DVK1	>5 μM	27
Lib-1-Fab.zip	mV-301	N	N	N	A	G	I	T	A	G	T	Y	A	R	E	S	S	T	G	G	·	Y	DVK1	90 nM	2
	mV-302	T	N	N	G	A	Y	S	A	G	N	Y	A	R	W	E	R	G	A	R	·	Y	DVK1	>5 μM	9
	mV-303	T	S	T	G	A	Y	S	Y	S	T	Y	A	R	W	S	R	R	N	K	·	Y	DVK1	600 nM	2
	mV-304	T	N	N	W	A	W	S	S	S	Y	Y	A	R	G	D	A	S	G	R	·	Y	DVK1	47 nM	57
	mV-305	N	N	N	W	G	V	T	N	S	A	D	A	S	Y	R	T	D	D	Y	·	A	DVK2	>5 μM	13
	mV-306	S	G	N	D	A	I	T	Y	G	Y	Y	A	K	A	A	G	X	A	G	·	Y	DVK1	>5 μM	6
	mV-307	T	N	N	G	A	X	Y	Y	S	Y	T	A	K	X	D	A	X	X	G	·	Y	DVK1	41 nM	4
	mV-308	N	S	S	G	G	F	T	Y	D	Y	D	A	R	G	X	S	W	T	R	·	Y	DVK1	110 nM	2
	mV-309	T	G	N	G	A	Y	S	T	G	S	Y	A	R	W	S	W	G	T	G	·	Y	DVK1	>5 μM	4
Lib-2	mV-401	S	D	Y	W	A	G	T	A	G	Y	Y	A	R	F	V	F	F	L	P	·	Y	NNS1	0.6 nM	65
	mV-402	T	G	S	S	A	R	S	A	G	Y	D	A	R	Y	F	R	W	Y	M	·	A	NNS2	80 nM	25
	mV-403	T	G	S	G	G	W	Y	Y	S	N	Y	A	R	A	L	W	A	F	V	·	A	NNS2	25 nM	10
	mV-404	N	A	S	W	G	A	Y	Y	S	Y	N	A	R	W	G	H	S	T	S	P	W	NVT3	44 nM	100[a]

Deduced amino acids sequences at the positions that were randomized in the libraries and the source of the H3 oligonucleotides (H3 oligo) are listed. Sequences with ambiguities were marked as X. The binding affinities were measured with competitive ELISA and represented as IC_{50} values. The frequency (%) of each clone among the sequenced clones (see Table 3) is listed in the last column.

[a] Clone mV-404 was the sole clone identified from a separate sorting of Lib-2 against mVEGF.

codons, which is a reduction from the 18 codons contained within the DVK codon. Therefore Lib-2-NVT contains lower DNA degeneracy in CDR-H3 compared with Lib-2-DVK (Table 2) and, thus, there is a smaller gap between the theoretical diversity (the number of unique codon combinations encoded by the mutagenic oligonucleotides) and the actual library size. Furthermore, the use of an NVT degenerate codon reduces the number of non-functional clones, since, unlike the DVK codon, it does not include a stop codon. One shortcoming of the NVT codon is that it does not encode Trp, which is commonly found to make contact with antigens.[40,41] We addressed this issue by doping one Trp codon through the positions 95–100 (Table 2) and using a mixture of oligonucleotides in library construction. The NNS degenerate codon contains 32 codons that encode for all 20 naturally occurring amino acids, so the gap between the actual and theoretical library size is the highest in Lib-2-NNS.

The three libraries were constructed separately and pooled for use in binding selections against antigen. Binding selections were performed in a manner similar to that used for the first-generation libraries by allowing phage pools to bind to mVEGF immobilized in 96-well Immunoplates. Following three rounds of binding selection, 80% of the clones were found to bind specifically to mVEGF and DNA sequencing of 50 clones revealed three unique sequences (Table 3). An additional unique clone (mV-404) was identified from a separate solution phase sorting strategy as used in light chain affinity improvement described below. The affinities of the four clones were estimated with competitive phage ELISAs, and the best clone (mV-401) exhibited a sub-nanomolar IC_{50} value, which was a significant improvement over the affinities obtained from Lib-1. Three of the four unique clones, including that with the highest affinity, came from Lib-2-NNS, and this suggested that allowing all 20 amino acids in CDR-H3 was important for finding a high-affinity clone. We have observed this phenomenon with other antigens (C.V.L., unpublished results). Indeed, the CDR-H3 sequence of the highest-affinity clone could have been generated only by an NNS codon, as it contained amino acids not encoded by either the DVK or NVT codon.

Construction of the third-generation CDR-H3 library

We next expanded the heavy chain library by incorporating multiple CDR-H3 lengths (Table 5). In addition, we utilized a novel degenerate codon, which was designed to encode for all 20 amino acids but, unlike the NNS codon, with frequencies that mimicked more closely those observed in natural CDR-H3 sequences. To design this codon, we examined the amino acid composition of natural CDR-H3 sequences in the Kabat database (Figure 2).[34] Since the lengths of natural CDR-H3s vary greatly, we did not align the sequences. Instead, we summed the occurrences of each amino acid within the region bounded by position 94 and the position preceding position 101, as this is the most variable region among natural antibodies. These sums were used to calculate the percentage frequency of each amino acid within the hypervariable CDR-H3 sequences. As reported,[32] we observed that the amino acid composition was more diverse than that observed in CDR-H1 and CDR-H2, but there were significant biases (Figure 2). For example, Tyr was the most frequent aromatic amino acid, and Arg was significantly more common than Lys or His amongst the basic amino acids. None of the degenerate codons used in the first and second-generation libraries could effectively mimic the amino acid composition of natural CDR-H3s (Figure 2). We therefore created a modified version of the NNS codon, called the XYZ codon, to bias the diversity toward the amino acid usage in natural CDR-H3s. Unlike standard degenerate codons that contain equimolar quantities of two, three or four of the nucleotide bases at degenerate positions, the XYZ codon contains different proportions of the nucleotides at each of the three codon positions (as described in Materials and Methods), so that the coded amino acid distribution resembles that found in natural CDR-H3 sequences better than other codons; nevertheless, the over-abundances of Tyr in natural sequences cannot be reproduced (Figure 2). Oligonucleotides to encode for CDR-H3s with lengths that varied from seven to 19 residues were designed so that the C-terminal regions were restricted to resemble the sequences of natural CDR-H3s and the framework position 94 was allowed a limited diversification to mirror the sequences of natural antibodies (Table 5). Degeneracies were introduced by either NNS or XYZ codons within the hypervariable region. The NNS codon was included for the shorter CDR-H3s, since it had the advantage of coding cysteine less frequently than the XYZ codon, but the longer CDR-H3s ($\geqq 14$) were designed exclusively with XYZ codons. A total of 150 clones from libraries designed with XYZ codons were sequenced to demonstrate the actual amino acid distribution matched closely with the theoretical design (Figure 2).

Separate libraries were constructed for each CDR-H3 length and, again, the same CDR-H1 and CDR-H2 designs were used (Table 1); each library contained 2×10^9 to 4×10^9 unique members. The libraries were constructed in a Fab.zip format to enable bivalent display, since this would increase the efficiency of binding selections and thus the probability of finding positive clones for a broad range of antigens.[38] The individual libraries were pooled to produce the third-generation library (Lib-3), which contained a total of $\sim 4 \times 10^{10}$ unique members. Lib-3 was used to select against a panel of 13 protein antigens, and individual clones were screened after four rounds of selection against immobilized antigens. For most antigens,

Table 5. Design for the CDR-H3 in the length diversity library, Lib-3

Oligonucleotide	CDR-H3 (95-102)																				Length
	93	94	95	96	97	98													101	102	
H3-7a	A	R/K	*NNK*	*NNK*	*NNK*	*NNK*	·	·	·	·	·	·	·	·	·	·	·	·	F	D	Y	7
H3-7b	A	R/K	*XYZ*	*XYZ*	*XYZ*	*XYZ*	·	·	·	·	·	·	·	·	·	·	·	·	F	D/A	Y	7
H3-7c	A	R/H/S/N	*XYZ*	*XYZ*	*XYZ*	*XYZ*	·	·	·	·	·	·	·	·	·	·	·	·	F/L	G/V/D/A	Y	7
H3-8a	A	R/K	*NNK*	*NNK*	*NNK*	*NNK*	*NNK*	·	·	·	·	·	·	·	·	·	·	·	F	D	Y	8
H3-8b	A	R/H/S/N	*XYZ*	*XYZ*	*XYZ*	*XYZ*	*XYZ*	·	·	·	·	·	·	·	·	·	·	·	F/L	G/V/D/A	Y	8
H3-8c	A	R/H/S/N	*XYZ*	*XYZ*	*XYZ*	*XYZ*	*XYZ*	·	·	·	·	·	·	·	·	·	·	·	F/L	D/A	Y	8
H3-9a	A	R	*NNS*	*NNS*	*NNS*	*NNS*	Y	A/G/V	·	·	·	·	·	·	·	·	·	·	M	D	Y	9
H3-9b	A	R	*NNS*	*NNS*	*NNS*	*NNS*	W/S/A/G	A/G/V	·	·	·	·	·	·	·	·	·	·	M	D	Y	9
H3-9c	A	R/K	*NNK*	*NNK*	*NNK*	*NNK*	*NNK*	*NNK*	·	·	·	·	·	·	·	·	·	·	F	D	Y	9
H3-9d	A	R/K	*XYZ*	*XYZ*	*XYZ*	*XYZ*	*XYZ*	*XYZ*	·	·	·	·	·	·	·	·	·	·	F	D/A	Y	9
H3-9e	A	R/K	*XYZ*	*XYZ*	*XYZ*	*XYZ*	Y	A	·	·	·	·	·	·	·	·	·	·	M	D	Y	9
H3-9f	A	R/K	*XYZ*	*XYZ*	*XYZ*	*XYZ*	W/S/A/G	A	·	·	·	·	·	·	·	·	·	·	M	D	Y	9
H3-10a	A	R	*NNS*	*NNS*	*NNS*	*NNS*	*NNS*	Y	A/G/V	·	·	·	·	·	·	·	·	·	M	D	Y	10
H3-10b	A	R	*NNS*	*NNS*	*NNS*	*NNS*	*NNS*	W/S/A/G	A/G/V	·	·	·	·	·	·	·	·	·	M	D	Y	10
H3-10c	A	R/K	*NNK*	*NNK*	*NNK*	*NNK*	*NNK*	*NNK*	*NNK*	·	·	·	·	·	·	·	·	·	F	D	Y	10
H3-10d	A	R/K	*XYZ*	*XYZ*	*XYZ*	*XYZ*	*XYZ*	*XYZ*	*XYZ*	·	·	·	·	·	·	·	·	·	F	D	Y	10
H3-10e	A	R/K	*XYZ*	*XYZ*	*XYZ*	*XYZ*	*XYZ*	*XYZ*	*XYZ*	·	·	·	·	·	·	·	·	·	F/L	G/V/D/A	Y	10
H3-11a	A	R	*NNS*	*NNS*	*NNS*	*NNS*	*NNS*	*NNS*	Y	A/G/V	·	·	·	·	·	·	·	·	M	D	Y	11
H3-11b	A	R	*NNS*	*NNS*	*NNS*	*NNS*	*NNS*	*NNS*	W/S/A/G	A/G/V	·	·	·	·	·	·	·	·	M	D	Y	11
H3-11c	A	R/K	*XYZ*	*XYZ*	*XYZ*	*XYZ*	*XYZ*	*XYZ*	*XYZ*	*XYZ*	·	·	·	·	·	·	·	·	F	D	Y	11
H3-11d	A	R/H/S/N	*XYZ*	*XYZ*	*XYZ*	*XYZ*	*XYZ*	*XYZ*	W/S/A/G	G/V/D/A	·	·	·	·	·	·	·	·	M	D	Y	11
H3-11e	A	R/H/S/N	*XYZ*	*XYZ*	*XYZ*	*XYZ*	*XYZ*	*XYZ*	Y	G/V/D/A	·	·	·	·	·	·	·	·	M	D	Y	11
H3-12a	A	R	*NNS*	*NNS*	*NNS*	*NNS*	*NNS*	*NNS*	*NNS*	W/S/A/G	A/G/V	·	·	·	·	·	·	·	M	D	Y	12
H3-12b	A	R	*NNS*	*NNS*	*NNS*	*NNS*	*NNS*	*NNS*	*NNS*	Y	A/G/V	·	·	·	·	·	·	·	M	D	Y	12
H3-12c	A	R	*XYZ*	*XYZ*	*XYZ*	*XYZ*	*XYZ*	*XYZ*	*XYZ*	*XYZ*	*XYZ*	·	·	·	·	·	·	·	F/L	D	Y	12
H3-12d	A	R/K	*XYZ*	*XYZ*	*XYZ*	*XYZ*	*XYZ*	*XYZ*	*XYZ*	W/S/A/G	A	·	·	·	·	·	·	·	M	D	Y	12
H3-12e	A	R/H/S/N	*XYZ*	*XYZ*	*XYZ*	*XYZ*	*XYZ*	*XYZ*	*XYZ*	W/S/A/G	G/V/D/A	·	·	·	·	·	·	·	M	D	Y	12
H3-12f	A	R/H/S/N	*XYZ*	*XYZ*	*XYZ*	*XYZ*	*XYZ*	*XYZ*	*XYZ*	Y	G/V/D/A	·	·	·	·	·	·	·	M	D	Y	12
H3-13a	A	R	*XYZ*	*XYZ*	*XYZ*	*XYZ*	*XYZ*	*XYZ*	*XYZ*	*XYZ*	*XYZ*	*XYZ*	·	·	·	·	·	·	F/L	D	Y	13
H3-13b	A	R	*NNS*	*NNS*	*NNS*	*NNS*	*NNS*	*NNS*	*NNS*	*NNS*	Y	A/G/V	·	·	·	·	·	·	M	D	Y	13
H3-13c	A	R	*NNS*	*NNS*	*NNS*	*NNS*	*NNS*	*NNS*	*NNS*	*NNS*	W/S/A/G	A/G/V	·	·	·	·	·	·	M	D	Y	13
H3-13d	A	R/K	*XYZ*	*XYZ*	*XYZ*	*XYZ*	*XYZ*	*XYZ*	*XYZ*	*XYZ*	Y	A	·	·	·	·	·	·	M	D	Y	13
H3-13e	A	R/K	*XYZ*	*XYZ*	*XYZ*	*XYZ*	*XYZ*	*XYZ*	*XYZ*	*XYZ*	W/S/A/G	A	·	·	·	·	·	·	M	D	Y	13
H3-13f	A	R/K	*XYZ*	*XYZ*	*XYZ*	*XYZ*	*XYZ*	*XYZ*	*XYZ*	*XYZ*	Y	A/G/V	·	·	·	·	·	·	M	D	Y	13
H3-13g	A	R/K	*XYZ*	*XYZ*	*XYZ*	*XYZ*	*XYZ*	*XYZ*	*XYZ*	*XYZ*	W/S/A/G	A/G/V	·	·	·	·	·	·	M	D	Y	13
H3-14a	A	R/K	*XYZ*	*XYZ*	*XYZ*	*XYZ*	*XYZ*	*XYZ*	*XYZ*	*XYZ*	*XYZ*	Y	A	·	·	·	·	·	M	D	Y	14
H3-14b	A	R/K	*XYZ*	*XYZ*	*XYZ*	*XYZ*	*XYZ*	*XYZ*	*XYZ*	*XYZ*	*XYZ*	W/S/A/G	A/G/V	·	·	·	·	·	M	D	Y	14
H3-15a	A	R/K	*XYZ*	*XYZ*	*XYZ*	*XYZ*	*XYZ*	*XYZ*	*XYZ*	*XYZ*	*XYZ*	*XYZ*	Y	A/G/V	·	·	·	·	M	D	Y	15
H3-15b	A	R/K	*XYZ*	*XYZ*	*XYZ*	*XYZ*	*XYZ*	*XYZ*	*XYZ*	*XYZ*	*XYZ*	*XYZ*	W/S/A/G	A/G/V	·	·	·	·	M	D	Y	15
H3-16a	A	R	*XYZ*	*XYZ*	*XYZ*	*XYZ*	*XYZ*	*XYZ*	*XYZ*	*XYZ*	*XYZ*	*XYZ*	*XYZ*	W/S/A/G	A/G/V	·	·	·	M	D	Y	16
H3-16b	A	R	*XYZ*	*XYZ*	*XYZ*	*XYZ*	*XYZ*	*XYZ*	*XYZ*	*XYZ*	*XYZ*	*XYZ*	*XYZ*	Y	A/G/V	·	·	·	M	D	Y	16
H3-17a	A	R	*XYZ*	*XYZ*	*XYZ*	*XYZ*	*XYZ*	*XYZ*	*XYZ*	*XYZ*	*XYZ*	*XYZ*	*XYZ*	*XYZ*	W/S/A/G	A/G/V	·	·	M	D	Y	17
H3-17b	A	R	*XYZ*	*XYZ*	*XYZ*	*XYZ*	*XYZ*	*XYZ*	*XYZ*	*XYZ*	*XYZ*	*XYZ*	*XYZ*	*XYZ*	Y	A/G/V	·	·	M	D	Y	17
H3-18a	A	R	*XYZ*	*XYZ*	*XYZ*	*XYZ*	*XYZ*	*XYZ*	*XYZ*	*XYZ*	*XYZ*	*XYZ*	*XYZ*	*XYZ*	*XYZ*	W/S/A/G	A/G/V	·	M	D	Y	18
H3-18b	A	R	*XYZ*	*XYZ*	*XYZ*	*XYZ*	*XYZ*	*XYZ*	*XYZ*	*XYZ*	*XYZ*	*XYZ*	*XYZ*	*XYZ*	*XYZ*	Y	A/G/V	·	M	D	Y	18
H3-19	A	R	*XYZ*	*XYZ*	*XYZ*	*XYZ*	*XYZ*	*XYZ*	*XYZ*	*XYZ*	*XYZ*	*XYZ*	*XYZ*	*XYZ*	*XYZ*	*XYZ*	Y	A/G/V	M	D	Y	19

Designs for CDR-H3 sequences with lengths of seven to 19 residues are listed. CDR-H3 positions 95–102 and a framework position 94 were diversified (Kabat numbering).[34] Degeneracies are shown as either degenerate codons (italics) or amino acids (plain text). The XYZ codon is a modified version of the NNK codon with unequal proportions of nucleotides (see Materials and Methods).

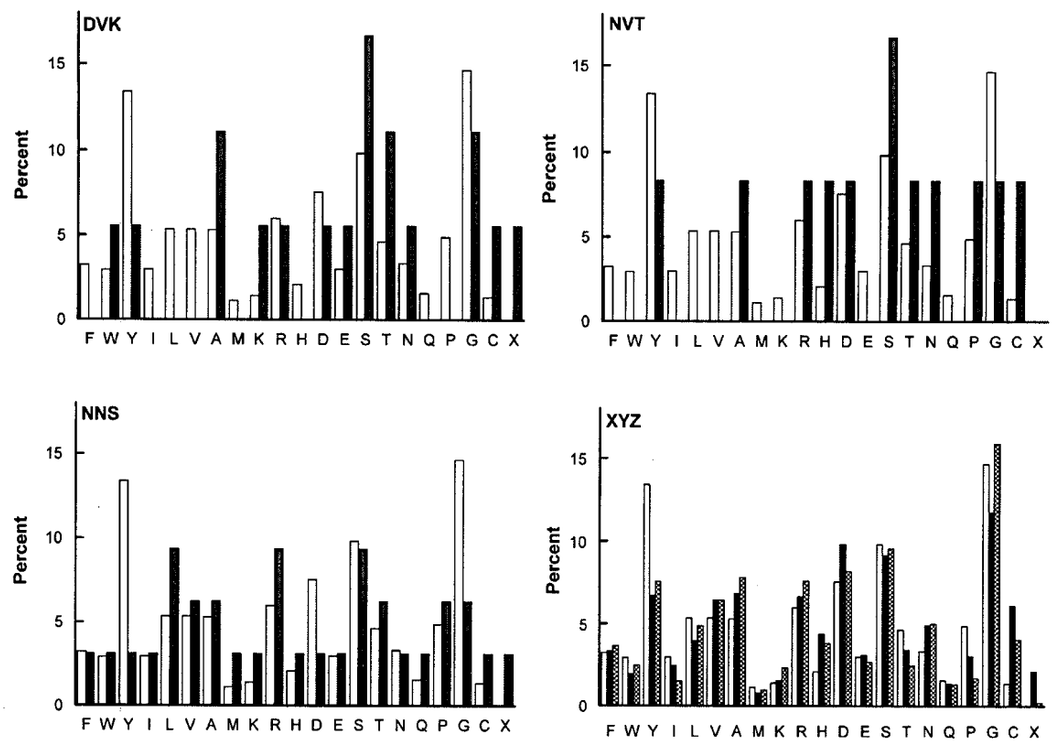

Figure 2. Relative amino acid composition of human CDR-H3 sequences compared to the compositions coded by various degenerate codons. The occurrences of each amino acid within the region bounded by position 94 and the position preceding position 101 were calculated for over 3600 human antibodies from Kabat database (white bars). The theoretical compositions of amino acids coded by DVK, NVT, NNS (or NNK) or XYZ (black bars) and the actual composition by sequencing 150 clones of XYZ-coded libraries (grey bars) were compared to the natural frequencies (white bars). The standard single-letter code for amino acids was used and X represents stop codons. See Materials and Methods for a detailed description of the XYZ codon.

specific binding clones were obtained with relatively high frequency at round 4 (Table 6). For each of the 13 antigens, between two and 15 unique clones were found by sequencing five to 72 binding clones (Table 6). Affinities of these unique clones were measured with phage competition ELISAs. For nine out of the 13 antigens, we identified antibodies with better than 10 nM affinities, and for the rest of the antigens, low nanomolar binders (25–130 nM) were found and the highest-affinity clones were often the dominant clones. The heavy chain CDR sequences of the Fabs selected for binding to some of the antigens are shown in Table 7. Some of the best clones were purified as free Fab or IgG proteins and binding affinities were confirmed with solution-phase binding assays (Table 7).

Next we compared the distribution of lengths and amino acid composition of the CDR-H3 sequences of the 70 unique binding clones isolated against the 13 protein antigens to those observed in natural CDR-H3 sequences (Figure 3).[32] The distribution of length of the synthetic CDR-H3s was similar to that of natural CDR-H3s in that lengths of between 11 and 13 amino acid residues were

Table 6. The sorting results of Lib-3 with expanded CDR-H3 length

Protein antigen	Positive (%)	Unique/sequenced
mNKG2D ECD	88	6/28
mIgE	84	6/26
mTissue Factor	34	4/32
mAPRIL ECD	56	15/18
TENB2 ECD	16	5/10
c-Met ECD	6	5/5
HGF 2 chain	87	3/56
Matriptase	12	3/6
Cthrc1 full length	51	3/24
Cthrc1 short form	83	5/72
Cystatin S	83	2/40
TFF-1	79	2/37
SPINK4	89	11/42

The performance of Lib-3 against 13 targets after four rounds of selection is shown with the percentage of specific binding clones (Positive (%)) and the number of unique sequences amongst the number sequenced (Unique/Sequenced). Antigens include murine proteins (indicated by the prefix m), and human proteins. The following abbreviations are used: Cthrc 1, collagen triple helix repeat containing 1; TFF-1, trefoil factor 1; SPINK4, serine protease inhibitor Kazal type 4.

Table 7. Sequences of the randomized heavy chain CDR residues of the some selected antibodies from Lib-3

Antigens	CDR-H1				CDR-H2								CDR-H3															CDR-H3 Length	IC_{50} (nM)	CDR-H3 Oligo source	CDR-H3 Codon
	30	31	32	33	49	50	52	53	54	56	58	93	94	95	96	97	98											101	102				
mNKG2D	T	G	S	G	G	I	A	A	D	S	Y	A	R	A	W	F	N	G	V	·	·	·	·	·	·	·	·	M	D	Y	9	> 2000	H3-9b	*NNS*
	S	D	Y	D	G	F	D	H	G	Y	Y	A	R	A	R	Q	R	·	·	·	·	·	·	·	·	·	·	F	D	Y	7	684	H3-7b	*XYZ*
	S	D	S	D	G	F	A	A	G	Y	Y	A	R	G	G	L	N	G	L	W	·	·	·	·	·	·	·	F	D	Y	10	222	H3-10d	*XYZ*
	N	G	N	W	A	W	Y	A	G	D	Y	A	R	L	R	N	V	·	·	·	·	·	·	·	·	·	·	F	A	Y	7	3[a]	H3-7b	*XYZ*
	N	D	T	Y	G	F	D	D	G	Y	Y	A	R	G	S	D	G	S	D	N	R	P	F	Y	A	·	·	M	D	Y	15	578	H3-15a	*XYZ*
mAPRIL	S	D	Y	D	G	W	S	D	G	S	N	A	R	V	L	D	N	F	L	Y	G	·	·	·	·	·	·	M	D	Y	11	50	H3-11a	*NNS*
	T	D	Y	A	G	F	Y	D	D	A	N	A	H	D	Q	G	W	I	G	W	G	·	·	·	·	·	·	M	D	Y	11	4.1[a]	H3-11d	*XYZ*
	N	D	S	D	A	E	T	Y	S	Y	N	A	R	W	D	E	W	H	N	H	W	D	·	·	·	·	·	M	D	Y	12	100	H3-12e	*XYZ*
	S	D	Y	S	A	W	S	A	D	S	N	A	R	L	M	L	A	P	W	W	G	V	·	·	·	·	·	M	D	Y	12	> 1000	H3-12a	*NNS*
	S	G	N	Y	G	W	S	N	N	S	Y	A	R	G	G	D	Y	S	P	C	G	Y	G	·	·	·	·	M	D	Y	13	> 1000	H3-13b	*NNS*
	T	D	Y	A	A	Y	S	N	N	S	N	A	R	D	V	D	E	G	G	M	G	V	V	S	V	·	·	M	D	Y	15	100	H3-15b	*XYZ*
	T	N	N	G	G	W	N	S	N	S	Y	A	R	Y	M	Y	E	E	A	G	W	D	L	G	G	·	·	M	D	Y	15	80	H3-15b	*XYZ*
	N	D	T	W	A	G	T	A	N	A	N	A	R	D	Y	A	W	L	V	N	S	W	N	Y	Y	G	·	M	D	Y	16	50	H3-16b	*XYZ*
	T	N	Y	A	A	W	N	D	G	S	N	A	R	D	G	G	D	F	G	R	R	D	Y	G	W	A	·	M	D	Y	16	50	H3-16a	*XYZ*
	T	S	S	D	G	F	S	T	G	A	N	A	R	N	I	L	A	Y	H	S	N	W	N	E	I	W	G	V	·	M	D	Y	18	100	H3-18a	*XYZ*
	N	D	N	W	G	D	S	D	G	A	Y	A	R	E	Y	D	G	S	Y	T	V	Q	N	N	D	A	Y	V	·	M	D	Y	18	ND	H3-18b	*XYZ*
	N	D	Y	S	A	G	N	T	N	S	N	A	R	D	W	G	R	F	H	L	H	D	L	Y	F	S	A	V	·	M	D	Y	18	50	H3-18a	*XYZ*
	S	D	T	W	A	I	N	S	N	A	N	A	R	D	S	N	L	F	E	I	A	S	Y	S	D	L	S	Y	A	M	D	Y	19	50	H3-19	*XYZ*
	S	N	Y	G	G	F	Y	D	D	T	N	A	R	D	N	Y	V	G	G	G	V	F	R	D	G	N	G	Y	A	M	D	Y	19	100	H3-19	*XYZ*
	N	D	N	W	G	W	S	A	N	A	Y	A	R	Q	D	V	G	F	G	D	Y	Y	L	G	A	Y	D	Y	G	M	D	Y	19	1.4[a]	H3-19	*XYZ*
mIgE	N	N	S	W	G	Y	S	S	G	S	N	A	R	E	G	R	T	V	K	Q	C	D	M	R	D	S	G	A		M	D	Y	18	ND	H3-18a	*XYZ*
	T	N	Y	G	A	V	N	A	S	S	N	A	R	M	D	W	D	H	D	G	G	V	·	·	·	·	·	·	·	M	D	Y	12	17	H3-12a	*NNS*
	S	S	S	S	G	Y	Y	T	D	Y	Y	A	R	L	G	V	S	P	G	A	·	·	·	·	·	·	·	·	·	M	D	Y	10	9.8	H3-10b	*NNS*
	N	G	S	W	G	Y	N	A	D	T	D	A	R	S	I	E	D	G	G	A	S	G	S	V	·	·	·	·	·	M	D	Y	14	ND	H3-14b	*XYZ*
	S	G	S	S	G	Y	Y	T	D	Y	Y	A	R	L	G	V	S	P	G	A	·	·	·	·	·	·	·	·	·	M	D	Y	10	16	H3-10b	*NNS*
	S	S	Y	S	G	R	Y	A	D	D	Y	A	R	S	D	R	V	C	G	D	V	G	V	·	·	·	·	·	·	M	D	Y	13	ND	H3-13c	*NNS*
mTF	S	D	Y	Y	G	I	N	S	D	A	Y	A	R	D	C	G	D	E	L	M	G	H	C	G	G	·	·	·	·	M	D	Y	15	11	H3-15b	*XYZ*
	S	D	S	D	A	A	N	A	G	Y	Y	A	R	T	M	N	N	R	G	A	·	·	·	·	·	·	·	·	·	M	D	Y	10	ND	H3-10b	*NNS*
	T	G	N	A	G	W	S	P	S	S	Y	A	R	R	R	G	A	A	W	V	W	Y	V	·	·	·	·	·	·	M	D	Y	13	ND	H3-13b	*NNS*
	S	N	N	A	A	R	A	Y	G	S	D	A	R	R	C	V	S	·	·	·	·	·	·	·	·	·	·	·	·	F	A	Y	7	ND	H3-7b	*XYZ*

Deduced amino acid sequences, CDR-H3 lengths and sources of some selected clones from Lib-3 are listed. CDR-H3 sequences in bold text in these clone and other clones from Lib-3 were used for the calculations of amino acid compositions depicted in Figure 3. Affinities were measured with phage competition ELISAs. ND indicates that these values were not determined.

[a] Some clones were purified as free Fab (mAPRIL- and mNKG2D-binding clones) and/or IgG (mNKG2D-binding clone) proteins and their affinities were measured with solution competition binding ELISAs as IC_{50} values.

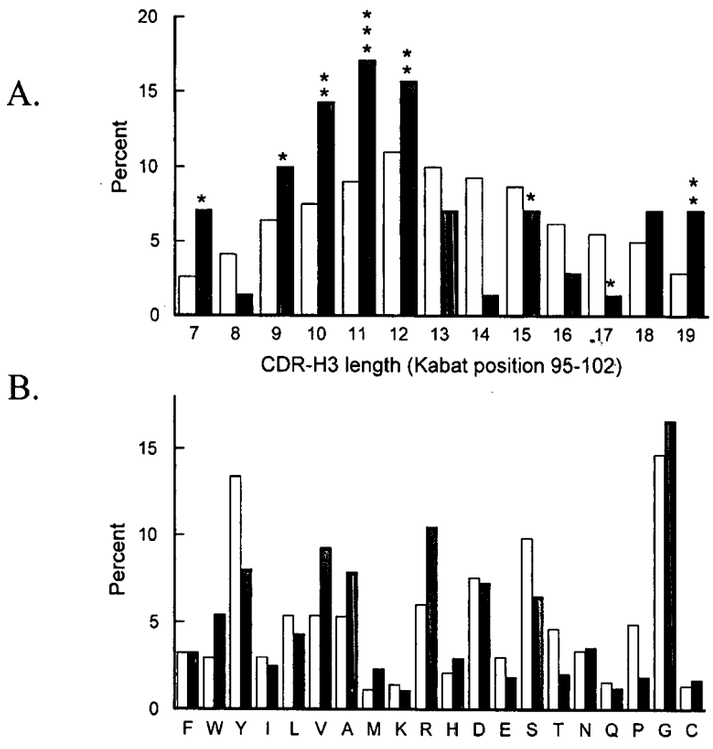

Figure 3. The CDR-H3 length distribution and amino acid composition of binding clones from Lib-3, which contains libraries with CDR-H3 sequences ranging from seven to 19 residues in length. The sequences of 70 clones selected for binding to 13 antigens were compiled to determine (A) the distribution of CDR-H3 lengths and (B) the amino acid composition (black bars) and compared to Kabat Database[32] for CDR-H3 length and amino acid composition (white bar). The asterisks in (A) indicate the CDR-H3 length for the best binding clone isolated against each of the 13 antigens.

most prevalent (Figure 3A). The CDR-H3 lengths that contributed to the highest-affinity clones for the 13 antigens (asterisks in Figure 3A) spanned the entire allowed range of lengths. Furthermore, the amino acid composition of the synthetic CDR-H3s was similar to that of natural CDR-H3s (Figure 3B). As we characterize more functional antibodies from this library, it will be interesting to further compare the sequences to those of natural antibodies.

Affinity maturation by the introduction of light chain diversity

In all of the libraries described above, the light chain was held constant and diversities were introduced in the heavy chain CDRs alone. Thus, we next investigated whether we could exploit light chain diversity as a means of further improving the affinity of a selected heavy chain sequence. We chose light chain CDR positions for the introduction of diversity based on the principles applied to the heavy chain CDR design; positions that were highly solvent-accessible in the crystal structure of h4D5[42] and/or were highly variable in the Kabat database were randomized using the diversity of natural light chains as a guide (Table 8).[34] Target diversity was defined by calculating the prevalence of the different amino acids within each light chain position in approximately 1500 human kappa light chain sequences, as described above for CDR-H1 and CDR-H2. The randomization at each site was tailored to ideally cover at least 70% of the natural diversity without encoding additional, rare amino acids (Table 8). In total, 13 positions within the three light chain CDRs were chosen as sites for the introduction of additional diversity (Figure 1).

The light chain library was combined with the heavy chain sequence of anti-mVEGF clone mV401 (designated G6) displayed as Fab. Following stringent selections for high-affinity binding (see Materials and Methods), 70 clones were sequenced and we found that most of the clones were unique. The results suggested that mutations in the light chain are sufficiently diverse that the library contained many clones that retained or improved upon the binding affinity of the G6 parent. A high-throughput affinity-screening assay was used to estimate the affinities of the selected clones, and 16 G6 descendants with new light chains and improved affinities were identified (Figure 4A). All of the improved G6 descendants had new CDR-L3 sequences but most retained the original CDR-L1 and CDR-L2 sequences. This could be due to the design of the template with stop codon embedded only in CDR-L3 and therefore the high occurrence of parental CDR-L1 and CDR-L2.

Three of the affinity-matured Fabs (G6-8, G6-23 and G6-31) were purified as Fab proteins, and their affinities for mVEGF were compared to G6 by using surface plasmon resonance (SPR) tech-

Table 8. Target diversity and design diversity of CDR-L1, CDR-L2 and CDR-L3

Positions	Target diversity										Design diversity			
	Prevalence in natural antibodies%										Codon	Residues encoded	Coverage%	Oligonucleotide
L1-D28	S	N	V	D	G	I					*RDT*	SNVDGI	94	L1
	33	17	17	12	12	3								
L1-V29	I	S	V	G	N						*RKT*	ISVG	86	L1
	40	18	16	12	10									
L1-S30	S	N	K	G	R	Y	T	D	A		*RVM*	SNKGRTDA E	93	L1
	55	11	11	6	5	4	2	2	1					
L1-T31	S	N	T	R	I	D	K	G			*ANW*	SNTRIK	94	L1
	44	32	11	3	2	2	2	1						
L1-A32	Y	N	W	F	S	D	R				*THT*	YFS	76	L1
	67	8	6	5	4	3	2							
L1-V33	L	V									*CTG*	L	94	L1
	94	2												
L2-S50	G	A	D	W	K	L	E	S			*KBG*	GAWLS V	65	L2
	25	22	19	10	8	6	3	2						
L2-F53	S	N	T	K	I	R					*AVC*	SNT	92	L2
	36	29	27	3	2	1								
L2-Y55	A	Q	E	F	D						*GMA*	AE	64	L2
	45	24	19	3	3									
L3-S91	Y	S	R	A	G	H					*TMT*	YS	66	L3 a,b
	54	12	11	7	4	3					*SRT*	RGH **D**	18	L3 c,d
L3-Y92	Y	G	N	S	D	L	T	H	I		*DMC*	YNSDT **A**	61	L3 a-d
	23	22	15	12	7	6	4	3	2					
L3-T93	S	N	Q	T	H	G	D	R			*RVT*	SNTGD **A**	79	L3 a-d
	46	21	7	6	4	3	3	2						
L3-T94	S	T	W	Y	L	F	A	P	V	I	*NHT*	STYLFAPVI **NDH**	79	L3 a-d
	24	23	18	11	7	5	3	3	2	1				
L3-P96	L	Y	W	F	I	R	P				*TWT*	YF	22	L3 a,c
	22	13	11	9	7	7	3				*YKG*	LLWR	40	L3 b,d

Positions chosen for randomization in CDR-L1, CDR-L2 and CDR-L3 are listed with h4D5 residues. Target diversity is a group of residues that cover over 90% of approximately 1600 human antibodies in the Kabat database.[34] The prevalence (%) of each amino acid at a given position is shown. Design diversity is a group of residues encoded by a tailored degenerate codon (italics) chosen so that the coverage of natural target diversity by one codon or a combination of codons is close to 70% or higher. Each codon was designed to minimize amino acids not present in the target diversity (bold text). Several oligonucleotides were mixed for the library construction as described in Materials and Methods.

nology with VEGF immobilized on a sensor chip for the rate of dissociation (off rate, k_{off}) and fluorescence quenching in solution for the rate of association (on rate, k_{on}) (Figure 4A and B) From initial SPR experiments, it was noted that there was significant k_{on} improvement, but the k_{on} determinations from SPR method for the affinity-improved Fabs were not statistically acceptable. The estimated k_{on} of the improved clones were about three- to sixfold lower than the measurements by solution-based fluorescence quenching assay, whereas k_{on} measurements for parent G6 Fab from SPR was statistically sound and within 1.2-fold difference with fluorescence quenching assays. It is possible that using BIAcore SPR technology for fast on-rate measurements was limited by the complex flow dynamics, or there could be some differences in protein behaviors between the parent clone and affinity-improved clones, though aggregation problems were not observed with these proteins. On the basis of the fluorescence assays, the three Fabs exhibited improvements over G6 in the on-rate by six-, eight- or 20-fold for G6-8, G6-31 or G6-23, respectively. Fab-G6-31 also exhibited an approximately fourfold improvement in the off-rate, and as a result, the affinity of Fab-G6-31 (K_d = 16 pM) and Fab-G6-23 (K_d = 21 pM) was ~40–60-fold improved compared to the G6 parent (K_d = 910 pM). It was consistent with the solution phase competition assays, which showed a 20–60-fold improvement in IC_{50} value for G6-31 (30 pM) or G6-23 (10 pM) in comparison with G6 (0.67 nM). We applied the light chain affinity maturation strategy to five other heavy chain sequences and have observed tenfold to 30-fold improvements in binding affinities (data not shown). Unlike G6, many improved clones adopted new sequences for all three light chain CDRs. Thus, our two-step strategy of heavy chain CDR randomization followed by light chain CDR randomization has proven capable of generating Fabs with binding affinities in the sub-nanomolar and even low picomolar range (Figure 5).

Discussion

We have constructed fully synthetic antibody phage libraries with a single Fab framework and randomized CDRs in a two-step manner: heavy chain and then light chain. The strategy of mimicking the biased diversity of natural CDRs by fine-tuned synthetic design was employed to restrict the degeneracy of the synthetic antibody library, and to generate antibodies with sequences similar to those of natural antibodies. Fabs with affinities

(A)

Clone	CDR-L1						CDR-L2			CDR-L3					Affinity			
	28	29	30	31	32	33	50	53	55	91	92	93	94	96	IC50 (nM)	k_{on} (10^5 $M^{-1}S^{-1}$)	k_{off}(10^{-4} S^{-1})	Kd (nM)
G6	D	V	S	T	A	V	S	F	Y	S	Y	T	T	P	0.60	1.75 (1.93)	1.60	0.91
G6-6a	N	V	A	T	F	L	S	N	A	S	Y	G	S	L	0.02	n/d	n/d	n/d
G6-23	D	V	S	T	A	V	S	F	Y	G	Y	A	N	W	0.01	56.6	1.21	0.021
G6-31	D	V	S	T	A	V	S	F	Y	G	Y	G	N	F	0.03	21.6	0.35	0.016
G6-2a	D	V	S	T	A	V	S	F	Y	G	Y	G	S	L	0.05	n/d	n/d	n/d
G6-2b	G	G	T	T	S	L	S	N	A	G	Y	G	S	F	0.07	n/d	n/d	n/d
G6-6b	I	V	T	N	S	L	L	S	A	G	A	T	D	R	0.22	n/d	n/d	n/d
G6-48	D	V	S	T	A	V	S	F	Y	G	T	S	S	P	0.06	n/d	n/d	n/d
G6-1a	D	V	S	T	A	V	S	F	Y	G	T	G	N	P	0.02	n/d	n/d	n/d
G6-8	D	V	S	T	A	V	S	F	Y	G	A	G	S	L	0.06	16.8	1.29	0.077
G6-3	D	V	S	T	A	V	A	F	Y	G	S	G	H	F	0.60	n/d	n/d	n/d
G6-34	D	V	S	T	A	V	S	F	Y	G	T	G	S	L	0.07	n/d	n/d	n/d
G6-4a	D	V	S	T	A	V	S	F	Y	G	S	G	N	F	0.06	n/d	n/d	n/d
G6-1a	D	V	S	T	A	V	S	F	Y	G	T	G	N	L	0.07	n/d	n/d	n/d
G6-4b	D	V	S	T	A	V	S	F	Y	G	S	G	S	F	0.04	n/d	n/d	n/d
G6-5	D	V	S	T	A	V	S	F	Y	G	A	G	S	F	0.04	n/d	n/d	n/d
G6-15	D	V	S	T	A	V	S	F	Y	G	V	N	S	L	0.06	n/d	n/d	n/d

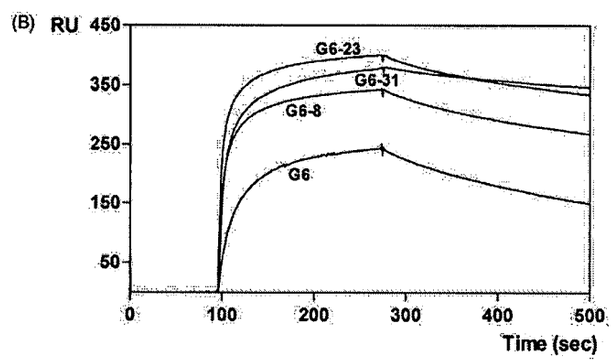

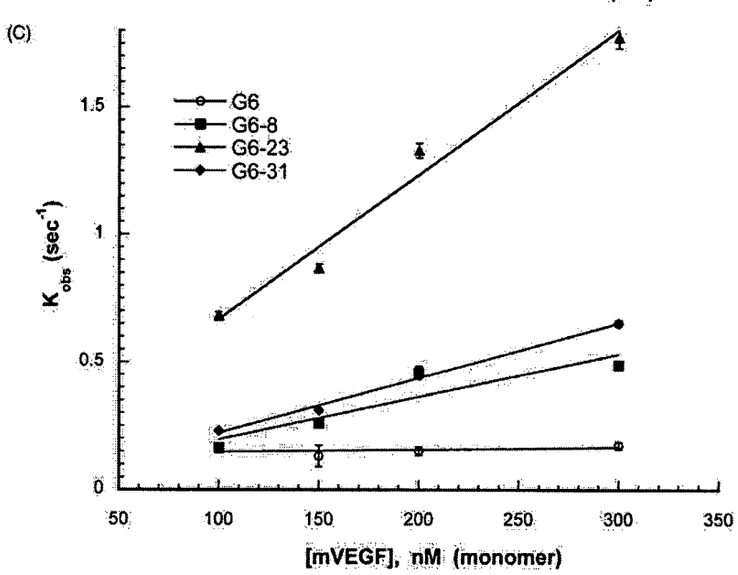

Figure 4. The affinity improvement of the anti-mVEGF Fab G6 by light chain randomization. Light chain CDR residues were chosen and randomized as described in Table 8, and in Materials and Methods. (A) The deduced amino acids sequences of the improved G6 clones at randomized light chain positions are shown. The residues that were the same as the parental G6 sequence are shaded. Each clone was analyzed with a competition phage ELISA to compare its affinity with the G6 parent as an IC_{50} value. The errors from three independent assays were in the range of 5–50%. Binding kinetic parameters of the Fab proteins of clones G6, G6-23, G6-31, G6-8 were determined with fluorescence quenching solution assay for k_{on} and surface plasmon resonance experiments using a BIAcore™ – 2000 for k_{off} at 25 °C. For G6, k_{on} from BIAcore SPR method is given in parentheses. The K_d values were derived by dividing k_{off} with k_{on}. The representative data from three sets of experiments are shown and the errors were within 50%. See Materials and Methods for details. (B) The sensograms for injection of 500 nM Fab at 37 °C over mVEGF immobilized

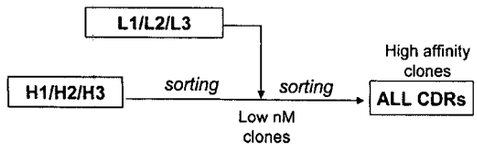

Figure 5. Two-step method of obtaining high-affinity antibodies from synthetic antibody phage libraries. Libraries with randomized heavy chain CDRs were used in the first step to select low nanomolar binders against antigen. If higher affinities are needed, the light chain CDR was randomized to obtain high-affinity clones in the second step.

in the low nanomolar range were obtained for most antigens from the first step of selection with heavy chain libraries. If a clone showed desired properties and higher affinities were required, the second step of affinity improvement could then be carried out to yield antibodies with sub-nanomolar or even picomolar affinities.

The ultimate goal for a combinatorial antibody library is to have a universal library capable of generating high-affinity antibodies against any antigen without the need for affinity maturation; this has been difficult to achieve for synthetic antibody libraries using a single-template framework. We have advanced significantly toward that goal by producing a library that can reliably provide antibodies of low nanomolar affinities to many target antigens. This library is comparable to other libraries utilizing multiple frameworks. Many elements contributed to the success; the significant increase in binding affinities from ~100 nM (Lib-1) to sub-nanomolar and low nanomolar (Lib-2) arising from a difference in the diversity design indicates clearly that the diversity design can play an important role in the performances of synthetic antibody libraries. Moreover, the optimized framework used to support the functional display of diverse CDRs was an important foundation for success. The framework of humanized 4D5, derived from one of the most frequently used germline origin (V_k1-1 and V_H3-23), was used, since it displayed well on phage as Fab and scFv, monovalently or bivalently.[30,38] The Fab format was chosen, since it is stable and converts reliably to IgG, even though it displayed less well than scFv. The option of bivalent Fab display increased avidity to assist in the isolation of weak-affinity clones but still allowed selection based on affinity. Fab and Fab.zip libraries resulted in smaller numbers of distinct clones than scFv libraries, but the best clones from each selection provided information on the performance of the library, and various diversity designs were clearly differentiated without having to sort through the larger number of different clones isolated from an scFv library.[30]

The optimum diversity design requires a balance between having diversity large enough to include high-affinity antibodies and restrictive enough in sequence space to be productive, so that diversity would not overly exceed the capacity of the library ($\sim 10^{10}$). In our heavy chain library, we chose 17 residues for randomization. Without tailored codons to restrict the diversity, the degeneracy ($32^{17} = 10^{25}$) would be overwhelmingly greater than the actual library size. While we found that restricted diversity in CDR-H1 and CDR-H2 improved library performance, we found that the libraries benefited from highly diverse CDR-H3 sequences, even at the cost of having a large DNA degeneracy. Thus, our successful Fab libraries proved to be those in which CDR-H1 and CDR-H2 diversities were highly restricted but CDR-H3 was highly diverse in both length and amino acid composition.

The diversity of natural antibodies provided the necessary guidance for where and how to restrict synthetic diversity. The amino acid compositions at most CDR positions of natural antibodies are highly biased, and the diversity increases incrementally from CDR-H1 to CDR-H2 to CDR-H3, with CDR-H3 being the most diverse of the three. In our design, we devoted 10^2, 10^4 and $>10^6$–10^{20} (length 7–19) in designed diversity for CDR-H1, CDR-H2 and CDR-H3, respectively, to mimic that hierarchy. Further, when examining the diversity within natural CDR-H1 and CDR-H2 sequences, we observed a hierarchy among the different positions. For example, positions 33 and 50 are the most diverse positions in CDR-H1 and -H2, respectively (Table 1). It is interesting to note that residues at these positions cluster structurally near the center of the antigen-binding site where CDR loops H1, H2, H3 and L3 are in close proximity (Figure 1). We believe that this arrangement provides a glimpse into how antibodies harness the power of the combinatorial diversity of the CDR loops, as the residues within this region (e.g. heavy chain positions 33, 50, 95, and 100 and light chain positions 91 and 96) have often been shown to be functionally important for antigen binding.[43,44] It will be interesting to see if these positions will be the functional hotspots for the antibodies derived from our synthetic phage libraries since the diversity design of the library had attempted to mimic this hierarchy (Table 1).

BIAcore chip demonstrate the off rate and on rate improvements. (C) From the fluorescence quenching assays, the observed rate (k_{obs}, s^{-1}) of complex formation between G6 and variant Fabs and mVEGF as the rate of the decrease of fluorescence intensity was plotted against the concentrations of mVEGF (nM) used and the slope based on the pseudo-first-order analysis was the on-rate ($\times 10^9\ M^{-1}\ s^{-1}$).

CDR-H3 design was shown to be key for obtaining high-affinity binding clones. We observed that restricting CDR-H3 diversity with a tailored genetic codon (DVK) in scFv (Lib-v1), Fab (Lib-1-Fab) and Fab-zip (Lib-1-Fab.zip) libraries yielded antibodies against mVEGF with moderate affinities in the 100 nM range. When all 20 amino acids were allowed in CDR-H3 in subsequent libraries (Lib-2), the affinities of the positive clones improved to the low nanomolar or even sub-nanomolar range. This could arise if some amino acid types were needed for optimal binding sequences but not included or in low supply in the restricted CDR-H3 codons, or if the prevalence of the undesired amino acid types was decreased in the codon that covers all 20 amino acids. The preference or rejection of particular amino acid types could certainly vary with individual antigen target of different chemical and structural characteristics. It is unlikely that any one design for CDR-H3 will be universally optimal and equally productive. Indeed, the number of acquired unique clones varied greatly from antigen to antigen. We rely on the supposition that multiple solutions exist for each protein–protein interaction. NNS and XYZ may not be the final synthetic design for CDR-H3, but they clearly were sufficiently productive in the present work. With the recent availability of trinucleotides‡, the coverage of natural diversity in CDR-H3 could conceivably be improved by increasing the prevalence of Tyr as in natural antibodies, which XYZ does not mimic adequately. As we expanded the diversity of CDR-H3 lengths in Lib-3, we observed that the best binding clones for different antigens utilized different CDR-H3 lengths. These results suggest that highly diverse CDR-H3 sequences, in terms of both length and amino acid composition, were important for obtaining high-affinity clones from the synthetic antibody libraries. This is consistent with the fact that in natural antibodies, CDR-H3 is the most diverse hypervariable region, and it is a major determinant for binding specificity and affinity.[26,27,35–37] Indeed, one of the first experiments with synthetic antibody libraries demonstrated that CDR-H3 diversity alone could generate antibodies with respectable affinities in the micromolar to sub-micromolar range.[18]

Besides optimizing the diversity design, the other important element for antibody phage library is the library size. For any combinatorial library intended for use in finding novel binding clones, the ideal situation is a library sufficiently large that it fully represents the designed sequence space. However, for antibody libraries, or other combinatorial libraries, the sequence space is often bigger than library size due to practical limitation in generating libraries. Thus, larger libraries can be expected to perform better. For natural antibody libraries, it was shown that the library size was important for finding high-affinity antibodies.[13,14] For our synthetic antibody library, we found that optimum diversity design, as well as library size, played a significant role. Phage libraries with diversities of 10^9–10^{10} could be constructed with relative ease using optimized methods,[45] but we observed that a larger library (Lib-2-DVK, 4.1×10^9) performed worse than a smaller library (Lib-2-NNS, 8×10^8) when they differed in diversity design. With any desired diversity design, a larger library will be beneficial if it narrows the gap between intended and actual library diversity. For our final library (Lib-3), we expanded the length of the CDR-H3. The degeneracies increased exponentially with increased lengths. Lib-3, in fact, had a wider gap between actual and designed degeneracy even with a library size of 4×10^{10}, than earlier libraries with restricted CDR-H3 lengths (e.g. Lib-2 of size $\sim 10^9$). XYZ was intended to narrow the gap by biasing the library toward productive sequences and it was quite successful. To further improve the library, reducing the gap will be important. Possible strategies include closer examination of the bias among different positions within CDR-H3 of different lengths and using trinucleotide synthesis to mimic the biased amino acid compositions for all three heavy chain CDRs.

It is a common notion that the light chain is much less important than the heavy chain for interacting with antigen. There were cases in natural antibodies where the light chain had no contact at all with antigen,[46] and indeed, the light chain has been totally dispensed within a significant proportion of the camelid immune repertoire.[47] Semi-synthetic libraries with multiple V_H germlines and synthetic CDR-H3 together with a single light chain was shown to be able to produced specific antibodies to some antigens with moderate affinities.[11] The heavy chain libraries we constructed with a single light chain yielded antibodies with high affinities and specificities. Altering light chain sequences, however, was known to influence the affinities of antibodies; one early example used light chain shuffling for affinity improvements.[48] Previous synthetic antibody libraries reported by others included mostly CDR-L3 in randomization together with heavy chain.[19,20,22] As we employed light chain randomization to improve the affinities of our antibodies from the heavy chain library, many new light chain sequences disrupted the antigen binding. In fact, over 80% of the light chain-randomized clones that displayed well lost their antigen-binding function (data not shown). Nevertheless, the remaining library members were sufficiently diverse to provide many solutions with improved binding affinities, and clones with improvements in both the on and off rates were identified. It will be interesting to compare the results of other methods for affinity maturation to those obtained from light chain randomization. For example, further limited randomization of selected heavy chain CDR sequences could lead to affinity

‡http://www.glenres.com

improvements, since the naïve library could not fully represent all possible heavy chain sequences.

In conclusion, fully synthetic antibody libraries were generated with a single framework by tailored randomization of the heavy chain CDRs to mimic natural diversity. Restricted diversity in CDR-H1 and CDR-H2 combined with high diversity in CDR-H3 was important for the generation of high-affinity Fabs from naïve synthetic repertoires. The affinity of selected heavy chain fragments could be further improved by the subsequent introduction of diversity in the light chain. In the end, low picomolar affinities were obtained with antibodies that contained synthetic diversity in the hypervariable loops.

Materials and Methods

Materials

Enzymes and M13-KO7 helper phage were from New England Biolabs. *E. coli* XL1-Blue was from Stratagene. Bovine serum albumin (BSA), ovalbumin, and Tween 20 were from Sigma. Neutravidin, casein and Superblock were from Pierce. Immobilized protein G and anti-M13 conjugated horse-radish peroxidase (HRP) were from Amersham Pharmacia. Maxisorp immunoplates were from NUNC (Roskilde, Denmark). Tetramethylbenzidine (TMB) substrate was from Kirkegaard and Perry Laboratories (Gaithersburg, MD). All protein antigens were generated by research groups at Genentech, Inc. DNA degeneracies were represented using the IUB code and represent equimolar mixtures unless indicated otherwise: N = A/C/G/T, D = A/G/T, V = A/C/G, B = C/G/T, H = A/C/T, K = G/T, M = A/C, R = A/G, S = G/C, W = A/T, Y = C/T.

Phagemid vectors for library construction

Phagemids pV0350-2b and pV0350-4, were designed to display h4D5 Fab monovalently or bivalently, respectively, on the surfaces of M13 phage particles. The vector pV0350-2b was constructed by modifying a previously described phagemid (pHGHam-gIII) that has been used for the phage display of human growth hormone (hGH) under the control of a phoA promoter.[38,49] An open reading frame in phGHam-gIII that encodes for the stII secretion signal sequence and hGH fused to the C-terminal domain of the M13 minor coat protein P3 (cP3) was replaced with a DNA fragment containing two open reading frames. The first open reading frame encoded for the h4D5 light chain and the second encoded for the variable (V_H) and first constant (C_H1) domains of the h4D5 heavy chain fused to cP3; each protein was directed for secretion by an N-terminal stII signal sequence. The amber stop codon between the heavy chain fragment and cP3 was deleted, as this modification has been shown to increase the levels of Fab displayed on phage.[38] An epitope tag (gD tag, amino acid sequence: MADPNRFRGKDLGG)[50] was added to the C terminus of the h4D5 light chain. The vector for bivalent display (pV0350-4) was identical with pV0350-2b, except for the insertion of a DNA fragment encoding for a GCN4 leucine zipper between the heavy chain C_H1 domain and cP3 as described.[38] The light chain gene was further modified in both phagemids at three positions to encode for amino acids most commonly found in the Kabat database of natural antibody sequences; specifically, Arg66 was changed to Gly and Asn30 and His91 were changed to Ser. These changes were found to increase Fab expression and display on phage. Standard molecular biology techniques were used for vector and library construction, as described.[45] Site-directed mutagenesis was performed using the method of Kunkel *et al.*[51]

Library construction

Phage-displayed libraries were generated using oligonucleotide-directed mutagenesis and "stop template" versions of pV0350-2b or pV0350-4 as described.[30] Stop codons (TAA) were embedded in all three heavy-chain CDRs. These were repaired during the mutagenesis reaction by a mixture of degenerate oligonucleotides that annealed over the sequences encoding for CDR-H1, -H2 and -H3 and replaced codons at the positions chosen for randomization with tailored degenerate codons. Mutagenesis reactions were electroporated into *E. coli* SS320 cells, and the cultures were grown overnight at 30 °C in 2YT broth supplemented with KO7 helper phage, 50 μg/ml of carbenicillin and 50 μg/ml of kanamycin. Phage were harvested from the culture medium by precipitation with PEG/NaCl as described.[45] Each electroporation reaction used $\sim 10^{11}$ *E. coli* cells and ~ 10 μg of DNA and resulted in 1×10^9–5×10^9 transformants.

Three distinct libraries were made with degenerate oligonucleotides tailored to mimic the natural diversity of CDR-H1 and CDR-H2 (Table 1): library 1 with Fab or Fab.zip template (Lib-1-Fab and Lib-1-Fab.zip), library 2 (Lib-2) with Fab template and library 3 (Lib-3) with Fab.zip template. Two to four oligonucleotides for CDR-H1 and CDR-H2 were combined to increase the coverage of natural diversity. Lib-1 used oligonuleotides H1a and H1b in the ratio of 2 : 1 for CDR-H1, and H2a and H2b in the ratio of 1 : 2 for CDR-H2. Lib-2 used oligonucleotides H1a-d (ratio 2 : 1 : 2 :1) for CDR-H1 and H2a and H2b (ratio 1 : 2) for CDR-H2. Lib-3 used oligonucleotides H1a and H1b (ratio 2 : 1) and H2a-c (ratio 1 :2 : 0.1) for CDR-H1 and CDR-H2, respectively (see Table 1 for a description of the oligonucleotides).

For positions 95–100 in CDR-H3, Lib-1 used a DVK codon, which encompasses 18 codons and encodes for 12 amino acids (Tyr, Ala, Arg, His, Asp, Ser, Thr, Asn, Pro, Gly, Trp and Cys) (Table 2), and the CDR-H3 length was fixed at 11 amino acid residues (positions 95–102). Lib-2 consists of a set of libraries that use different degenerate codons (DVK, NVT or NNS) for CDR-H3 (Table 2). Lib-2-DVK used three lengths of CDR-H3 (11, 12, or 13 amino acid residues) with DVK codons and was generated with three separate electroporations, one for each CDR-H3 length. The NVT codon encompasses 12 codons and encodes for 11 amino acids (Tyr, Ala, Arg, His, Asp, Ser, Thr, Asn, Gly, Pro, and Cys) while the NNS codon encompasses 32 codons and encodes for all 20 amino acids. Lib-2-NVT and Lib-2-NNS were constructed separately, but in each case, the different CDR-H3 oligonucleotides were combined in a single mutagenesis reaction. Lib-3 consists of a set of libraries with expanded CDR-H3 lengths containing either NNS codons (or NNK codons) or a modified version of the NNS codon (the XYZ codon) that contained unequal nucleotide ratios at each position of the codon triplet. X contained 38% G, 19% A, 26% T and 17% C; Y contained 31% G, 34% A, 17% T and 18% C; and Z contained

24% G and 76% C. The CDR-H3 design for Lib-3 is described in Table 5. Separate mutagenesis reactions were performed and electroporated for each CDR-H3 length, except for lengths seven and eight residues, which were electroporated together.

Phage display of complete Fabs in each library was examined by measuring the binding of 48 randomly picked clones to anti-gD antibody. Lib-1-Fab and Lib-1-Fab.zip had Fab protein displayed on 40–55% or 50–60% of the clones, respectively. Lib-2 with different designs of CDR-H3 displayed similarly with 50%, 46% and 56% positive clones for the DVK, NVT and NNS libraries, respectively. For Lib-3, similar levels of display were observed for the different CDR-H3 lengths, except that libraries incorporating the longest CDR-H3s (from 15–19 residues) had a reduced percentage of Fab displaying clones (15–30%). This may reflect the reduced mutagenesis efficiency when using very long synthetic oligonucleotides.

Library sorting and screening

For sorting, protein antigens were immobilized on Maxisorp immunoplates and libraries were cycled through four to five rounds of binding selections, as described.[30] Wells were blocked alternately using BSA, ovalbumin or casein. Random clones selected from rounds 3 through 5 were assayed using a phage ELISA to compare binding to target antigen, an anti-gD antibody, and two non-relevant proteins for checking non-specific binding. Clones that bound to only the anti-gD antibody and target protein were considered to be specific positives. The PCR fragments of the amplified V_H regions were sequenced.

Light chain randomization for affinity improvement

To generate a light chain library for the affinity maturation of anti-mVEGF clone mV401, a stop template was generated by placing stop codons (TAA) in positions 91–96 in CDR-L3. For library construction, an equimolar mixture of four oligonucleotides designed for the mutagenesis of CDR-L3 (L3-a-d) was mixed with oligonucleotides designed for the mutagenesis of CDR-L1 and CDR-L2 at 1 : 1 : 1 ratio (see Table 8 for oligonucleotide designs). The combined oligonucleotide mixture was annealed to the mV401 stop template phagemid,[51] and published procedures were used to perform a mutagenesis reaction and *E. coli* electroporation. Since the template had stop codons embedded only within CDR-L3, mutagenesis of CDR-L3 alone would result in functional display of a library member. Thus, mutagenesis of CDR-L3 was obligatory for functional display, while mutagenesis of CDR-L1 and CDR-L2 was optional. Library phage was prepared as described above. The first round of binding selection was performed with mVEGF immobilized on immunoplates, and the following rounds were performed by a solution-phase sorting method with increasing stringency as described below.

Solution-phase sorting

A solution-phase sorting method was developed to enhance the efficiency of affinity-based selection. First, purified phage were incubated with biotinylated mVEGF for one to two hours at room temperature in PBS with 0.05% (v/v) Tween20, and 0.5% Superblock (Pierce) (PST). Second, the mixture was diluted five- to tenfold with PST and added to neutravidin-coated wells for a brief (five minutes) capture of biotinylated mVEGF. A reaction lacking biotinylated mVEGF served as a control to monitor background phage binding. The plate was washed with PBS with 0.05% Tween20 (PBT) and eluted with 0.1 M HCl for 20 minutes. Stringency was modulated by the concentration of biotinylated mVEGF, the addition of excess non-biotinylated mVEGF to compete for binding before capturing on neutravidin-coated wells, and the duration and temperature of the binding and competition steps. For the affinity improvement of mV-401, the first round of solution sorting employed 1.0 nM biotinylated mVEGF incubated with phage for one hour at room temperature, followed by the addition of 1.0 μM non-biotinylated mVEGF for 15 minutes at room temperature. The mixture was then diluted tenfold with PST and captured using neutravidin-coated wells for five minutes. The second round used 0.1 nM biotinylated mVEGF followed by an incubation with 100 nM non-biotinylated mVEGF at 37 °C for 30 minutes. The third round used 0.1 nM biotinylated mVEGF followed by incubation with 100 nM non-biotinylated mVEGF at 37 °C for two hours or six hours before capturing with neutravidin-coated wells.

Single-point competitive ELISA

A high-throughput, single-point competitive ELISA was used to screen for high-affinity clones.[30] Briefly, phagemid clones in *E. coli* XL1-Blue were grown in 150 μl of 2YT broth supplemented with carbenicillin and M13-KO7 helper phage; the cultures were grown with shaking overnight at 37 °C in a 96-well format. Culture supernatants containing phage were diluted fivefold in PBST (PBT with 0.5% (w/v) BSA) with or without the addition of 20 nM mVEGF. After incubation for one hour at room temperature, the mixtures were transferred to a plate coated with mVEGF and incubated for ten minutes. The plate was washed with PBT and incubated for 30 minutes with anti-M13 antibody horseradish peroxidase conjugate diluted 5000-fold to ~1 nM in PBST. The plates were washed, developed with TMB substrate for approximately five minutes, quenched with 1.0 M H_3PO_4, and read spectrophotometrically at 450 nm. The ratio of the absorbance in the presence of solution-phase mVEGF to that in the absence of solution-phase mVEGF was used as an indication of the affinity. A low ratio would indicate that most of the Fab-phage were bound to solution-phase mVEGF in the initial incubation stage and, therefore, were unavailable for capture by immobilized mVEGF. Clones with low ratios were chosen for further analysis.

Competitive phage-binding ELISA for IC_{50} measurement

Phage clones were propagated from a single colony by growing in 40 ml of 2YT culture supplemented with carbenicillin and KO7 helper phage overnight at 30 °C. Phage purified by precipitation in PEG/NaCl were first diluted serially in PBST and tested for binding to an antigen-coated plate. The dilution that gave 50–70% saturating signal was used in the solution binding assay in which phage were first incubated with increasing concentration of antigen for one to two hours and then transferred to antigen-coated plates for 10–15 minutes to capture the unbound phage. IC_{50} was calculated as the concentration of antigen in solution-binding stage

that inhibited 50% of the phage from binding to immobilized antigen.

Fab and IgG production, and affinity determination

To generate Fab or IgG proteins for affinity assays, we cloned the variable domain into vectors designed for Fab expression in *E. coli* or transient IgG expression in mammalian cells. The Fab expression vector was derived from the phage display phagemid by deleting the sequence encoding for cP3 and adding an λ terminator sequence (GCTCGGTTGCCGCCGGGCGTTTTTTAT) about 20 nucleotides downstream from the stop codon at the end of C_H1. Fab protein was generated by growing the transformed 34B8 *E. coli* cells in AP5 medium at 30 °C for 24 hours as described.[52] IgG was purified with protein A columns and Fab was purified with protein G affinity chromatography. The production yield for Fab was typically 5–10 mg/l in small-scale shake flask growth and 0.5–3 g/l in fermenter growth. IgG production was reasonably high at 10–50 mg/l in small-scale culture with some clone to clone differences.

For affinity determinations of anti-mVEGF Fabs, we used SPR assays on a BIAcore™-2000 with immobilized mVEGF CM5 chips at ~100 response units (RU) as described.[53] Fab samples of increasing concentration from 3 nM to 500 nM were injected at 20 μl/minute, and binding responses on mVEGF were corrected by subtracting of RU from a blank flow-cell. For kinetics analysis, 1 : 1 Languir model of simultaneous fitting of k_{on} and k_{off} was used. For G6 variants that had increased affinities, all available models were tried but the simultaneous fitting was unsatisfactory with k_{on} determinations being unfittable to any models available. We therefore utilized fluorescence quenching assays to measure the k_{on} in solution. The change of fluorescence intensity in complexing the Fab and VEGF was used to determine the rate of association as developed for the on-rate determination of Avastin variants and VEGF.[54] We first determined that the fluorescence intensity with an excitation wavelength of 280 nm of G6 (or variants)-VEGF complex was lower than the sum of individual components using an 8000 series SLM-Aminco spectrophometer (Thermo-Spectronic) by adding 100 nM VEGF to a stirred cuvette containing 20 nM Fab in PBS (pH 7.2), at 25 °C. Next, increasing concentrations of VEGF (100–400 nM) was mixed with equal volumes of 40 nM Fab in a stop-flow (Aviv Instruments) equipped spectrophotometer to observe the rate of the decrease of fluorescence intensity at 25 °C. For each experiment, nine measurements were performed for each concentration and fit to a single-exponential curve. The observed rate was then plotted against VEGF concentrations for pseudo-first-order analysis, and the slope is the rate of association. Two or three independent experiments were carried out and the differences were within 50%. For Fab and IgG binding to other antigens, IC_{50} values from solution competition assays were reported. The solution competition binding assay used biotinylated protein antigens equilibrated with serial dilutions of purified Fab or IgG proteins, and the unbound biotin-antigen was captured with immobilized Fab or IgG coated on Maxisorb plates and was detected with streptavidin-conjugated HRP. Alternatively, Fab or IgG proteins were equilibrated with serial dilutions of protein antigen, and the unbound Fab or IgG was captured with immobilized antigen and detected with protein A-HRP.

Acknowledgements

We are grateful to the Genentech Automation Technology group for screening assays, the DNA Synthesis group for oligonucleotides and the DNA Sequencing group for sequencing. We thank Jenny Bostrom and Jonathan Marvin for technical consultation, and Robert Kelley, Henry Lowman, and Abraham de Vos for helpful discussions.

References

1. Smith, G. P. & Scott, J. K. (1993). Libraries of peptides and proteins displayed on filamentous phage. *Methods Enzymol.* **217**, 228–257.
2. Hoogenboom, H. R. (2002). Overview of antibody phage-display technology and its applications. *Methods Mol. Biol.* **178**, 1–37.
3. Rader, C. & Barbas, C. F. (1997). Phage display of combinatorial antibody libraries. *Curr. Opin. Biotechnol.* **8**, 503–508.
4. Hanes, J. & Pluckthun, A. (1997). *In vitro* selection and evolution of functional proteins by using ribosome display. *Proc. Natl Acad. Sci. USA*, **94**, 4937–4942.
5. Georgiou, G., Stathopoulos, C., Daugherty, P. S., Nayak, A. R., Iverson, B. L. & Curtiss, R. (1997). Display of heterologous proteins on the surface of microorganism from the screening of combinatorial libraries to live recombinant vaccines. *Nature Biotechnol.* **15**, 29–34.
6. Kieke, M. C., Cho, B. K., Boder, E. T., Kranz, D. M. & Wittrup, K. D. (1997). Isolation of anti-T cell receptor scFv mutants by yeast display. *Protein Eng.* **10**, 1303–1310.
7. Kretzschmar, T. & von Ruden, T. (2002). Antibody discovery: phage display. *Curr. Opin. Biotechnol.* **13**, 598–602.
8. de Kruif, J., Boel, E. & Logtenberg, T. (1995). Selection and application of human single chain Fv antibody fragments from a semi-synthetic phage antibody display library with designed CDR3 regions. *J. Mol. Biol.* **248**, 97–105.
9. Griffiths, A. D., Williams, S. C., Hartley, O., Tomlinson, I. M., Waterhous, P., Crosby, W. L. *et al.* (1994). Isolation of high affinity human antibodies directly from large synthetic repertoires. *EMBO J.* **13**, 3245–3260.
10. Nissim, A., Hoogenboom, H. R., Tomlinson, I. M., Flynn, G., Midgley, C., Lane, D. & Winter, G. (1994). Antibody fragments from a 'single pot' phage display library as immunochemical reagents. *EMBO J.* **13**, 692–698.
11. Hoogenboom, H. R. & Winter, G. (1992). By-passing immunisation. Human antibodies from synthetic repertoires of germline VH gene segments rearranged *in vitro*. *J. Mol. Biol.* **227**, 381–388.
12. Marks, J. D., Hoogenboom, H. R., Bonnert, T. P., McCafferty, J., Griffiths, A. D. & Winter, G. (1991). By-passing immunization: human antibodies from V-gene libraries displayed on phage. *J. Mol. Biol.* **222**, 581–597.
13. Vaughan, T. J., Williams, A. J., Pritchard, K., Osbourn, J. K., Pope, A. R., Earnshaw, J. C. *et al.* (1996). Human antibodies with sub-nanomolar affinities isolated from a large non-immunized phage display library. *Nature Biotechnol.* **14**, 309–314.

14. Sheets, M. D., Amersdorfer, P., Finnern, R., Sargent, P., Lindqvist, E. A., Shier, R. *et al.* (1998). Efficient construction of a large nonimmune phage antibody library: the production of high-affinity human single-chain antibodies to protein antigens. *Proc. Natl Acad. Sci. USA*, **95**, 6157–6162.
15. Clackson, T., Hoogenbroom, H. R., Griffiths, A. D. & Winter, G. (1991). Making antibody fragments using phage display libraries. *Nature*, **352**, 624–628.
16. Barbas, C. F., Kang, A. S., Lerner, R. A. & Benkovic, S. J. (1991). Assembly of combinatorial antibody libraries on phage surfaces: the gene III site. *Proc. Natl Acad. Sci. USA*, **88**, 7978–7982.
17. Sblattero, D. & Bradbury, A. (2000). Exploiting recombination in single bacteria to make large phage antibody libraries. *Nature Biotechnol.* **18**, 75–80.
18. Barbas, C. F., Bain, J. D., Hoekstra, D. M. & Lerner, R. A. (1992). Semisynthetic combinatorial Ab libraries: a chemical solution to the diversity problem. *Proc. Natl Acad. Sci. USA*, **89**, 4457–4461.
19. Garrard, L. J. & Henner, D. J. (1993). Selection of an anti-IGF-1 Fab from a Fab phage library created by mutagenesis of multiple CDR loops. *Gene*, **128**, 103–109.
20. de Wildt, R. M. T., Mundy, C. R., Gorick, B. D. & Tomlinson, I. M. (2000). Antibody arrays for high-throughput screening of antibody–antigen interactions. *Nature Biotechnol.* **18**, 989–994.
21. Desiderio, A., Fanconi, R., Lopez, M., E., V. M., Viti, F., Chiaraluce, R. *et al.* (2001). A semi-synthetic repertoire of intrinsically stable antibody fragments derived from a single-framework scaffold. *J. Mol. Biol.* **310**, 603–615.
22. Knappik, A., Ge, L., Honegger, A., Pack, P., Fischer, M., Wellnhofer, G. *et al.* (2000). Fully synthetic human combinatorial antibody libraries (HuCAL) based on modular consensus frameworks and CDRs randomized with trinucleotides. *J. Mol. Biol.* **296**, 57–86.
23. Hanes, J., Schaffitzel, C., Knappik, A. & Pluckthun, A. (2000). Picomolar affinity antibodies from a fully synthetic naive library selected and evolved by ribosome display. *Nature Biotechnol.* **18**, 1287–1292.
24. Krebs, B., Rauchenberger, R., Reiffert, S., Rothe, C., Tesar, M., Thomassen, E. *et al.* (2001). High-throughput generation and engineering of recombinant human antibodies. *J. Immunol. Methods*, **254**, 67–84.
25. Carter, P., Kelley, R. F., Rodrigues, M. L., Snedecor, B., Covarrubias, M., Velligan, M. D. *et al.* (1992). High level *Escherichia coli* expression and production of a bivalent humanized antibody fragment. *Bio/Tech*, **10**, 163–167.
26. Chothia, C. & Lesk, A. M. (1987). Canonical structures for the hypervariable regions of immunoglobulins. *J. Mol. Biol.* **196**, 901–917.
27. Chothia, C., Lesk, A. M., Tramontano, A., Levitt, M., Smith-Gill, S. J., Air, G. *et al.* (1989). Conformations of immunoglobulin hypervariable regions. *Nature*, **342**, 877–883.
28. Chothia, C., Lesk, A. M., Gherardi, E., Tomlinson, I. M., Walter, G., Marks, J. D. *et al.* (1992). Structural repertoire of the human V_H segments. *J. Mol. Biol.* **227**, 799–817.
29. Carter, P., Presta, L., Gorman, C. M., Ridgway, J. B. B., Henner, D., Wong, W. L. T. *et al.* (1992). Humanization of an anti-p185HER2 antibody for human cancer therapy. *Proc. Natl Acad. Sci. USA*, **89**, 4285–4289.
30. Sidhu, S. S., Li, B., Fellouse, F., Eigenbrot, C. & Fuh, G. (2004). Phage-displayed antibody libraries of synthetic heavy chain complementarity determining regions. *J. Mol. Biol.* **338**, 299–310.
31. Wu, T. T., Johnson, G. & Kabat, E. A. (1993). Length distribution of CDRH3 in antibodies. *Proteins: Struct. Funct. Genet.* **16**, 1–7.
32. Zemlin, M., Klinger, M., Link, J., Zemlin, C., Bauer, K., Engler, J. A. *et al.* (2003). Expressed murine and human CDR-H3 intervals of equal length exhibit distinct repertoires that differ in their amino acid composition and predicted range of structures. *J. Mol. Biol.* **334**, 733–749.
33. Collis, A. V. J., Brouwer, A. P. & Martin, A. C. R. (2003). Analysis of the antigen combining site: correlations between length and sequence composition of the hypervariable loops and the nature of the antigen. *J. Mol. Biol.* **325**, 337–354.
34. Johnson, G. & Wu, T. T. (2000). Kabat database and its applications: 30 years after the first variability plot. *Nucl. Acids Res.* **28**, 214–218.
35. Wilson, I. A. & Stanfield, R. L. (1994). Antibody–antigen interactions: new structures and new conformational changes. *Curr. Opin. Struct. Biol.* **4**, 857–867.
36. Padlan, E. A. (1994). Anatomy of the antibody molecule. *Mol. Immunol.* **31**, 169–217.
37. Xu, J. L. & Davis, M. M. (2000). Diversity in the CDR3 region of V(H) is sufficient for most antibody specificities. *Immunity*, **13**, 37–45.
38. Lee, C. V., Sidhu, S. S. & Fuh, G. (2004). Bivalent antibody phage display mimics natural immunoglobulin. *J. Immunol. Methods*, **284**, 119–132.
39. O'Connell, D., Becerril, B., Roy-Burman, A., Daws, M. & Marks, J. D. (2002). Phage *versus* phagemid libraries for generation of human monoclonal antibodies. *J. Mol. Biol.* **321**, 49–56.
40. Padlan, E. A. (1990). On the nature of antibody combining sites: unusual structural features that may confer on these sites an enhanced capacity for binding ligands. *Proteins: Struct. Funct. Genet.* **7**, 112–124.
41. Mian, I. S., Bradbury, A. & Olson, A. J. (1991). Structure, function and properties of antibody binding sites. *J. Mol. Biol.* **217**, 133–151.
42. Eigenbrot, C., Randal, M., Presta, L., Carter, P. & Kossiakoff, A. A. (1993). X-ray structures of the antigen-binding domains from three variants of humanized anti-p185HER2 antibody 4D5 and comparison with molecular modeling. *J. Mol. Biol.* **229**, 969–995.
43. MacCallum, R. M., Martin, A. C. & Thornton, J. M. (1996). Antibody–antigen interactions: contact analysis and binding site topology. *J. Mol. Biol.* **262**, 732–745.
44. Jirholt, P., Strandberg, L., Jansson, B., Krambovitis, E., Soderland, E., Borrebaeck, C. A. *et al.* (2001). A central core structure in an antibody variable domain determine antigen specificity. *Protein Eng.* **14**, 67–74.
45. Sidhu, S. S., Lowman, H. B., Cunningham, B. C. & Wells, J. A. (2000). Phage display for selection of novel binding peptides. *Methods Enzymol.* **328**, 333–363.
46. Muller, Y. A., Chen, Y., Christinger, H. W., Li, B., Cunningham, B. C., Lowman, H. B. & de Vos, A. M. (1998). VEGF and the FAB fragment of a humanized neutralizing antibody: crystal structure of the complex at 2.4 Å resolution and mutational analysis of the interface. *Structure*, **6**, 1153–1167.
47. Hamers-Casterman, C., Atarhouch, T., Muyldermans, S., Robinson, G., Hamers, C., Songa,

E. B. *et al.* (1993). Naturally occurring antibodies devoid of light chains. *Nature*, **363**, 446–448.
48. Marks, J. D., Griffiths, A. D., Malmqvist, M., Clackson, T., Bye, J. M. & Winter, G. (1992). Bypassing immunization: high affinity human antibodies by chain shuffling. *Bio/Tech*, **10**, 779–783.
49. Lowman, H. B., Bass, S. H., Simpson, N. & Wells, J. A. (1991). Selecting high-affinity binding proteins by monovalent phage display. *Biochemistry*, **30**, 10832–10838.
50. Lasky, L. A. & Dowbenko, D. J. (1984). DNA sequence analysis of the type-common glycoprotein-D genes of herpes simplex virus types 1 and 2. *DNA*, **3**, 23–29.
51. Kunkel, T. A., Roberts, J. D. & Zakour, R. A. (1987). Rapid and efficient site-specific mutagenesis without phenotypic selection. *Methods Enzymol.* **154**, 367–382.
52. Presta, L. G., Chen, H., O'Connor, S. J., Chisholm, V., Meng, Y. G., Krummen, L. *et al.* (1997). Humanization of an anti-vascular endothelial growth factor monoclonal antibody for the therapy of solid tumors and other disorders. *Cancer Res.* **57**, 4593–4599.
53. Chen, Y., Weismann, C., Fuh, G., Li, B., Christinger, H. W., McKay, P. *et al.* (1999). Selection and analysis of an optimized anti-VEGF antibody: crystal structure of an affinity-matured Fab in complex with antigen. *J. Mol. Biol.* **293**, 865–881.
54. Marvin, J. S. & Lowman, H. B. (2003). Redesigning an antibody fragment for faster association with its antigen. *Biochemistry*, **42**, 7077–7083.

Edited by I. Wilson

(Received 27 February 2004; received in revised form 25 May 2004; accepted 25 May 2004)